

Dissertation zur Erlangung des Doktorgrades
der Fakultät für Chemie und Pharmazie
der Ludwig-Maximilians-Universität München

**Formulation development of a
highly concentrated suspension
of Cilengitide**

Gudrun Charlotte Birk

aus

Villingen-Schwenningen, Deutschland

2015

Erklärung

Diese Dissertation wurde im Sinne von § 7 der Promotionsordnung vom 28. November 2011 von Herrn Prof. Dr. Wolfgang Frieß betreut.

Eidesstattliche Versicherung

Diese Dissertation wurde eigenständig und ohne unerlaubte Hilfe erarbeitet.

München,

.....
Gudrun Birk

| | |
|--------------------------------|--------------------------|
| Dissertation eingereicht am | 11. September 2015 |
| 1. Gutachterin / 1. Gutachter: | Prof. Dr. Wolfgang Frieß |
| 2. Gutachterin / 2. Gutachter: | Prof. Dr. Gerhard Winter |
| Mündliche Prüfung am | 20. Oktober 2015 |



Acknowledgement

The present thesis was prepared as cooperation between the Department of Pharmacy, Pharmaceutical Technology and Biopharmaceutics at the Ludwig-Maximilians-University of Munich and the Drug Product Development and Life Cycle Management Department at Merck Serono, Darmstadt under the supervision of Prof. Dr. Wolfgang Frieß.

First and foremost, I want to express my deepest gratitude to Prof. Dr. Wolfgang Frieß for his scientific guidance and his ongoing and encouraging support of my work. I would like to thank for the constructive discussions, the patience and consistency to critical questioning. Moreover, I appreciate the open and welcoming atmosphere of the team which I joined irregularly.

I also would like to thank Prof. Dr. Gerhard Winter for taking over the co-referee of the thesis. Thank you for the valuable contributions during the Thursdays' seminars.

I am deeply grateful to my supervisor Dr. Sandra Kucera for continuously supporting me in the last one and a half year. I really appreciate your scientific enthusiasm and comprehensive approach to questions. Thank you very much for the time and energy you spent for our discussions. It was a pleasure to work with you.

Dr. Anke Stabenau is cordially acknowledged for her dedicated supervision throughout the first half of the thesis. Thank you for your ongoing interest and support of my work.

Many thanks for all the colleagues at Merck for their scientific support and enjoyable breaks. Thank you for the pleasant working atmosphere. Particularly, I want to thank Dr. Alena Wieber for her comprehensive and ongoing support. I really appreciate our friendship and our cooperation. Many thanks to Dr. Adela Kasselkuß for her helpful advice and for the enjoyable time together with Alena. I am grateful to Stefanie Herold, Tim-Nikolas Hoffman and Reiner Vonderschmitt for their strong and continuous help in the formulation laboratory. I also want to thank Dr. Andreas Marx for the intensive support in NMR analytics and constant motivation. Dr. Meike Harms is warmly acknowledged for the scientific discussions and helpful input. Great thanks are addressed to Dr. Dirk Wandschneider and Stephan von der Au for the support in particle analysis.

Acknowledgement

Thanks also to my Ph.D. colleagues for the discussions and weekly breakfast. I recall with pleasure the “Blutwurst aus dem Glas”.

Moreover, I would like to thank the research groups of Prof. Dr. Frieß and Prof. Dr. Winter. Especially, I would like to thank Verena Saller for her support and for providing me an accommodation during the excursions.

Finally, I sincerely thank my family and especially my sister for their encouragement and strong support. Thanks for all you made possible for me.

Table of content

| | | |
|----------|---|-----------|
| 1 | Introduction | 1 |
| | 1.1 General introduction | 1 |
| | 1.2 Suspensions | 2 |
| | 1.2.1 Classification of suspensions..... | 2 |
| | 1.2.2 Interaction between particles in suspension | 2 |
| | 1.2.3 Physical stability of a suspension | 4 |
| | 1.2.4 Rheological properties..... | 5 |
| | 1.2.5 Parameter influencing the viscosity | 9 |
| | 1.3 Aim of the thesis | 13 |
| 2 | Materials..... | 14 |
| 3 | Methods..... | 14 |
| | 3.1 Analytical methods..... | 14 |
| | 3.1.1 Characterization of the raw material | 14 |
| | 3.1.2 Flowability | 15 |
| | 3.1.3 Angle of repose | 15 |
| | 3.1.4 Thermogravimetric analysis..... | 15 |
| | 3.1.5 Dynamic vapor sorption..... | 15 |
| | 3.2 Characterization of the suspension | 16 |
| | 3.2.1 Particle size measurement | 16 |
| | 3.2.2 Microscopy | 16 |
| | 3.2.3 Stereomicroscopy..... | 16 |
| | 3.2.4 Scanning electron microscopy..... | 16 |
| | 3.2.5 Zeta potential..... | 16 |
| | 3.2.6 Streaming potential..... | 17 |
| | 3.2.7 Turbidimetry | 17 |

| | | |
|----------|---|-----------|
| 3.2.8 | Dynamic light scattering | 18 |
| 3.2.9 | Cryo-transmission electron microscopy | 18 |
| 3.2.10 | Nuclear magnetic resonance (NMR) spectroscopy | 18 |
| 3.2.11 | Surface tension | 19 |
| 3.2.12 | Sedimentation analysis..... | 19 |
| 3.2.13 | Rheometry..... | 19 |
| 3.2.14 | Resuspendability | 20 |
| 3.2.15 | Syringeability | 20 |
| 3.2.16 | Injectability | 20 |
| 3.3 | Manufacturing process | 21 |
| 3.3.1 | Milling of API | 21 |
| 3.3.2 | Preparation of suspensions | 21 |
| 3.4 | Storage stability study..... | 21 |
| 4 | General properties, solid-state and powder characterization of the drug substance..... | 23 |
| 4.1 | Crystallinity and polymorphism | 23 |
| 4.2 | pKa values..... | 26 |
| 4.3 | Particle size | 26 |
| 4.4 | Flow properties of raw material..... | 29 |
| 4.5 | Conclusion..... | 29 |
| 5 | Characterization of aqueous Cilengitide suspension | 30 |
| 5.1 | Parameters influencing the particle size | 30 |
| 5.1.1 | Stirring time and raw material particle size | 30 |
| 5.1.2 | Application of comminuting methods with higher energy levels | 37 |
| 5.1.3 | Influence of drug substance concentration in suspension..... | 39 |
| 5.2 | Particle size stability upon storage | 39 |
| 5.3 | Sedimentation behavior | 43 |

| | | |
|----------|--|-----------|
| 5.3.1 | Sedimentation rate analyzed by transmission and backscattering detection..... | 44 |
| 5.3.2 | Macroscopic sedimentation behavior..... | 44 |
| 5.4 | Rheological characterization..... | 47 |
| 5.4.1 | Influence of concentration on rheological properties..... | 48 |
| 5.5 | Injectability of different concentrated formulations..... | 51 |
| 5.6 | Conclusion..... | 52 |
| 6 | Formulation development for 300 mg/mL Cilengitide suspensions | 54 |
| 6.1 | Parameters influencing the suspension viscosity | 54 |
| 6.1.1 | Effect of varying pH on viscosity of 300 mg/mL API suspension..... | 54 |
| 6.1.2 | Influence of ions on viscosity of 300 mg/mL API suspension..... | 58 |
| 6.1.3 | Effect of particle size on viscosity of 300 mg/mL API suspension..... | 59 |
| 6.1.4 | Effect of phospholipids on suspension viscosity | 61 |
| 6.1.5 | Effect of varying pH on viscosity of 300 mg/mL Cilengitide suspensions containing 2 mg/mL DMPG | 70 |
| 6.1.6 | Interaction model for Cilengitide and DMPG at varying pH values..... | 78 |
| 6.1.7 | Addition of phospholipids with alternative chain length to confirm the interaction model | 81 |
| 6.1.8 | Polysorbate 80 and sorbitan monooleat as alternative surfactants | 83 |
| 6.1.9 | Influence of pH on viscosity of suspensions containing 2 mg/mL DMPG or 5 mg/mL PS 80/SO (40/60)..... | 88 |
| 6.2 | Physical stability during storage of suspensions containing 300 mg/mL Cilengitide and 2 mg/mL DMPG or 5 mg/mL PS 80/SO (40/60) | 90 |
| 6.2.1 | Initial characteristics | 91 |
| 6.2.2 | Particle size stability | 92 |
| 6.2.3 | Sedimentation rate of DMPG and PS 80/SO containing suspensions | 94 |
| 6.2.4 | Resuspendability | 96 |
| 6.2.5 | Syringeability | 97 |

Table of content

| | | |
|----------|--|------------|
| 6.2.6 | Injectability | 98 |
| 6.3 | Conclusion..... | 99 |
| 7 | Final summary of the thesis | 102 |
| 8 | References | 105 |

1 Introduction

1.1 General introduction

Many drugs, especially peptides and proteins require parenteral delivery for bypassing the hepatic first-pass effect and avoiding enzymatic degradation in the gastrointestinal tract. Therefore, injections in the form of sterile solutions, emulsions or suspensions are indicated. Among these formulations, injected suspensions can be efficient depot formulations with prolonged drug release compared to solutions [1]. They provide advantages to deliver higher doses and insoluble or poorly soluble pharmaceutical ingredients can be administered. Resistance to degradation, including hydrolysis, oxidations or microbial activity is further improved by using the solid drug form [2]. The subcutaneous or intramuscular administration route offers benefits as it enables self-application of the drug, resulting in lower medical costs and better compliance of the patients. However, only small volumes up to 1.5 mL may be injected [3] and therefore either high concentrations or a high potency of the active ingredient are required. Highly concentrated formulations for subcutaneous administration are frequently suspensions due to the limited solubility of many drugs. A sufficiently low viscosity of these suspensions is pivotal to allow a subcutaneous injection via 25 to 27 Gauge needles [4]. Moreover, the needle size creates limitations for the drug particle size in order to avoid needle clogging. One drawback, however, is that subcutaneously applied suspensions may produce irritations, indurations, sloughing or abscess formation, which can be painful to the patients [5]. In addition, the injection site must be changed if regular injections are required [5].

A subcutaneously applied suspension is the drug formulation of choice for Cilengitide (EMD 121974), an antineoplastic therapeuticum. Cilengitide is a cyclized pentapeptide consisting of the amino acid sequence L-Arg-Gly-L-Asp-D-Phe-N(Me)-L-Val [6]. Several polymorphs are known, whereby the polymorph A1 is most stable and least water-soluble and therefore most suitable for a suspension formulation [7]. The RGD-sequence (L-Arg-Gly-L-Asp) of the peptide binds to the integrin receptors $\alpha\beta3$ and $\alpha\beta5$ and leads to the inhibition of angiogenesis and apoptosis. Intended indications have been glioblastoma [8], prostate cancer [9], non small cell lung cancer [10] or recurrent and/or metastatic squamous cell carcinoma of the head and neck [11].

1.2 Suspensions

1.2.1 Classification of suspensions

Suspensions can be generally classified according to various criteria. Coarse suspensions contain dispersed particles larger than 1 μm , while particles are smaller than 1 μm in colloidal suspensions [12]. Regarding the intended route of delivery, pharmaceutical suspensions are broadly divided into three general classes [13]: orally administered (sometimes referred to as mixtures), externally applied (topical lotions) and injectable (parenteral) suspensions. The solid content varies, depending on the use of the suspension, between 0.5 % and 40 %. Diluted suspensions with a solid concentration between 0.5 and 5 % are used for parenteral application, except for insoluble forms of penicillin with antibiotic concentration exceeding 30 % [14]. Further well-known parenteral crystal suspensions contain NPH-insulin (neutral protamine hagedorn or isophane insulin) or a corticoid (Volon[®], Diprosone[®] Depot) with concentration up to 40 mg/mL (Volon[®]). They are efficient depot formulations.

Taking the electrokinetic nature of solid particles into consideration, suspensions may be classified as flocculated or deflocculated systems. Deflocculated suspensions are characterized by separated, uniformly dispersed particles which settle slowly whereas the supernatant remains cloudy. The sediment can be closely packed ("cake") and can be difficult to redisperse [2]. In flocculated suspensions, particles form loose aggregates which settle rapidly. The sediment is easy to redisperse due to its scaffold-like structure [2]. A continuous rigid three-dimensional particulate network structure is built at quiescent conditions when the volume fraction is above the percolation threshold or most recently named the gel point ϕ_g [15]. The appearance is somewhat unsightly due to the rapid sedimentation and the presence of an obvious, clear supernatant. This can be optimized by increasing the volume of the sediment. Flocculated formulations are the most common type of parenteral suspension [2]. They have less potential to cause physical stability problems, above all caking [2].

1.2.2 Interaction between particles in suspension

The aggregation potential of dispersions is defined by attractive and repulsive forces which exist between the suspended particles [16]. The result of particle interaction is explained by the DLVO theory, which in fact applies for colloidal dispersion, but is also valid for coarse suspension systems as confirmed by Kayes [17].

The potential energy of interaction, V_T is the result of repulsion V_R and attraction V_A [Eq. 1]:

$$V_T = V_R + V_A \quad [\text{Eq. 1}]$$

The repulsive potential V_R is influenced by the zeta potential, the particle radius, the interparticular distance and the dielectric constant of the medium. The attractive potential V_A depends mainly on the particle radius and the interparticular distance [16, 18]. Figure 1 shows the interaction energy as a function of the distance between two particles [16].

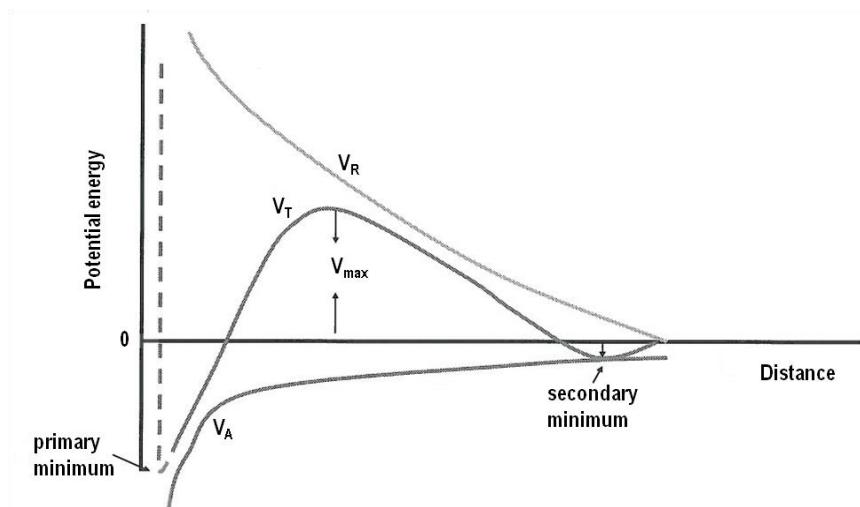


Figure 1: Schematic representation of the variation of potential energy with distance according to the Derjaguin-Landay-Verwey-Overbeek (DLVO) theory pursuant to [19].

If a particle approaches another particle, it will enter a radius of long-range forces of attraction, the secondary minimum. At this minimum, flocculated suspensions are formed which are easy to resuspend. However, the secondary minimum does not occur in all cases [20] as it depends on specific conditions (e.g. certain electrolyte concentrations) [18]. Further reduction in the distance leads to increased repulsive forces, which stabilize suspensions in the deflocculated state [16]. If these repulsive forces are overcome by particles with high kinetic energy, these particles will enter the primary minimum, a state characterized by dense particle packing and strong attractive forces. A hard cake will be formed which is very difficult to redisperse [16]. Stable dispersions can be obtained by electrostatic stabilization or by steric stabilization due to adsorption of a non-ionic polymer, e.g. gum or cellulosic or surfactant, e.g. polysorbate 80 [1, 12, 16, 18] which both affect the repulsive potential V_R [18] and thus, the potential energy of interaction V_T . The steric stabilization is relatively insensitive to the presence of electrolytes in the aqueous vehicle [1].

1.2.3 Physical stability of a suspension

Sedimentation and floating

Formulation development of suspensions is very complex and challenging from a physicochemical point of view due to the coexistence of a solid (internal) and a liquid (external) phase prone to physical instabilities [16]. In addition to caking, sedimentation and flotation are further phenomena of suspension instability which compromise dosing uniformity. Sedimentation or flotation occur as soon as differences in density exist between the solid and liquid phase [16]. The settling kinetics of diluted dispersions with spherical, monodispersed particles can be described by the Stokes' equations [20]:

$$v = \frac{2r^2(\rho_S - \rho_L)g}{9\eta} \quad \text{[Eq. 2]}$$

The velocity (v) of sedimentation (or flotation) at specific differences in density ($\rho_S - \rho_L$) between the solid (ρ_S) and liquid (ρ_L) phase depends on the radius r of the dispersed particles and on the viscosity of the liquid phase η . At a given density difference, a lower rate of sedimentation can be achieved by particle size reduction or an increase in the viscosity of the medium, respectively. Common viscosity enhancers used in parenteral suspensions are cellulose derivatives, gelatin or polyvinyl pyrrolidone. Floating can be prevented by wetting agents such as surfactants [16].

However, Stokes' law is invalid for suspensions containing more than 2 % of solids as the higher solid content imparts additionally viscosity to the system and particle-particle interactions increase [16]. Furthermore, Stokes' law does not account for the dielectric constant, which has an influence on the zeta potential and thus, on the settling rate as well as Brownian movement which counteracts sedimentation to a measurable extent [16].

Particle size stability

Crystal growth, also known as Ostwald ripening, is another phenomenon of physical instability of suspensions. The solubility of a compound is constant for larger particles and depends on the compound, the dispersion medium and the temperature. Smaller particles exhibit higher surface free energy and are therefore more soluble in the dispersion medium. This effect is described by the Ostwald-Freundlich equation [21]

$$\rho v \frac{RT}{M} \ln \frac{S_r}{S_\infty} = \frac{2 \gamma_{sl}}{r} \quad \text{[Eq. 3]}$$

where S_r is the solubility of particles of radius r , S_∞ the normal solubility value, γ_{sl} is the interfacial tension, and ν represents the number of moles of ions formed from one mole of electrolyte and ρ the density of the solid. M is the molecular weight, R the gas constant and T the absolute temperature. A drug concentration gradient between the small and large particles is created, leading to molecule diffusion from the higher concentration surrounding small particles to areas around larger particles with lower drug concentration. The drug crystallizes onto the large particles as supersaturation is generated. The diffusion process creates an unsaturated solution around the small particles causing further dissolution of the molecules from the small particles into the bulk medium. As a consequence, the smaller particles dissolve over time while larger particles will grow in size, leading to a shift in particle size distribution of the suspension. Factors that promote crystal growth are a wide particle size distribution, changes in pH and temperature, dissolution and recrystallization processes as well as polymorphism and solvate formation [1, 2]. Using a narrow particle size distribution, the least soluble polymorph and solvate form and choosing appropriate storage conditions [1, 2], the risk can be minimized. Viscosity enhancing agents may prevent Ostwald ripening as the mobility of the suspended particles in the coherent phase decreases. Certain hydrophilic gums [1, 2] or surfactants [1, 16] may adsorb at the particle surface and retard crystal growth due to a film barrier or dissipating the free surface energy of particles by reducing the interfacial tension, respectively. However, the tolerable viscosity of subcutaneous formulations is limited due to requirements with regard to syringeability and injectability, limiting the use of viscosity enhancers. Syringeability is defined as the ability of a parenteral solution or suspension to pass easily through a hypodermic needle during the transfer of the product from a vial to a hypodermic syringe prior to injection [22]. Injectability refers to the subsequent ejection of the formulation into the desirable site of administration [22]. Increased viscosity of suspensions hinders syringeability as well as injectability [1, 2] and further promotes syringe clogging [2].

1.2.4 Rheological properties

Diluted suspensions as commonly used for the parenteral route contain 0.5 - 5 % of the API [14] and behave like low-viscous, Newtonian systems. However, concentrated suspensions typically follow non-Newtonian flow [16], where viscosity changes with applied shear rate. They show a maximum viscosity at rest caused by high interparticular interaction [16]. The viscosity decreases considerably when the yield point is overcome by applying a minimum force. Beyond that point, viscosity either remains constant for Bingham plastic systems (plastic flow) or further decreases with increasing shear rate (pseudoplastic flow / shear thinning) [16, 19].

Pseudoplastic flow is beneficial for parenteral suspensions as the reduced viscosity of the sheared system facilitates syringeability and injectability [16].

In pharmaceutical literature, viscosity reduction of suspensions is rarely discussed as viscosity enhancement is more often required to stabilize the formulation. Highly concentrated protein solutions such as monoclonal antibodies which have gained interest recently, often suffer from high viscosities, leading to some reports discussing the viscosity of parenteral solutions [23]. Viscosity reduction of suspensions is more often requested in the field of process technology. Coal-water mixtures exhibit high viscosities, so that they are difficult to pump [24]. The knowledge of the rheological properties of bentonite clays is of great importance as they are used as thickening agents in many industrial preparations such as drilling fluids, cement and paint [25]. Another field that requires viscosity reduction is the process of ceramics fabrication, where polymer dispersants are generally added in order to control aggregation properties and obtain highly concentrated suspensions [26].

Viscosity is strongly influenced by the nature and magnitude of the interparticular forces [23, 24, 27, 28] as well as the interactions of the suspended particles with the solvent and co-solutes [23]. Generally, three different forces can be distinguished in suspensions [28]. Hydrodynamic forces, which are existent in all flowing suspensions, result from the relative motion of particles to the surrounding fluid and particles. Brownian force, noticeable for systems containing submicron particles ($< 1 \mu\text{m}$), is a fluctuating force which is the consequence of particle collisions with molecules of the fluid. Colloidal forces in immobile suspensions can be attractive or repulsive. Van der Waals, electrostatic attractive and hydrophobic interactions, bridging and depletion are attractive forces. Repulsive forces include electrostatic repulsion, steric hindrance, hydration and structural forces [28]. The sum of all effects determines the particular interaction, as already mentioned discussing the DLVO theory, and can be influenced by the nature of solids, the properties of the dispersion medium and the addition of excipients.

The probability of solute or particle interaction increases with concentration as the spatial distances between the particles or dissolved molecules are reduced [23, 29]. Hence, short-range interactions such as van der Waals forces, dipole-dipole and hydrophobic interactions, hydrogen bonding and specific ionic attractions [30] can play a significant role in concentrated compositions [23, 31]. Important physical parameters influencing the interaction and thus, the viscosity of the preparation are the dispersed phase content ϕ , the particle shape, size and size distribution, the nature of the dispersion medium and the temperature. The dispersed phase content is defined as the ratio in volume (weight) of the dispersed phase to the total volume (weight) of the dispersion and has the greatest impact on viscosity [32, 33]. The

viscosity increases with increasing phase content as described by the Einstein equation ([Eq. 4]) for very diluted suspensions ($\phi < 0.01$) of hard, noninteracting spheres [19].

$$\eta_S = \eta_0(1 + 2.5 \phi) \quad \text{[Eq. 4]}$$

In more concentrated suspensions, aggregates are formed due to more interparticular attractions and the dispersion medium is trapped within the aggregates [16], increasing the effective volume of the solid phase ϕ_e of the flocculated system and thus, the viscosity [Eq. 5] including a as the two-body interaction parameter between the particles, is more accurate [32]:

$$\eta_S = \eta_0(1 + 2.5 \phi_e + a \phi_e^2) \quad \text{[Eq. 5]}$$

The semiempirical Thomas equation describes the viscosity of suspensions for ϕ values up to 0.6 [Eq. 6].

$$\eta_S = \eta_0(1 + 2.5\phi_e + 10.05 \phi_e^2 + 0.00273 e^{16.6 \phi_e}) \quad \text{[Eq. 6]}$$

The last term becomes more important as ϕ increases and the viscosity increases exponentially [32].

Another way to calculate the viscosity of concentrated suspensions is the Krieger-Dougherty equation [Eq. 7] with the intrinsic viscosity $[\eta_0]$ and the maximum packing fraction ϕ_m , which describes the maximum volume that particles occupy without deformation [34].

$$\eta_S = \eta_0 \left(1 - \frac{\phi}{\phi_m}\right)^{-\phi_m [\eta]} \quad \text{[Eq. 7]}$$

For monodisperse particles, ϕ_m is between 0.6 and 0.64 approximately [32].

When a colloidal solid particle is partly soluble in the medium, solvation layers are built and lead to an apparent swelling of the particle which increases ϕ and hence the viscosity [16]. [Eq. 8] includes this effect.

$$\eta_s = \eta_0 \left[1 + 2.5 \left(1 + \frac{t_i}{R} \right)^3 \phi \right] = \eta_0 \left[1 + 2.5 \left(1 + \frac{t_i * \rho A_{sp}}{3} \right)^3 \phi \right] \quad \text{[Eq. 8]}$$

t_i is the thickness of the solvation layer, ρ is the density of the dispersed phase and A_{sp} is the specific surface area of the solid particles, assuming spherical. All of the mentioned equations do not consider either particle size, shape or size distribution. Also, the non-Newtonian behavior of systems with ϕ values above 0.2 [32] is not considered.

1.2.5 Parameter influencing the viscosity

The effect of the particle size on the viscosity of concentrated suspensions is important and depends on the counterbalance of hydrodynamic and Brownian forces [16, 32]. Considering repulsive particle systems, the relative importance of electrostatic repulsive forces increases as the diameter is decreased as Boersma et al have shown [35]. Thereby, the effective volume fraction of smaller particles due to the larger double layer is increased and the mean distance between the particles is shorter for smaller particles, resulting in an extended double layer interaction [28]. Consequently, viscosity is increased, especially at low shear rates. Shi et al. [33] showed that slurries exhibited two different types of flow curves in dependence of particle size and total concentrations. Dilatant flow was observed for slurries with low solid concentration (15 %), where the viscosity increased with increasing fines content in addition to the development of a yield stress. At intermediate solids concentrations and coarse particle size (20 % < 38 μm) classic Bingham plastic flow occurred. The slurries behaved like pseudoplastics at the highest solid concentration (45 %) and higher fines content (> 20 %). In general, yield stress appeared by increasing the slurry concentration or fines content and the flow behavior changed from dilatant over plastic to pseudoplastic when the solid content was increased.

Flocculated systems also show higher viscosities as the density of inter-particle contacts is increased and the microstructure of the suspension affected [28].

In general, a wider particle size distribution leads to lower viscosity [32, 36], mainly at higher shear rates [28] as confirmed by [37, 38] due to an enhancement of packing efficiency [28]. Chang et. al found that a bimodal size distribution reduces the viscosity of polystyrene spheres [39] which was further confirmed by other authors [40, 41]. However, the amount of very fine particles remains important. The very fine particles and the continuous phase build a pseudocontinuous phase, decreasing the effective volume fraction. A further increase raises the viscosity due to colloidal interactions overcoming the effect of volume fraction reduction [28, 32].

Regarding the particle shape, suspensions with more irregularly shaped particles are more viscous compared to suspensions containing spherical particles [28, 32, 42, 43], confirmed by the study of Graham et al. [44] and Zhang et al. [45]. As particle shape deviates from sphericity, the maximum packing fraction ϕ_m decreases and thus, viscosity increases, according to the Krieger-Dougherty equation ([Eq. 7]). Additionally, $[\eta]$ is higher for unsymmetrical particles than for spherical and cubic particles due to an increasing disruption of the flow field, additionally contributing to the viscosity increase [28]. Non-spherical particle suspensions may exhibit

shear-thickening or shear-thinning flow behavior [32]. Shear-thickening occurs when particles interact more with each other under shearing as typically observed for glass rods, and is caused by shear-induced microstructural changes [28]. Shear-thinning is typical for fibers suspensions, where fibers align in the direction of shear at higher shear rates, minimizing their interactions [32].

A decrease in viscosity is generally observed with higher temperatures [32] as interfacial properties and the volume expansion of the phases are modified. The liquid medium expands more than the solid phase, leading to a lower solid content and a decrease in viscosity at higher temperature. Additionally, the viscosity of the continuous phase is reduced. Colloidal systems also exhibit higher Brownian dispersion force with increased temperature. However, if flocculation is induced, viscosity increases due to the increased effective volume fraction ϕ_e of the flocculated systems [46].

The interparticle forces can be chemically modified by varying the pH [3, 24, 25], the addition of electrolytes [47], surface-active agents [48-50] or polymers [26, 51]. The variation in pH influences the electrostatic force, whereby the van der Waals forces remain constant for a given system. At a pH near the isoelectric point, systems show the highest viscosity. As charge-charge repulsion is minimal between neutral molecules, attractive forces dominate at the isoelectric point, resulting in a flocculated system. This pH-effect was observed by Liu et al. [3] and Chari et al. [52] in antibody solutions. Desai et al. [48] demonstrated this pH dependence of the viscosity for a pyrophyllite - water slurry.

The addition of electrolytes influences the double layer thickness and the zeta potential of the suspended particles, affecting the electric double layer repulsive forces [28] and hence the rheological properties. Two different effects could be observed with increasing electrolyte concentrations [28]. The effective volume fraction of the solid phase is reduced due to the compressed double layer [28, 29]. Furthermore, the range and magnitude of the electrostatic repulsive force is decreased [28]. Low concentrations lead to a compressed double layer and reduced, but still repulsive forces, resulting in lower viscosities. Due to the limitation of the double layer compression, only the repulsive forces are reduced at high concentrations and cannot balance the attractive forces. Aggregates are built in the secondary minimum [29], and consequently, the viscosity increases [28].

This concept was confirmed by Zhou et. al [53] observing the effect of electrolytes on metal oxide suspensions and Heller et. al [54] analyzing montmorillonite suspensions. Chari et. al [52] and Liu et. al [3] found a viscosity reduction of antibody solutions with the addition of salt.

Zaman et. al [55] showed that bidisperse silica suspensions are more fluid with increased salt concentration. When increasing salt concentrations were added to a bentonite suspension, the viscosity decreased due to the above mentioned effects, leading to a change of flow properties from shear-thinning behavior to Newtonian and shear thickening [56].

Dispersants added to the suspension may exert a multitude effects influencing the rheology and the stability of the formulation [26]. Surfactants adsorbing to the surface of suspended particles may sterically or electrosterically stabilize the suspension or induce flocculation by bridging [26, 49]. Bridging flocculation occurs when a long (usually polymeric) surfactant molecule adsorbs onto two separated particles, holding them together [57]. This is mostly observed, when the particle surface is covered with a long chain polymer at low concentrations [57, 58]. This mechanism was identified by Heath and Tadros [59], investigating the effect of polyvinylalcohol on a sodium-montmorillonite suspension. They observed a maximum viscosity at an adsorption value corresponding to a quarter of full coverage, where the system is most flocculated due to polymer bridges. Further polymer addition reduced the flocculation and hence viscosity. Kamibayashi et al. found a drastic viscosity increase of a silica suspension by the addition of a polymer inducing flocculation [60]. Depletion flocculation occurs if the dispersant do not adsorb onto the particles and the interparticular distance is less than the length of the molecules, the molecules are excluded from the gap due to an osmotic pressure gradient between the particles and the surrounding solution. An effective attractive force is produced leading particles to come closer and flocculate or phase separate [28].

Steric stabilization induced by the addition of a surfactant prevents systems from flocculating [61]. For steric stabilization, the surface should be sufficiently covered with surfactant molecules for effective particle repulsion [28]. The adsorbed surfactants influence the electrical double layer interactions due to changes in the surface charge, displacement of counterions and changes in the dielectric constant. Secondary, the van der Waals interactions are weakened [61, 62] as the steric hindrance prevents the particle to get close in the range of attractive forces. Surfactants are effective in both aqueous and non-aqueous media and at low and higher solid concentrations [61] and the electrosteric stabilization is insensitive to the presence of electrolytes [63]. However, the steric repulsion is a short-range force and only present when the stabilizer layers overlap [29]. Schott et al. [64] observed a decrease in viscosity with an increase in polyoxyethylated nonionic detergent concentration. This was attributed to the deflocculation of the clay particles by steric separation. A viscosity reduction of a coal-water mixture with the nonionic surfactant Triton-X 405 achieved by increasing the interparticle repulsion forces was also reported by Aktaş [24]. A comparable short-range repulsive force can be obtained by electrosteric effects, involving a combination of steric and

electrostatic repulsion due to ionizable groups in surfactants. Desai et al. [48] investigated the influence of a cationic, anionic and nonionic surfactant on the viscosity and zeta potential of the pyrophyllite-water slurry. In general, the addition of an anionic surfactant reduced the viscosity as repulsive forces were increased. At very low anionic surfactant concentrations, they found a slight increase of viscosity due to bridging. Higher amounts did not further affect the fluidity in accordance with constant zeta potential values. The positively charged surfactant adsorbed onto the oppositely charged surface using the polar head group, leading to a hydrophobic surface. The clay showed a higher viscosity due to an increased coagulation tendency. With further addition of surfactant, bilayers were formed and the surface became positively charged, resulting in a viscosity reduction. In presence of the nonionic surfactant the formation of an enhanced hydration layer led to an increased viscosity in presence of the nonionic surfactant. Tunç et al. [65] investigated the effect of a cationic, anionic and nonionic surfactant on the electrokinetic and rheological properties of Na-bentonite and sepiolite suspensions. They showed that the used surfactants only altered the viscosity and the rheological behavior of the sepiolite suspensions, whereby the bentonite containing systems were unaffected. The anionic surfactant bound via hydrophobic interaction on the negatively charged surface, leading to increased electrostatic repulsion forces and resulting in a decrease in viscosity. The nonionic surfactant lowered the viscosity due to a decrease in flocculation. The addition of positively charged surfactant caused an overall viscosity reduction, but flocculation was observed at 1 mM surfactant concentration.

In conclusion, a variety of parameters influences the interactions of dispersed particles with each other and with the solvent and co-solutes and thus, determines the rheological properties of a system. Physical parameters include the phase content, the particle size and particle size distribution, the particle shape, the dispersion medium and the temperature, whereby the phase content has the biggest impact on the viscosity of a system. Chemical parameters include the pH, electrolytes or surface-active agents.

1.3 Aim of the thesis

The thesis aimed to develop a highly concentrated suspension of Cilengitide for subcutaneous application. The required solid content of the most stable polymorph A 1 of Cilengitide is 30 % (w/v) to deliver a target dose of 300 mg in 1 mL. The suspended API is evaluated in terms of its physical stability including the particle size and structure, sedimentation behavior and resuspendability and with respect to its performance parameter like viscosity, syringeability and injectability. This high amount of active pharmaceutical ingredient (API) suspended in water exhibited very high viscosity and a paste-like structure which is unsuitable for parenteral application. Therefore, the effect of particle size, pH, ions and the addition of surface active agents is examined to finally enable subcutaneous application via a 25 Gauge or even smaller needle. Main aspect of the thesis is the characterization of the rheological behavior, but also the surface potential and the potential stabilizing effect of phospholipids and other surfactants. The interaction of a phospholipid with the API particles, as well as the interactions with dissolved API are investigated in more details. Excipients should be acceptable for the parenteral route and if possible, commonly used in marketed products and the formulation should be simple for clinical practice.

2 Materials

Cilengitide (polymorph A1) was provided by Merck KGaA, Darmstadt, Germany. An optional micronization step was performed at the Gesellschaft für Mikronisierung, GfM, Bremen, Germany to obtain a narrow and specified particle size between 0.9 (D(10)) and 26 μm (D(90)). 1,2-Dimyristoyl-*sn*-glycero-3-phospho-*rac*-glycerin (sodium salt) (DMPG / Lipoid PG 14:0 / 14:0), 1,2-Dipalmitoyl-*sn*-glycero-3-phospho-*rac*-glycerol (sodium salt) (DPPG / Lipoid 16:0 / 16:0), 1,2-Distearoyl-*sn*-glycero-3-phospho-*rac*-glycerin (sodium salt) (DSPG / Lipoid PG 18:0 / 18:0) as well as N-(Carbonyl-methoxypolyethylene glycol-2000)-1,2-Distearoyl-*sn*-glycero-3-phosphoethanolamine (sodium salt) (DSPE-PEG 2000 / Lipoid PE 18:0 / 18:0 – PEG 2000) were acquired from Lipoid AG, Ludwigshafen, Germany. 1,2-Didecanoyl-*sn*-glycero-3-phospho-(1'-*rac*-glycerol) (sodium salt) (DDPG / PG 10:0 / 10:0) and 1,2-Dilauroyl-*sn*-glycero-3-phospho-(1'-*rac*-glycerol) (sodium salt) (DLPG / PG 12:0 / 12:0) were bought from Avanti Polar Lipids, Inc., Alabaster, Alabama.

Tween[®] 80 (polysorbate 80) and Span[®] 80 (sorbitan monooleate) were obtained from Croda, Nettetal, Germany.

Sodium chloride, potassium chloride, calcium chloride, hydrochloric acid, sodium hydroxide and glucose were purchased from Merck KGaA, Darmstadt, Germany.

For HPLC analysis acetonitrile, methanol, acetic acid, ammoniac, isopropanol and ammonium acetate were provided by Merck KGaA, Darmstadt, Germany.

For sample preparation, aqua ad injectabilia prepared by distillation was used.

3 Methods

3.1 Analytical methods

3.1.1 Characterization of the raw material

Bulk and tapped density

For the analysis of the bulk and tapped density the Sotax TD 2 was used (Sotax Corporation, Horsham, PA). The test was performed three times with the method 1 of the Ph. Eur. 100.0 g of the raw material were weighed into a 250 mL cylinder and the unsettled apparent volume V_0 was read. The tapped volume was determined after 10, 500 and 1250 taps. The difference between V_{500} and V_{1250} was less than 2 mL and thus, the V_{1250} was used for the calculation of the tapped density (= V_f). Finally, the Hausner ratio $HR = V_0 / V_f$ was calculated by using the determined volumes.

3.1.2 Flowability

The flowability was determined according to the Ph. Eur. using the Erweka GT (Erweka, Heusenstamm, Germany). The powder was introduced in a funnel with the 15 mm outlet nozzle. The flow time of the powder on the special GT balance which determined the weight of the falling sample was measured. For the micronized material, the outlet of the powder was supported by an agitator (level 1). The analysis was done three times.

3.1.3 Angle of repose

The angle of repose was determined by using the Erweka GT (Erweka, Heusenstamm, Germany). The height of the cone of powder on a fixed base is measured and calculated with the equation [Eq. 9].

$$\tan \alpha = \frac{\text{height}}{0.5 * \text{base}} \quad \text{[Eq. 9]}$$

A triplicate determination was done.

3.1.4 Thermogravimetric analysis

Thermogravimetric analysis were performed with a DSC 1/TGA (Mettler Toledo, Delaware, USA) with a 5 K/min heating rate up to 300 °C, under nitrogen. About 25 mg were weighed in an aluminium pan.

3.1.5 Dynamic vapor sorption

The moisture uptake and desorption at different humidity conditions were measured using Dynamic Vapor Sorption (Advantage, Surface Measurement systems Ltd, London, UK). The required humidity was generated by mixing dry nitrogen and water saturated nitrogen flows, in the corresponding proportions using mass flow controllers. The humidity range chosen was from 0 to 98 % r. H. in steps of 10% r. H. at 25 °C. The instrument was run in dm/dt mode to decide when equilibrium was reached, with the dm/dt set at 0.002 %/min within 10 min. The sample weight was approximately 25 mg.

3.2 Characterization of the suspension

3.2.1 Particle size measurement

The particle size distributions of the formulations were determined with a Mastersizer 2000 (Malvern Instruments Ltd, Worcestershire, UK). A saturated API-solution with appropriate excipients of the samples was used as dispersion medium. After background alignment with the dispersion medium, a representative sample of the homogenized suspension was injected into the sample cell. The amount was dependent on the API-concentration of the sample and selected to obtain an obscuration of 10 – 15 %.

3.2.2 Microscopy

Microparticles were visualized with a light microscope (Olympus Bx 60, Olympus GmbH, Hamburg, Germany). The API-concentration was limited to 60 mg/mL by transparency, so that a dilution step with saturated API-solution was required. 20 µl of diluted suspension were dropped onto a microscope slide and covered with a slip to be examined at 50 and 100 fold magnification. Digital imaging of microparticles were taken with a ColorView camera (Olympus Soft Imaging Solutions GmbH, Münster, Germany).

3.2.3 Stereomicroscopy

The dissolution of a non-micronized crystal was observed using a stereomicroscope (Stereo Discovery V20, Carl Zeiss Microscopy GmbH, Jena, Germany). One large non-micronized particle was selected, transferred in a cuvette and suspended in water, 2 mg/mL DMPG, a non-saturated (4 mg/mL API) or a saturated API-solution (5 mg/mL API). The particle was observed over a period of 16 days maximum without agitation.

3.2.4 Scanning electron microscopy

The samples were imaged using a Leo Supra 35 (Carl Zeiss Microscopy GmbH, Jena, Germany). Acceleration voltage was kept constant at 5.0 kV. The sample was coated with Platinum.

3.2.5 Zeta potential

Measurements of the zeta potential (ζ) were performed with a Zetasizer Nano ZS (Malvern Instruments Ltd, Worcestershire, UK). The zeta potential was automatically

calculated from the electrophoretic mobility based on the Helmholtz-Smoluchowski relationship. The high-concentration cell was used to prevent sedimentation of the particles. The Cilengitide concentration was 15 mg/mL. Runs were performed in triplicate using an effective voltage of 30 mV.

3.2.6 Streaming potential

The streaming potential is analyzed by the measurement setup of the Müttek PCD-03 (BTG Müttek GmbH, Herrsching, Germany), (Figure 2). A piston sinusoidally moves up and down with a frequency of 4 Hz and forces the suspension to stream through the gap along the container wall. Particles, which interact with the container wall, are polarized according to the distortion of the diffuse double layer in the streaming liquid and an electrical potential – the so called streaming potential - is measurable between the electrodes. The obtained values are not absolute, because a calibration against a reference of known streaming potential is not possible. The measurements dependent on pH were conducted with 20 mL of a 50 mg/mL API aqueous suspension ($n = 6$). The DMPG-concentration was adapted to the formulation (0.33 mg/mL). The titration was performed with 0.1 M hydrochloric acid.

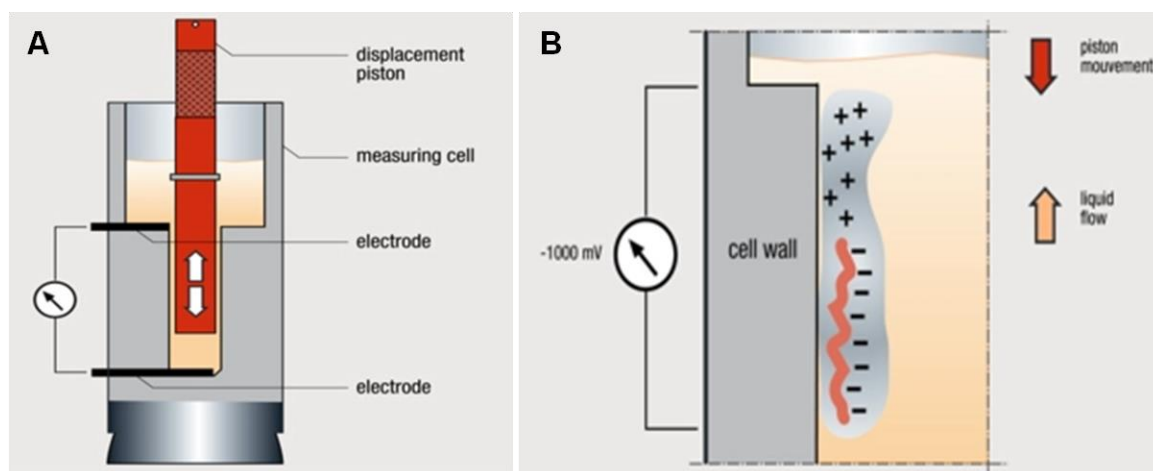


Figure 2: Measurement cell of the Müttek™ PCD-03 (A) and schematic illustration of the separation principle of counterions from adsorbed material (B).

3.2.7 Turbidimetry

The turbidimetry of DMPG dispersions ($n = 3$) containing dissolved API (4 mg/mL), and 150 mM sodium chloride where indicated, was measured with a turbidimeter (2100 AN, Hach Lange, Düsseldorf, Germany). The intensity of the light scattered by a sample under defined conditions was compared to the intensity of light scattered by a standard reference suspension

(400-600 nm, 90°). Size calibration was performed with four Gelex[®] secondary turbidity standards, covering the ranges of 0-2, 0-20, 0-200 and 200-4000 Nephelometric Turbidity Units (NTU).

3.2.8 Dynamic light scattering

Dynamic light scattering was used for the structural characterization of phospholipid and surfactant mixture dispersions. Size measurements of diluted excipient dispersions (0.05 mg/mL DMPG, 2 mg/mL polysorbate 80 / sorbitan monooleate with different ratios) as well as dispersions including 4 mg/mL API in solution were carried out with a Zetasizer Nano ZS (Malvern Instruments Ltd, Worcestershire, UK). The experiments were performed in triplicate.

3.2.9 Cryo-transmission electron microscopy

Cryo-transmission electron microscopy (Cryo-TEM) was conducted at the Albert-Ludwigs-University of Freiburg, Department of Pharmaceutical Technology with a Leo 912 OMEGA electron microscope equipped with a slow-scan CCD camera system (Proscan HSC 2 camera, Oxford Instruments, Abingdon, USA) and operating at 120 kV. A small drop (3 μ l) of the homogenized sample was placed onto a TEM-grid (400 x 100 mesh). Excess solution was removed with a filter paper and the sample was immediately shock-frozen by immersion into kryogen (90 K) and fixed in a sample holder for the transfer into the microscope. During the transfer the temperature was held below -170 °C. The samples were observed and digitalized under low exposure rate.

3.2.10 Nuclear magnetic resonance (NMR) spectroscopy

For NMR spectroscopy samples were prepared in D₂O containing 300 mg/mL Cilengitide and 2 mg/mL DMPG. The pD was adjusted to 4.6 (pH = 4.2), 5.8 (pH = 5.4) and 7.3 (pH = 6.9) with 0.1 M HCl. The samples were centrifuged (5 min, 12000 rpm) and the clear solution was transferred into a 5 mm NMR tube and equilibrated for 30 min. NMR spectra were measured at 700 MHz proton resonance frequency and 298 K measuring temperature on a Bruker Avance III 700 spectrometer (Billerica, USA) equipped with a CP-TCl probe. 2 D NOESY-NMR-spectra (Nuclear Overhauser Effect Spectroscopy) were obtained using the standard pulse sequences *noesyphprv* (80 ms mixing time).

3.2.11 Surface tension

The surface tension of a saturated API-solution and phospholipid dispersions of different concentrations was determined using a Wilhelmy plate tensiometer (Krüss Tensiometer K12, Krüss GmbH, Hamburg, Germany). The solutions were equilibrated at 20 °C for 10 min before measuring. Every 10 s a measurement step was performed automatically until the standard deviation was less than 0.02 for water and 0.1 for the samples (maximum 999 steps). The determination was performed in triplicate.

3.2.12 Sedimentation analysis

The sedimentation behavior was analyzed by imaging at different time points. The API amount was varied (15 – 300 mg/mL). Suspensions with 150 mg/mL API (highest possible concentration) were analyzed by the TurbiScan (TurbiScan LAb™, Formulation, L'Union, France) for a period of 13 h at 25 °C. In the first 30 min, the sample was scanned every minute, followed by measurements every 5 min for 2.5 h and every 15 min for 10 h.

During storage, suspensions with 300 mg/mL API were characterized by the sedimentation degree $F = V_e/V_0$ (V_e : final sediment volume, V_0 : volume at the beginning; $n = 3$). Therefore, the sediment and the total height were analyzed by using the IrfanView software.

3.2.13 Rheometry

Rheological properties of suspensions were investigated using a rotational rheometer (HAAKE Rheostress 1, Thermo Scientific, Karlsruhe, Germany). The shear stress (τ) of the samples was measured as a function of shear rate ($\dot{\gamma}$) at a constant temperature (20 °C \pm 0.1) using different plate geometries (P 20, P 35). The measurements were carried out with increasing (forward measurements) and decreasing (backward measurements) shear rates. The used shear rates depended on the method and were 50 - 1200 or 0.1 - 1000 1/s. Measurements were performed in triplicate. The yield point is calculated by using the Casson model with the following equation [Eq. 10]:

$$\sqrt{\sigma} = \sqrt{\sigma_c} + \sqrt{\eta c} * \sqrt{\dot{\gamma}} \quad \text{[Eq. 10]}$$

The calculation was performed in triplicate.

3.2.14 Resuspendability

The resuspendability of stored suspensions was investigated by subjecting the vials to a defined overhead rotation. In a tablet friabilator (TA of Erweka, Heusenstamm, Germany), vials were attached with clamps and moved with a constant rotation speed of 25 rpm (Figure 3). The time needed for resuspension until the sediment was completely detached from the bottom of the vial was measured (n = 3).



Figure 3: Measurement setup for the analysis of resuspendability.

3.2.15 Syringeability

Syringeability is defined as the ease of withdrawal of a product through a needle from the container. The set criterion was an easy withdrawal without air bubbles with a 25 Gauge needle (BD Microlance 3™, 25G x 5/8'', 0.5 mm x 16 mm, BD Becton Dickinson GmbH, Heidelberg, Germany) and a 1 mL syringe (Terumo Syringe without needle, Terumo Medical Corporation, New Jersey, USA). The time required for the withdrawal of 1 mL of the suspension was measured (n = 3).

3.2.16 Injectability

Injectability in general means the injection into the desirable site of administration. In case of the formulation development, the force required to eject the suspension through a 25 G needle into air was determined using a texture analyzer (XT plus, stable micro system Ltd, Surrey, UK) operated at a displacement speed of 5 mm/s and with 0.1 g force sensitivity. The average value of three samples was analyzed with the corresponding SMS' Exponent software and used for comparison.

3.3 Manufacturing process

3.3.1 Milling of API

The micronization of Cilengitide was performed at the Gesellschaft für Mikronisierung, GfM, Bremen, Germany, using an air jet mill (JM 100, Scheffler Metallverarbeitung, Bremen, Germany). Particle size specifications are shown in Table 1.

| D (0.1) [μm] | D (0.5) [μm] | D (0.9) [μm] |
|---------------------------|---------------------------|---------------------------|
| 0.9 - 2 | 5 - 8 | 16 - 26 |

Table 1: Particle size specification for micronization of Cilengitide.

3.3.2 Preparation of suspensions

Cilengitide suspensions were produced by suspending the adequate amount of API (w/v) in water and stirring at room temperature for 4 hours. To observe the effect of stirring on particle size as a function of time the samples were stirred at room temperature for up to 48 hours. Samples were taken at different time points and analyzed. Suspensions containing a phospholipid were prepared by dispersing the required amount of excipient (w/v) in 60 °C hot water and subsequent cooling down to room temperature while stirring. The API (w/v) was added and the suspensions were stirred for 4 hours with a magnetic stirrer. The isotonicity agents were then added. In formulations comprising surfactant mixtures, the adequate ratio (w/w) of polysorbate 80 and sorbitan monooleate were first homogenized by mixing with a magnetic stirrer before dispersing in water at 60 °C.

For the evaluation of the effect of higher energy levels the samples were subsequently treated for 30 s using the Sonotrode HD 2070 (Bandelin, Berlin, Germany) or using the Ultraturrax (T 10 basic ULTRA-TURRAX®, IKA®-Werke GmbH & Co. KG, Staufen, Germany). Short-time ball-milling was performed with the impact mill Pulverisette 23 (Fritsch, Idar-Oberstein, Germany) using zirconium spheres with a diameter of 1 mm or 5 mm. 4 mL were filled in the milling cup and milled for 10 min at 45 Hz.

3.4 Storage stability study

For the stability studies, 2 mL of the suspensions were filled into siliconized 2 mL vials (Fiolax Clear, Schott, Müllheim, Germany), stoppered (S2, Daikyo Seiko Ltd., Tokyo, Japan) and crimped under lab atmosphere. Three metal beads with a 1 mm diameter (ISOMETALL Handelsgesellschaft, Pleidelsheim, Germany) for resuspension were added in some samples

Methods

as indicated. Samples were stored at 2 – 8 °C (up to one year), 25 °C / 60 % r.H. (9 weeks) or 40 °C / 75 % r.H. (4 weeks).

The molecule exists in several polymorphic forms with the solvate S2, the tetrahydrate Ia and the anhydrous form A1 being the most stable and relevant ones [70]. Table 2 summarizes the physicochemical properties of these three polymorphic forms.

| | Form A1 | Form Ia | Form S2 |
|---|---|--|--|
| Modification | Ansolvate | Tetrahydrate | Unstoichiometric water-ethanol solvate |
| Unit cell | orthorhombic | orthorhombic | orthorhombic |
| Cell volume | 2940 Å ³ | 3396 Å ³ | 3373 Å ³ |
| Density | 1.330 g/cm ³ | 1.285 g/cm ³ | 1.319 g/cm ³ |
| Melting / degradation | 304 °C (onset) | 217 °C (onset) | 212 °C (onset) |
| Thermogravimetric Analysis weight loss | Less than 0.3 wt % up to 150 °C | 10.4 wt % up to 140 °C (step) | 13.2 wt % up to 180 °C (step) |
| Dynamic vapour sorption | - not hygroscopic acc. Ph. Eur. - no hints to hydrate conversion | - slightly hygroscopic acc. Ph. Eur. - formation of a lower hydrate | - slightly hygroscopic acc. Ph. Eur. |
| Solubility | 5 mg/mL | > 15 mg/mL → transition to A1 | > 15 mg/mL → transition to A1 |
| Stability | most stable | metastable | metastable |

Table 2: Physicochemical properties of the most relevant polymorphic forms A1, Ia and S2 of Cilengitide.

It has been demonstrated that the anhydrous form is the thermodynamically most stable form, even in presence of high relative humidity. The tetrahydrate and the water-ethanol solvate have similar cell volumes and lattice parameters and can convert to the anhydrous form during storage. The anhydrous form exhibits the lowest solubility (5 mg/mL), highest melting / degradation temperature (onset at 304 °C), lowest hygroscopicity and highest true density (1.330 g/cm³) when compared to the tetrahydrate and the solvate. Due to its highest stability and lowest solubility, the polymorph A1 was selected for the formulation development of a suspension.

This anhydrous A1 form crystallizes in the orthorhombic space group $P2_1 2_1 2_1$ with the lattice parameters $a = 9.7944 \text{ \AA}$, $b = 15.3877 \text{ \AA}$ and $c = 19.5090 \text{ \AA}$. Figure 5 shows the refined structure.

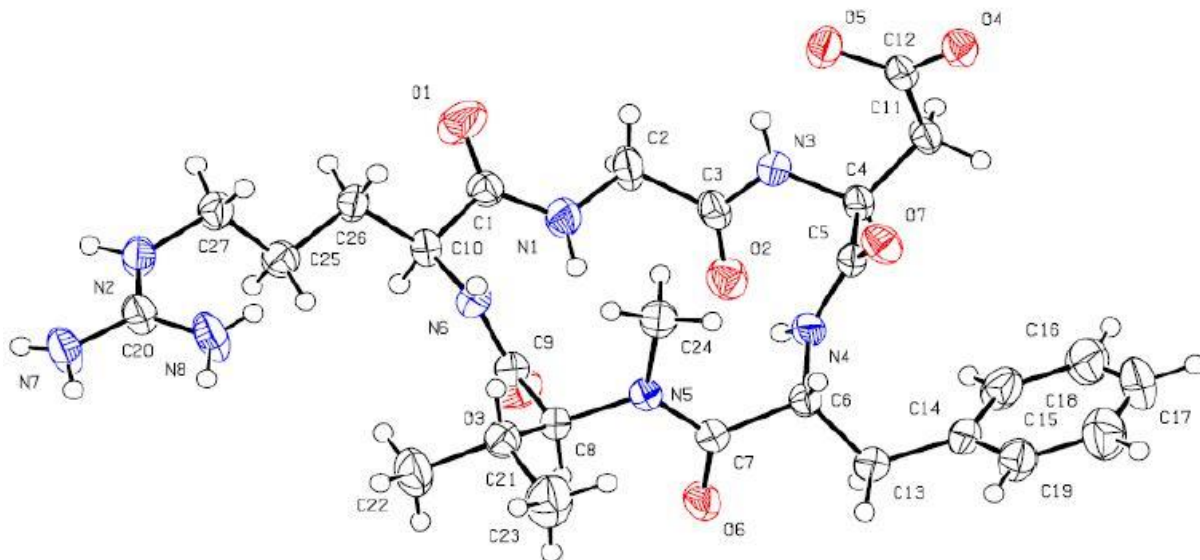


Figure 5: The refined structure of the anhydrous A1 Cilengitide crystal.

The entire unit cell consists of four molecules which are arranged as shown in Figure 6. The hydrophobic moieties of the amino acids phenylalanine and valine are outwardly orientated leading to a hydrophobic surface of the crystal.

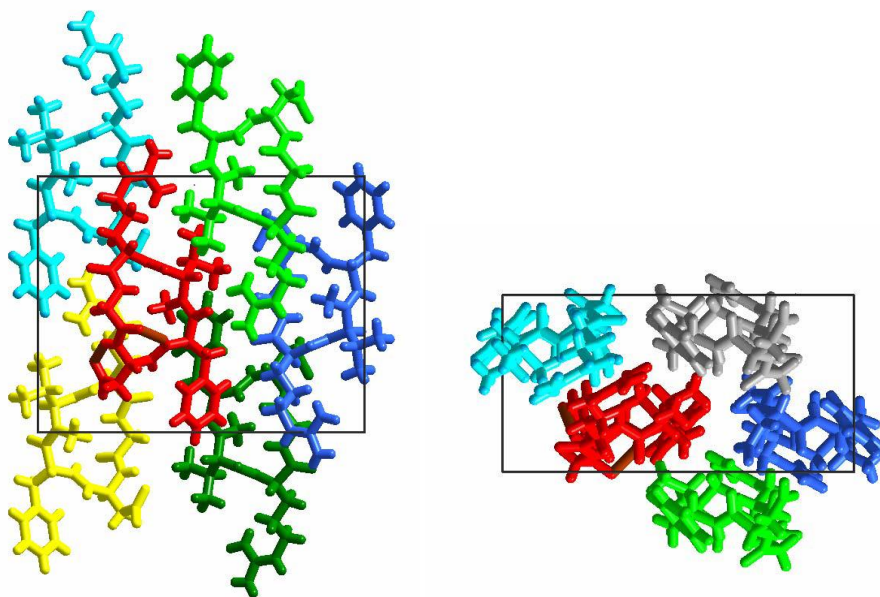


Figure 6: Arrangement of Cilengitide molecules in the unit cell of the A1 polymorph.

4.2 pKa values

In the anhydrous polymorph A1, the molecules are present in a zwitterionic form and stabilized by two intramolecular and six intermolecular hydrogen bridges (Figure 7).

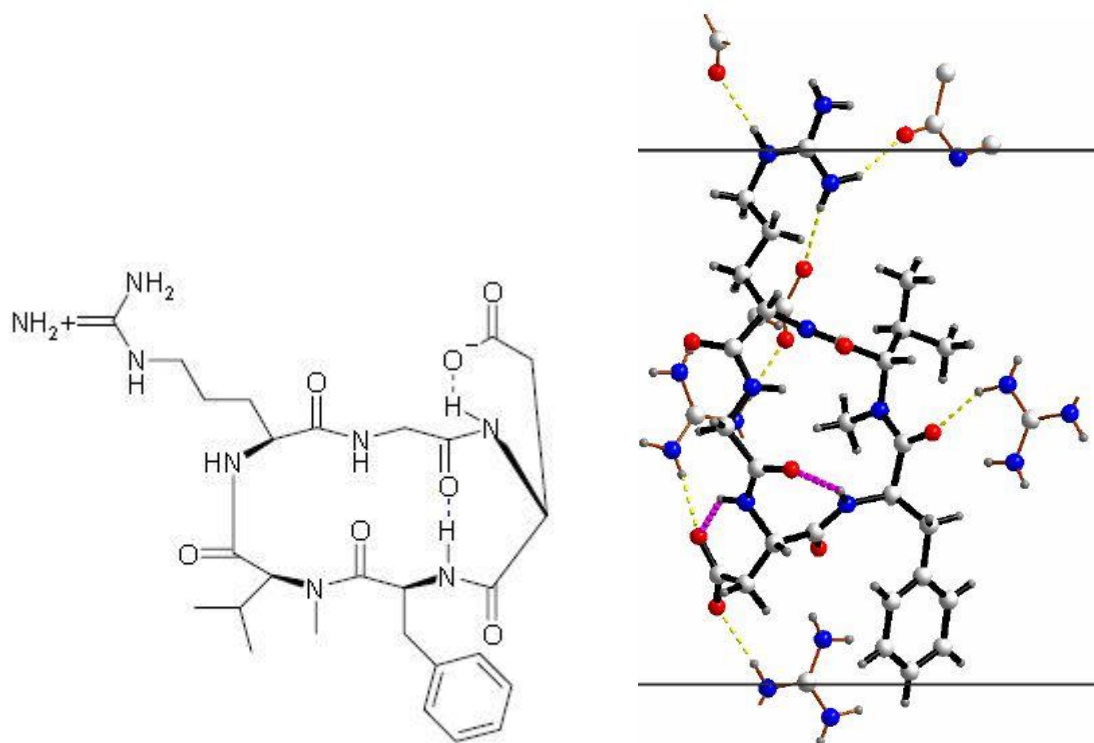


Figure 7: The anhydrous A1 form of Cilengitide with two intramolecular hydrogen bridges (left graph) and six intermolecular hydrogen bridges (right graph).

Two pKa values have been detected for dissolved Cilengitide molecules by potentiometric titration. The pKa value of 3.9 can be ascribed for the carboxylic acidic group of the aspartic acid and 11.1 for the guanidinium group of arginine. Thus, the calculated isoelectric point is around 7.5. However, measurements of the isoelectric point of suspended particles via Zeta and streaming potential showed a lower value of 5.5. As demonstrated in Figure 7 the arginine group is involved in intermolecular hydrogen bonds, and may therefore not be freely accessible for ionization.

4.3 Particle size

Generally, a narrow drug particle size distribution is preferred as particle size might have a significant impact on dissolution and absorption, mainly for compounds that show dissolution-dependent exposure [71]. A particle size reduction might improve the exposure of a compound. The effect of particle size on exposure is normally assessed in animals during preclinical evaluation [71]. Another limitation for subcutaneous application is the needle size. A maximum

particle size of one third of the inner diameter is recommended [2, 12, 14]. In case for a 25 Gauge needle this limits the particle size to 106 μm . Considering the particle shape a spherical shape is preferred as crystal with sharp edges or long, needle shapes may cause irritation or discomfort [72]. Nevertheless, there are products on the market containing needle shaped API particles as seen for Insuman[®] Basal (Sanofi Aventis) and Protaphane[®] Penfill (Novo Nordisk).

Drug substance as obtained after synthesis and purification consists of mainly needle- and rod-shaped particles (Figure 8) with a typical particle size distribution summarized in Table 3. This particle size of up to 569 μm is too large for subcutaneous applications, the drug substance typically needs to be micronized.

| Non-micronized drug substance batch | D(0.10) [μm] | D(0.50) [μm] | D(0.90) [μm] |
|--|---|---|---|
| 10/LL/017-03 | 6 | 117 | 366 |
| 11/LL/112-03 | 52 | 209 | 569 |

Table 3: Particle size distribution of the used non-micronized batches 10/LL/017-03 and 11/LL/112-03 of Cilengitide.

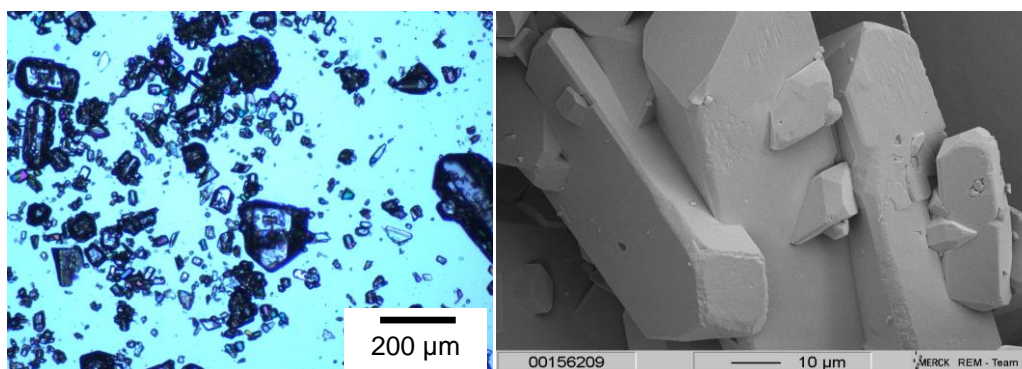


Figure 8: Microscopic image of non-micronized Cilengitide particles (batch 10/LL/017-03) suspended in water (left) and SEM graph of the raw material (right).

Micronization was performed with an air jet mill and reduced the particle size to the desired size of 1.2 - 1.3 μm for D(0.10), 6 - 7 μm for D(0.50) and 15 - 18 μm for D(0.90). Nevertheless, a few large needles of up to a length of 100 μm are still present. (Figure 9).

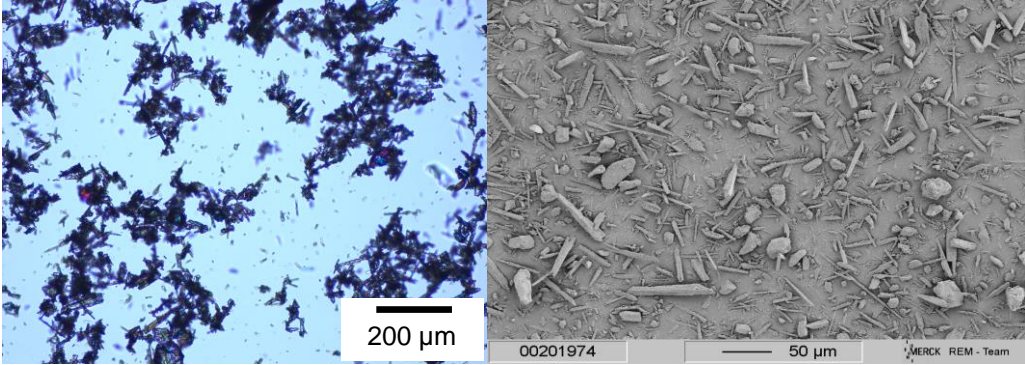


Figure 9: Microscopic image of micronized Cilengitide particles (batch 10/LL/017-03) suspended in water (left) and SEM graph of the raw material (right).

4.4 Flow properties of raw material

The addition of the solid material from the bulk storage container to the liquid phase is an essential process step during suspension manufacturing. Therefore, raw materials with acceptable flow properties are preferred to avoid difficulties, e.g. powder loss, powder sticking to the wall and intersection of the container. The bulk flow properties of non-micronized and micronized drug substance were characterized using the methods for powder characterization of the Ph. Eur. (Table 4). The non-micronized material offers “good” flow character considering the Hausner ratio (Ph. Eur.). The observed angle of repose also confirms “fair” flowability without any aid (Ph. Eur.). However, the flow properties of the micronized drug are inferior. The flowability is “very, very poor” (Ph. Eur.) according to the determined Hausner ratio. The determination of the angle of repose and the flowability through an orifice is not feasible even with the help of the agitator.

| Parameter | Non-micronized drug substance | Micronized drug substance |
|-------------------------|-------------------------------|---------------------------|
| Bulk density | 0.61 ± 0.02 g/mL | 0.24 ± 0.01 g/mL |
| Tapped density | 0.67 ± 0.01 g/mL | 0.42 ± 0.00 g/mL |
| Hausner ratio | 1.11 ± 0.01 | 1.62 ± 0.01 |
| Angle of repose | 37.3 ± 0.4 ° | - |
| Flow through an orifice | 3.65 ± 0.17 s | - |

Table 4: Characteristic flowability parameter for non-micronized and micronized drug substance.

In conclusion, the non-micronized raw material flows good in contrast to the micronized powder. However, the particle size of the non-micronized material is too large for an application via a 25 Gauge needle.

4.5 Conclusion

The anhydrous polymorph A1 of Cilengitide is the most stable form and thus, suitable for the development of a suspension formulation. The solubility of the compound is approximately 5 mg/mL API in water and the isoelectric point at pH 5.5. The surface of the API particle is hydrophobic due to the outwardly orientated phenylalanine and valine group. The non-micronized material contains needle- and rod-shaped particles offering good flowability contrary to the micronized powder. However, the particle size of the non-micronized API is too large for an application with a 25 Gauge needle.

5 Characterization of aqueous Cilengitide suspension

5.1 Parameters influencing the particle size

Generally, the particle size of a preclinical parenteral suspension formulation may impact drug absorption [71]. For poor soluble compounds a narrow particle size distribution is preferred with particles below 10 μm [71]. However, for drugs with a solubility higher than 1 mg/mL, as in the case of Cilengitide, particle size has low impact on dissolution or bioavailability, respectively [71]. In this case the size is mainly limited by the administration via a needle. A maximum particle size of one third of the needle diameter is recommended as larger particles can block the needle during injection [2, 12, 14]. For a 25 Gauge needle with an inner diameter of 0.318 mm the maximum particle size should be below 100 μm . Furthermore, a narrow particle size distribution is preferred with respect to storage stability. For Cilengitide particles, a particle size distribution of 2 D(0.10), 6 D(0.50), 24 D(0.90) and 35 D(0.95) μm is specified for the micronized raw material. In comparison, an injectable depot formulation comprising loperidone crystals shows a drug particle size of 15 to 70 μm [73]. The anti-inflammatory suspension Volon[®] for intramuscular application exhibits a Triamcinolonacetone D(0.50) value of 10 μm and D(0.90) value of 47 μm , respectively [74]. The insulin product Insuman[®] Basal contains drug particles of 2.5 μm (D(0.10)), 10 μm (D(0.50)) and 26 μm (D(0.90)) and Protaphane[®] Penfill particles of 1.4 μm ((D(0.10)), 5.1 μm (D(0.50)), 13 μm D(0.90)).

In the following part the use of non-micronized versus micronized material is evaluated with respect to the particle size. The non-micronized material offers the advantage of better flow properties and thus, easier handling for production. The influence of stirring time and mode in aqueous medium upon dispersing is analyzed as well as the effect of Cilengitide concentration. The storage stability is determined at different conditions over a period of one year. The particle size is measured by laser diffraction. Furthermore, microscopy complements the data and enables the characterization of the agglomeration behavior and the inner structure of the suspension.

5.1.1 Stirring time and raw material particle size

The non-micronized raw material with particles up to 700 μm has better flow properties and shows a lower tendency for electrostatic charges. Therefore, it has been evaluated if the particle size can be reduced to the recommended maximum size of approximately 100 μm by stirring during the suspension manufacture. The influence of stirring is also analyzed for suspensions with micronized material.

In suspensions containing non-micronized raw material the particle size decreases during stirring up to 48 hours as a function of time (Figure 10). After 48 hours of stirring, a particle size distribution similar to micronized raw material is detected. The D(0.95) value is reduced to 28.5 μm after 48 hours of stirring.

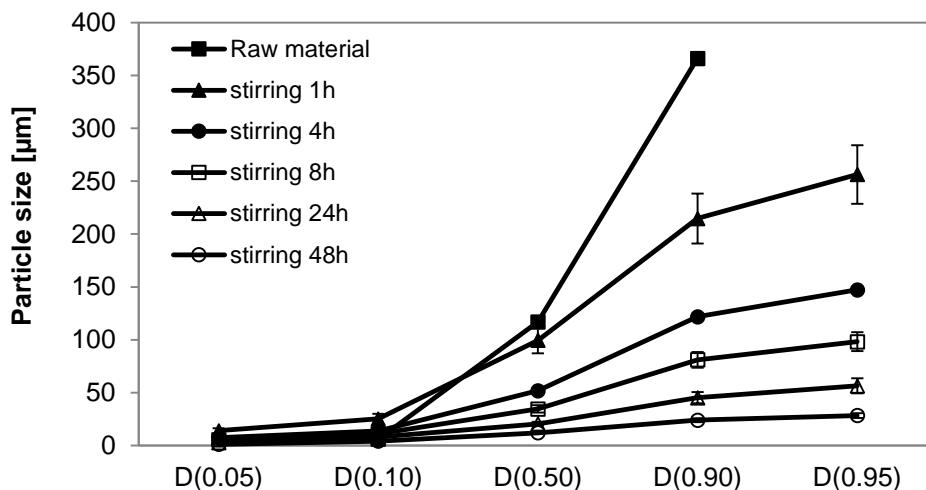


Figure 10: Particle size distribution of suspensions with 60 mg/mL non-micronized material in Wfl as a function of stirring time. Error bars represent standard deviations from triplicate measurements.

The particle size of suspensions with micronized raw material is less affected by the stirring process. Only the largest particles are reduced in size within the first four hours as indicated by the decrease of the D(0.95) by around 10 μm with a D(0.95) of 35.5 μm after 24 hours.

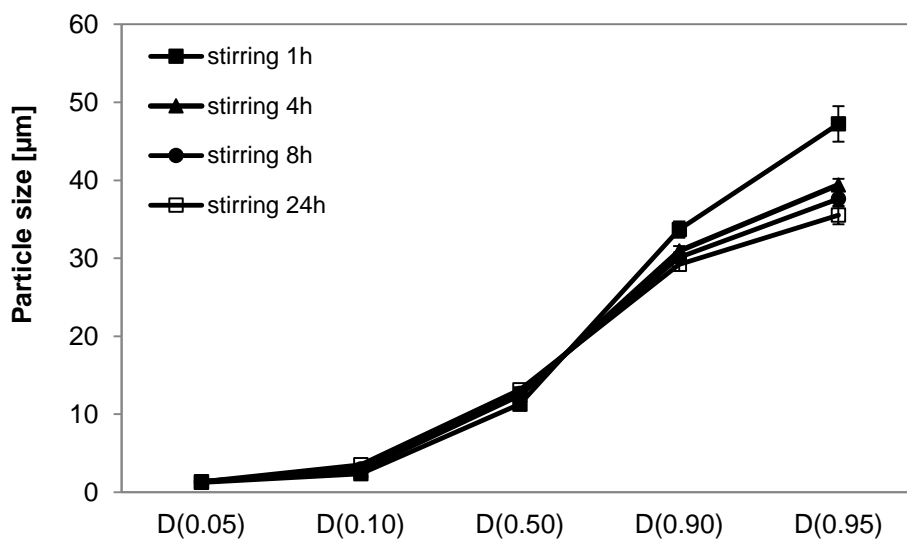


Figure 11: Particle size distribution of suspensions with 60 mg/mL micronized material in Wfl as a function of stirring time. Error bars represent standard deviations from triplicate measurements.

It is not possible to determine the particle size immediately after addition to water due to an inhomogeneous distribution. Comparing the particle size of the micronized raw material with an aqueous suspension after one hour of stirring (Table 5) indicates slightly larger sizes. This is due to still present agglomerates.

| | D(0.05) [μm] | D(0.10) [μm] | D(0.50) [μm] | D(0.90) [μm] | D(0.95) [μm] |
|-----------------------|------------------------------|------------------------------|------------------------------|------------------------------|------------------------------|
| Raw material | - | 2 | 6 | 24 | 35 |
| After 1 hour stirring | 1.3 | 2.4 | 11.3 | 33.7 | 47.2 |

Table 5: Comparison of particle size distribution of micronized raw material and of suspensions (60 mg/mL) after 1 hour of stirring.

The micrographs of suspensions prepared with micronized drug (Figure 12) indicate structural changes during stirring. Starting with inhomogeneously distributed particles and lumps the dispersion becomes more homogeneous with increasing stirring time. After four hours the smaller particles are attached to the larger ones and a continuous, scaffold-like structure is formed. A homogeneous distribution of lower (30 mg/mL) and higher (90 mg/mL) concentrated suspensions is also seen after 4 hours of stirring by microscopy.

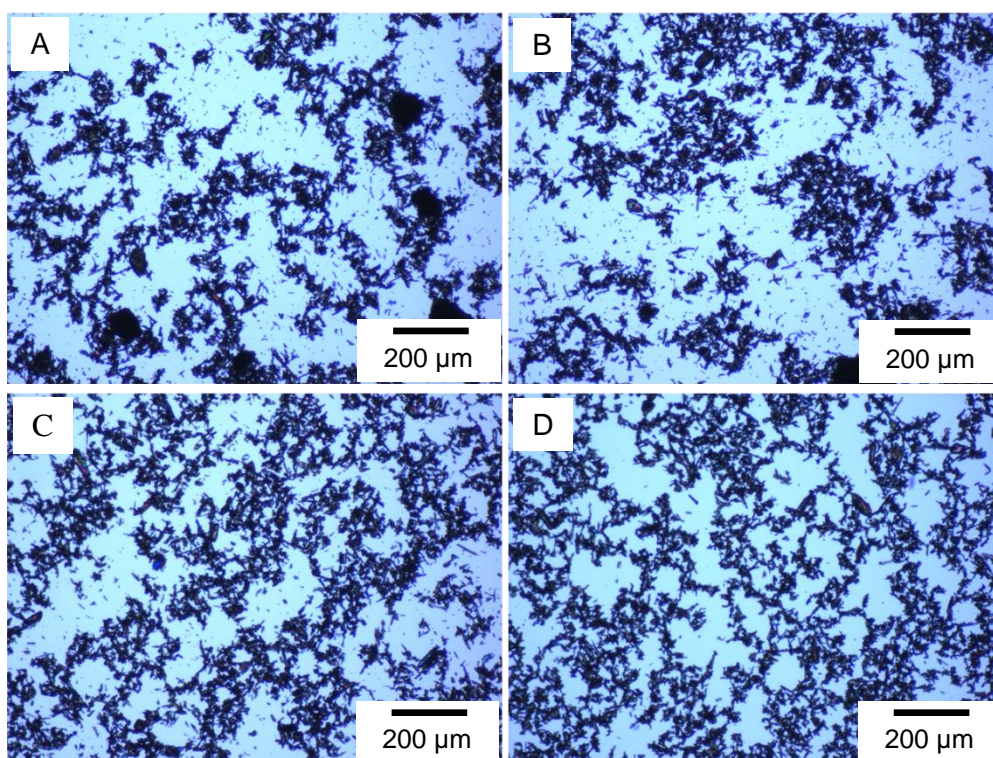


Figure 12: Micronized particles suspended in Wfl (60 mg/mL) at different stirring times (A) 0.5 min, (B) 5 min, (C) 20 min, (D) 4 h.

This continuous inner structure is also observed for the non-micronized material after 24 hours of stirring (Figure 13 D), corresponding to the similar particle sizes measured by laser diffraction. The non-micronized particles are initially separated before they become reduced in size and interact with each other to form this continuous structure.

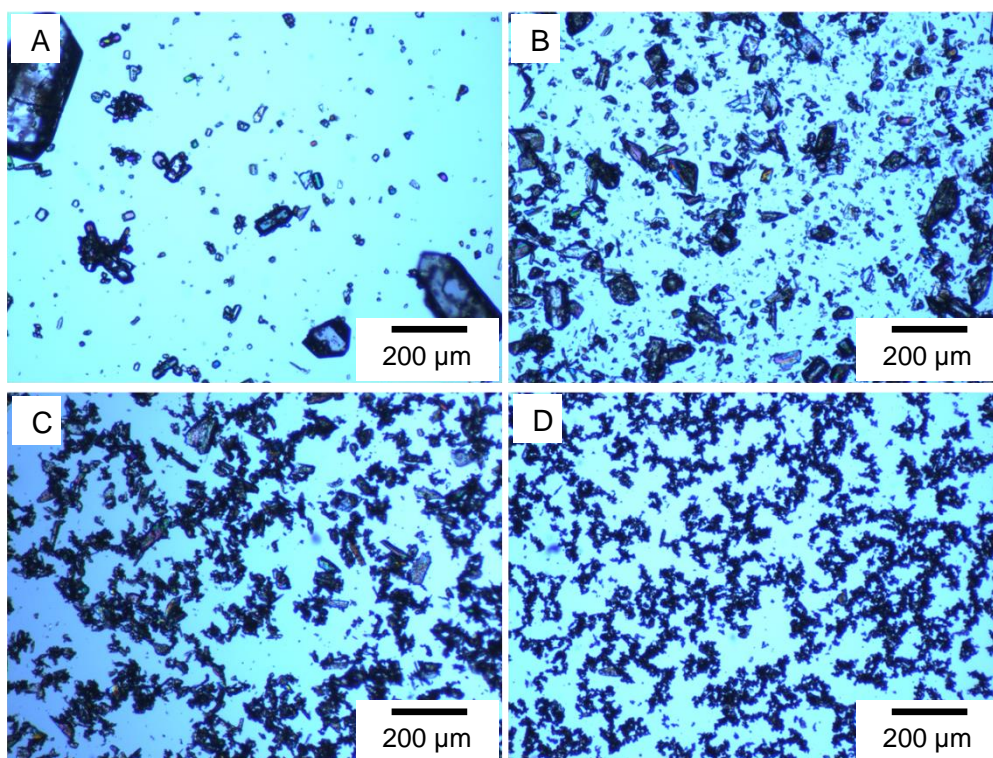


Figure 13: Non-micronized particles (60 mg/mL) suspended in Wfl after different stirring times (A) 0.5 min, (B) 30 min, (C) 4 h, (D) 24 h.

There are two possible mechanisms which can lead to the notable particle size decrease of the non-micronized suspension during stirring. On the one hand, particle dissolution can cause the size decrease. On the other hand, the particles might be comminuted by the mechanical energy imparted by the magnetic stirrer. If solution processes were mainly responsible for the observed reduction, the smallest particles would disappear resulting in an increase of the particle size distribution and the particles would not further decrease after the saturation level of the dispersion medium is reached. Furthermore, less particle size changes are expected for a higher concentrated suspension as a lower relative percentage is dissolved. On the other hand, particles suspended in a saturated solution would be comminuted to a comparable extend as seen in unsaturated medium if the decrease is mainly induced by mechanical energy.

To gain further insight on the mechanism of particle size decrease, the solubility of Cilengitide in water is determined as a function of time. Furthermore, non-micronized material (60 mg/mL) is suspended in a saturated API solution and stirred for 48 hours. The particle size distribution of a 300 mg/mL suspension over time is determined. Additionally, individual large particles were dispersed in different media Wfl, a non-saturated and saturated Cilengitide solution in a flat cuvette and observed by stereomicroscopy without stirring. The final saturation solubility of Cilengitide in water is already reached after 5 min indicating that size reduction is mechanically induced (Figure 14).

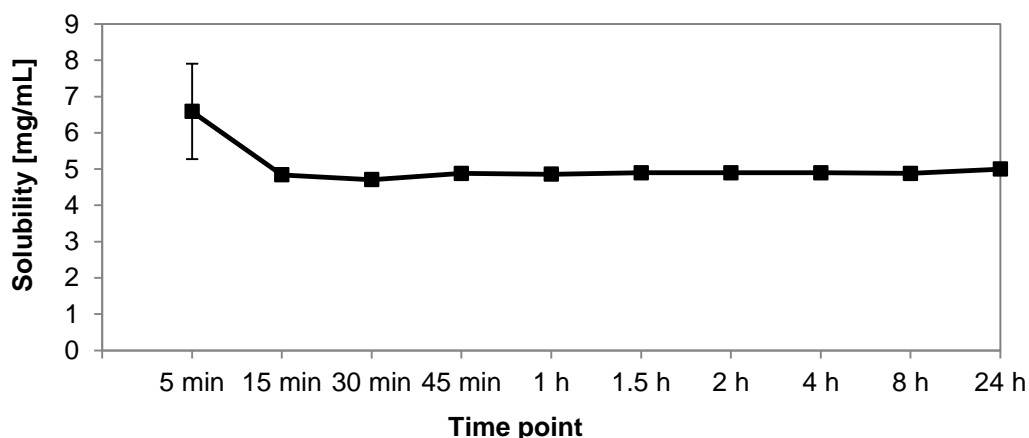


Figure 14: Solubility of Cilengitide in Wfl as a function of time. Error bars represent standard deviations from triplicate measurements.

Figure 15 A shows the particle size of 60 mg/mL API suspended in a saturated API solution as a function of stirring time. A similar particle size reduction is observed as for API particles suspended in water (Figure 10) demonstrating that mechanical size reduction prevails. For higher concentrated suspension, the absolute sizes cannot be compared as different raw material batches were used. Nevertheless, a similar trend is observed for particle size reduction of the concentrated suspension as for the lower concentrated (Figure 15 B).

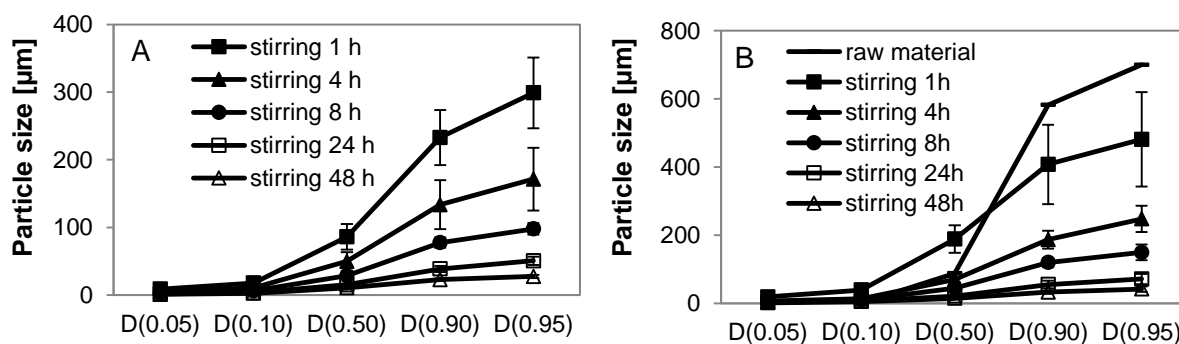


Figure 15: Particle size distribution of suspensions with 60 mg/mL non-micronized material in saturated API-solution (A) and of suspensions with 300 mg/mL non-micronized material in Wfl (B) as a function of stirring time. Error bars represent standard deviations from triplicate measurements.

A particle size distribution similar to the micronized powder is reached after 48 hours of stirring of 300 mg/mL as already seen for the 60 mg/mL suspensions in water (Table 6). When a non-micronized single particle is suspended in a non-stirred saturated API-solution the particle size and appearance do not change after 16 days (Figure 16).

| | 60 mg/mL API | 300 mg/mL API | Micronized raw material |
|---|------------------|------------------|-------------------------|
| D(0.05) [μm] | 1.23 \pm 0.07 | 1.59 \pm 0.08 | 1.35 |
| D(0.10) [μm] | 4.28 \pm 0.23 | 5.19 \pm 0.18 | 1.81 |
| D(0.50) [μm] | 12.05 \pm 0.69 | 14.60 \pm 0.86 | 6.14 |
| D(0.90) [μm] | 23.99 \pm 1.74 | 32.93 \pm 4.85 | 24.16 |
| D(0.95) [μm] | 28.48 \pm 2.23 | 41.55 \pm 7.77 | 35.19 |

Table 6: Particle size distribution of suspension with 60 and 300 mg/mL micronized API stirred for 48 hours and the micronized raw material powder. Standard deviations are from triplicate measurements.

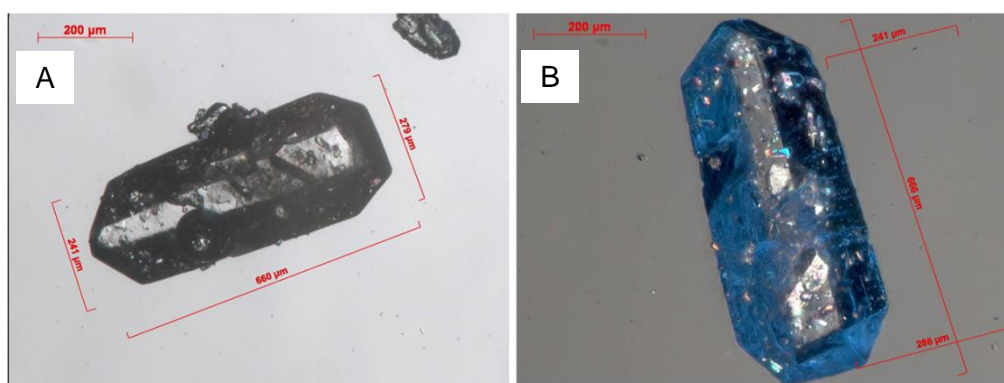


Figure 16: Non-micronized Cilengitide crystal in saturated API-solution at the beginning (A) and after 16 days (B).

In conclusion, all of the above mentioned results indicate that the dissolution process is not responsible for the substantial size reduction of Cilengitide particles upon dispersion in aqueous media. Instead the particles are reduced by the mechanical input of stirring. The particle size distribution of non-micronized material in suspension becomes similar to the size distribution of micronized drug substance raw material as well as of micronized substance in suspension. It can be speculated that the non-micronized particles are fragmented at predetermined breaking points either during stirring in suspension or jet-milling of the drug material. Stereomicrographs of a particle suspended in water show the formation of such predetermined breaking points during the solution (Figure 17).

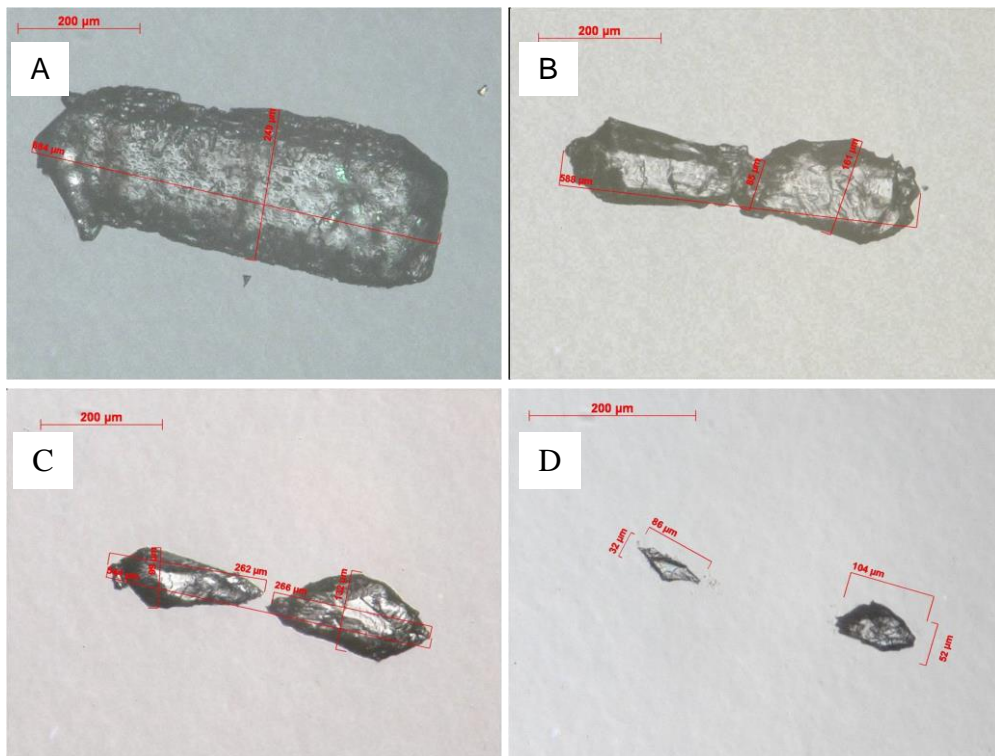


Figure 17: Non-micronized Cilengitide crystal in Wfl at the beginning (A), after 3.5 h (B), 5.25 h (C) and 8 h (D) of incubation.

A similar process occurs when a particle was suspended in a non-saturated API-solution. The particle dissolves and further, predetermined breaking points appear (Figure 18).

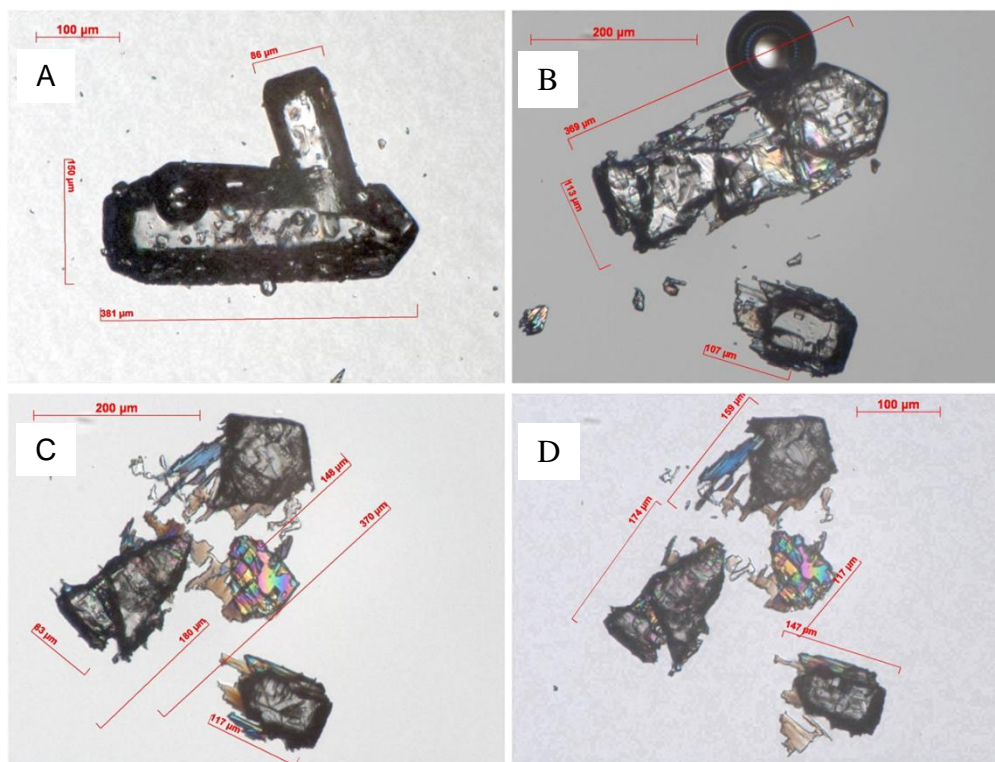


Figure 18: Non-micronized Cilengitide crystal in API-solution (4 mg/mL) at the beginning (A), after 3 d of storage (B), 8 d (C) and 12 d (D) of incubation.

5.1.2 Application of comminuting methods with higher energy levels

Additionally it was to be analyzed whether the application of high energy comminution leads to smaller particle sizes. For this purpose, suspensions containing micronized material that were stirred for 24 hours were additionally treated by either ultrasound (Sonotrode) or Ultraturrax for 30 s. Both treatment methods result in only a minimal decrease in particle size (Table 7).

| | Micronized, 24 h stirring | Micronized, ultrasound (30 s) | Micronized, Ultraturrax (30 s) |
|--------------|------------------------------|----------------------------------|-----------------------------------|
| D(0.05) [μm] | 1.35 | 1.23 | 1.24 |
| D(0.10) [μm] | 2.81 | 2.75 | 2.81 |
| D(0.50) [μm] | 13.16 | 10.91 | 10.90 |
| D(0.90) [μm] | 29.21 | 26.85 | 26.66 |
| D(0.95) [μm] | 35.54 | 34.67 | 34.22 |

Table 7: Particle size distribution of suspensions with 300 mg/mL micronized API after 24 h stirring and with ultrasound or Ultraturrax application.

As an alternative, suspensions with micronized raw material were ball milled. Only a slight but significant size reduction, especially of the larger particles (D(0.90) and D(0.95)) by milling with 1 mm for 10 min, is resulted (Figure 19). Smaller particles (D(0.10)) are not reduced in size. Milling with the larger balls does not affect the particle size distribution. Longer milling times could not be investigated as the suspension foams substantially.

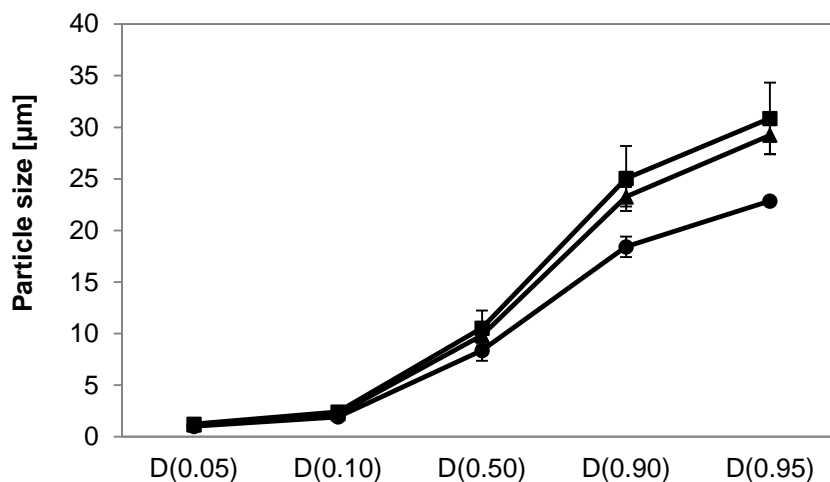


Figure 19: Particle size distribution of suspension with 300 mg/mL micronized API without milling (■) and after milling with 5 mm balls for 10 min (▲) or with 1 mm balls for 10 min (●), respectively. Error bars represent standard deviations from triplicate measurements.

5.1.3 Influence of drug substance concentration in suspension

The above mentioned results have shown that stirring with a magnetic stirrer strongly affects the particle size of suspensions with non-micronized raw material. However, the particle size of suspensions containing micronized API is hardly influenced by stirring and only slightly by ball-milling. In this part the influence of concentration on the final particle size of suspensions containing 30, 100 and 300 mg/mL micronized API after 4 h of stirring is analyzed. The results demonstrate that the size distribution of the lower concentrated suspension (30 and 100 mg/mL) is similar (Figure 20). The suspension containing 300 mg/mL API yields smaller particle sizes for the D(0.90) and D(0.95). The largest particles comminution may be more effective for higher concentration due to higher internal friction.

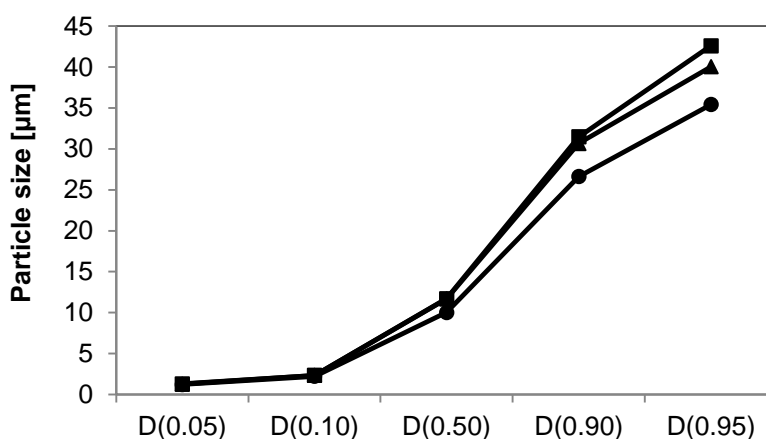


Figure 20: Particle size distribution of suspension with 30 mg/mL (■), 100 mg/mL (▲) and 300 mg/mL (●) micronized API.

5.2 Particle size stability upon storage

Particle size stability during storage is a crucial parameter for suspension development. As already mentioned before, large particles can compromise the injectability, physiological compatibility and dissolution kinetics. A wide particle size distribution can promote a particle size increase during storage [75] with a particle growth of the larger particles at the expense of smaller ones (Ostwald ripening). The temperature [75] and the volume fraction [76] can affect the ripening rate.

The stability of several formulations is analyzed at 2 – 8 °C over a time period of one year. The influence of the raw material (non-micronized stirred for 48 h in suspension versus micronized stirred for 4 h in suspension) besides the concentration is determined. The suspensions

containing 300 mg/mL micronized raw material are additionally stored at accelerated conditions for 4 weeks at 40 °C / 75 % r.H. or 9 weeks at 25 °C / 60 % r.H. Finally, the effect of beads on particle size during storage is analyzed for suspensions containing 300 mg/mL micronized Cilengitide. Three metal beads (2 mm diameter) per vial are added to facilitate the resuspension of the highly concentrated suspension.

The analyses over one year show good particle size stability for suspensions containing 300 mg/mL non-micronized API (Figure 21). The smallest particles (D(0.05)) grow about 0.2 µm (within one year) which means a percentage increase of 12 %. The D(0.95) value rises by about 4 µm corresponding to a percentage increase of 10 %.

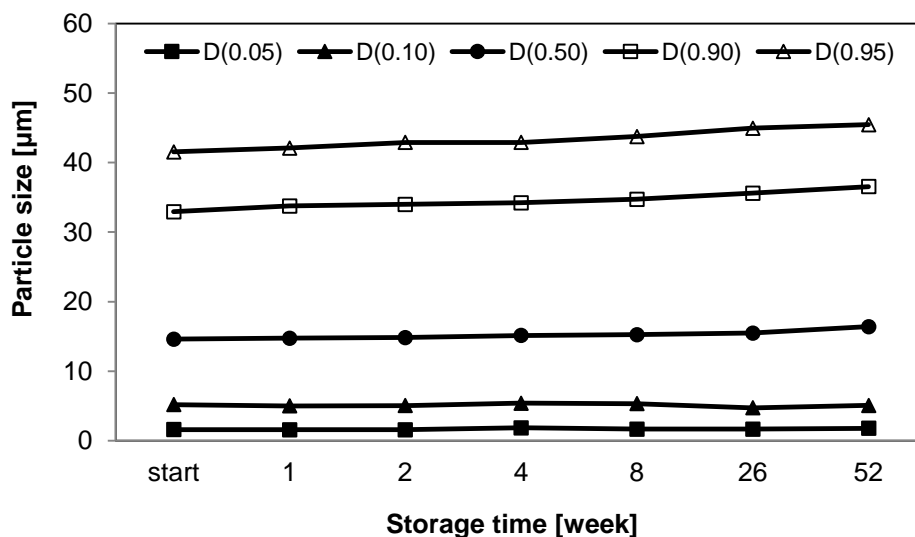


Figure 21: Particle size stability of suspensions containing 300 mg/mL non-micronized API stored at 2 - 8 °C over one year.

Compared to these results the change in particle size distribution of samples containing micronized raw material is more pronounced. The increase of the D(0.05) value is about 0.2 µm (16 %), the D(0.95) value rises by about 11 µm (31 %) within one year. However, the increase is still acceptable as neither the syringeability nor the injectability are compromised.

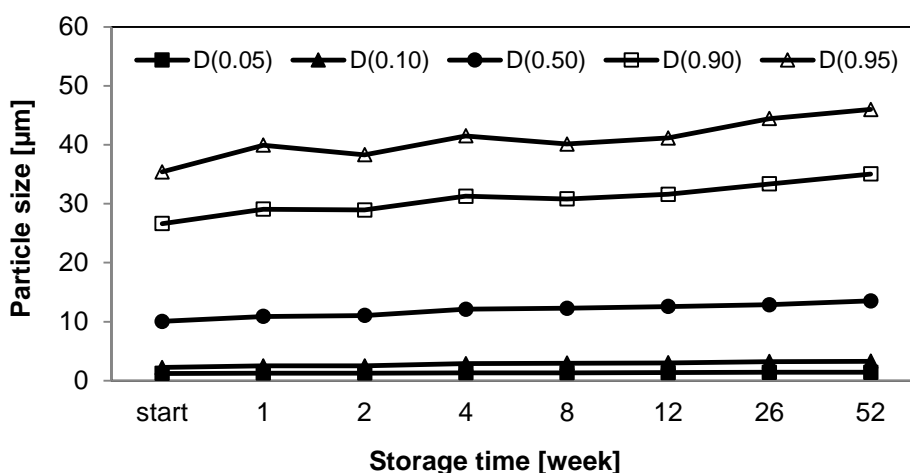


Figure 22: Particle size stability of suspensions containing 300 mg/mL micronized API stored at 2 - 8 °C over one year.

Even under accelerated storage conditions the particle size does not increase significantly (Table 8). The smallest particles (D(0.05)) do not change in size, the D(0.95) value is about 2 µm (5 %) higher at 40 °C / 75 % r.H. than the value after suspension storage at 2 – 8 °C for 4 weeks. Considering the storage at 25 °C / 60 % r.H. for 9 weeks the D(0.05) value rises by about 0.14 µm (10 %). The larger particles grow about 6 µm more which corresponds to a percentage increase of 16 %.

| | D(0.05) [µm] | D(0.10) [µm] | D(0.50) [µm] | D(0.90) [µm] | D(0.95) [µm] |
|------------------------------|--------------|--------------|--------------|--------------|--------------|
| Start | 1.33 ± 0.02 | 2.84 ± 0.14 | 12.47 ± 0.35 | 30.95 ± 0.63 | 39.42 ± 0.79 |
| 4 weeks, 2 – 8 °C | 1.46 ± 0.04 | 3.91 ± 0.11 | 14.19 ± 0.19 | 31.50 ± 0.57 | 38.37 ± 0.79 |
| 4 weeks, 40 °C / 75% r.H. | 1.40 ± 0.02 | 3.93 ± 0.12 | 14.41 ± 0.24 | 32.68 ± 0.12 | 40.16 ± 0.16 |
| 8 weeks, 2 – 8 °C | 1.42 ± 0.14 | 3.65 ± 0.40 | 12.74 ± 0.42 | 29.34 ± 2.18 | 36.93 ± 2.87 |
| 9 weeks, 25 °C / 60% r.H. | 1.56 ± 0.11 | 4.23 ± 0.18 | 14.84 ± 0.33 | 34.07 ± 0.90 | 42.42 ± 1.96 |

Table 8: Particle size distribution of suspension with 300 mg/mL micronized API stored at accelerated conditions.

Studying the influence of the concentration on the storage stability it can be noted that the D(0.95) values increase is similar with 9 µm increase for the 30 mg/mL suspension and 11 µm for the 100 and 300 mg/mL suspension (Figure 23).

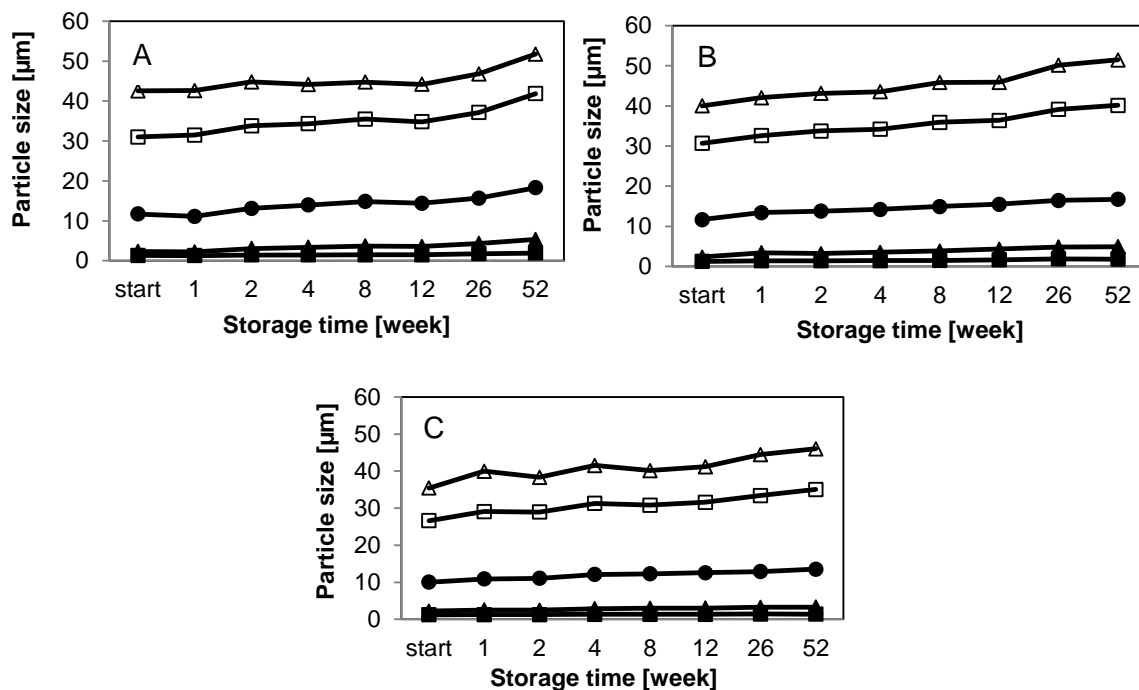


Figure 23: Particle size stability of suspensions containing 30 mg/mL (A), 100 mg/mL (B) and 300 mg/mL (C) micronized API stored at 2 – 8 °C over 1 year. D(0.05) (■), D(0.10) (▲), D(0.50) (●), D(0.90) (□) and D(0.95) (△) are shown.

For the evaluation of the influence of metal beads on the particle size, D(0.10), D(0.50), D(0.90) and D(0.95) values are shown in Figure 24. The beads do not influence the particle size distribution over the storage period.

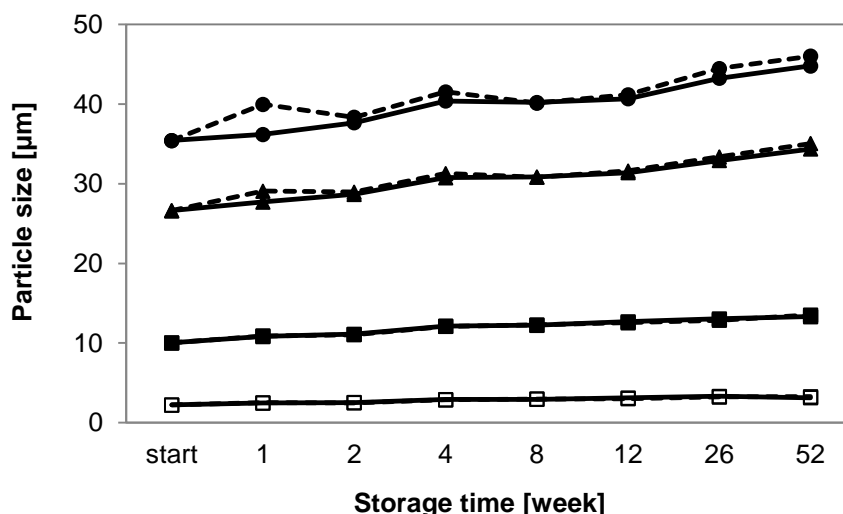


Figure 24: Particle size stability of suspensions with 300 mg/mL micronized API stored at 2 – 8 °C over 1 year with beads (—) and without beads (- -). D(0.10) (□), D(0.50) (■), D(0.90) (▲) and D(0.95) (●) are shown.

In summary, it can be noted that the suspended particles offer good size stability when stored over a period of one year or at accelerated conditions independent of the used raw material

and concentration. The final particle size of suspensions prepared with non-micronized raw material remarkably depends on the stirring time. Although a similar particle size compared to micronized raw material can be reached with the non-micronized material, long stirring times (48 hours) are needed which is not acceptable for a sterile manufacturing process. Thus, it was decided to use micronized material for future experiments although the material exhibit drawbacks with regard to flow properties. A stirring time of 4 hours of stirring is defined to obtain a homogeneous suspension with a continuous, scaffold-like structure using the micronized material. It should also be noted that the size of the micronized particles is less affected by application of ultrasound, Ultraturrax or additional short-time ball-milling.

5.3 Sedimentation behavior

The sedimentation rate of the suspended particles should be low to avoid resuspension difficulties during storage and to ensure the withdrawal of adequate doses after resuspension. Generally, there are two types of sedimentation behavior. On the one hand, agglomerated particles settle as flocs building a loosely packed sediment with a minimized caking risk. On the other hand, deflocculated particles settle as separated particles. The sedimentation rate of the latter is usually slower but a densely packed sediment is built which can cause difficulties in redispersing (caking). From microscopic pictures it is known that the suspended micronized Cilengitide particles interact with each other building a scaffold-like structure. Thus, it is expected that the particles settle as flocs. However, the sediment can be compressed during storage by the particles' own weight due to the large particle size, so the caking potential has to be analyzed.

The sedimentation rate is analyzed by measuring the transmission and backscattering of a near infrared diode as a function of the sample height. Thus, a fingerprint is obtained at given time points for a more detailed analysis. Measurement of the sedimentation rate was limited to a maximum API-concentration of 150 mg/mL. Photographs are taken at different time points using API concentrations of 15, 30 and 100 mg/mL. The caking potential of 300 mg/mL suspensions is determined by the evaluation of the sedimentation degree F . F is defined by the ratio of the sediment volume V_e after 52 weeks of storage to the sediment volume V_0 at the beginning (equal to overall volume for the 300 mg/mL suspension).

5.3.1 Sedimentation rate analyzed by transmission and backscattering detection

Figure 25 shows the results of the transmission and backscattering measurements of suspensions with 150 mg/mL API during 13 hours. The curves demonstrate the profiles at different time points. The transmission of the sample at 37.7 – 39.5 mm sample height increases up to 30 % after 13 hours (red curve) which indicates that the particles settle and a small more translucent supernatant is detected. The calculated sedimentation rate is 1.7 $\mu\text{m}/\text{min}$. The transmission increase goes ahead with a backscattering decrease at the mentioned sample height. However, a marginal increase of the backscattering is observed at the lower and middle zone of the cuvette, indicating that the sediment is becoming more concentrated. No distinct change at the vial bottom can be identified.

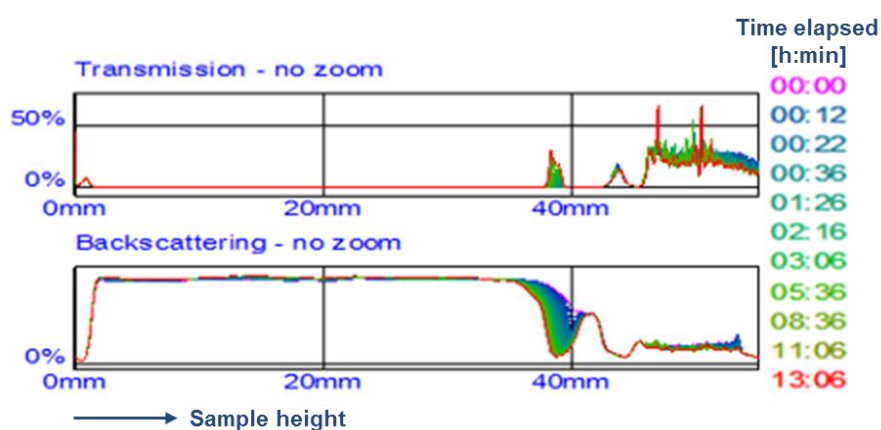


Figure 25: Transmission and backscattering profile of suspension with 150 mg/mL micronized API dependent on time over the sample height.

As discussed in chapter 5.4 an acceptable time for drawing out the suspension is 20 s. Within this time the particles should not show sedimentation. Considering the calculated sedimentation rate, the travelling distance would be 0.57 μm within 20 s. It can be concluded that the low settling rate does not compromise an adequate dosing even of the half concentrated 150 mg/mL suspension. The sedimentation rate of the double concentrated suspension is expected to be lower due to the increased steric hindrance of the particles. This is confirmed by the evaluation of the sedimentation degree during storage as discussed in the following.

5.3.2 Macroscopic sedimentation behavior

Deflocculated suspensions are characterized by separated particles which settle independent from each other. The larger particles sediment faster than the smaller, resulting in a turbid

supernatant until all particles are sedimented. However, flocculated particles settle as flocs with a clear supernatant as the smaller particles are attached to the larger. A settling particle front is visible for this type.

For the evaluation of the sedimentation behavior suspensions with 15, 30, 100 and 300 mg/mL are observed. The lower concentrations enable a better analysis. The samples are analyzed over a period of 24 hours, significant time points of each concentration are presented.

In 15 mg/mL suspensions the particles are homogeneously distributed at the beginning (Figure 26, “start”). Already after 1 minute, most particles have sedimented and only the smallest particles stay suspended. After 20 minutes, the supernatant is almost clear. The sedimentation is too fast to gain information about the sedimentation behavior (flocculated / separated particles). Nevertheless, a magnification of the suspended particles suggests that they are flocculated.

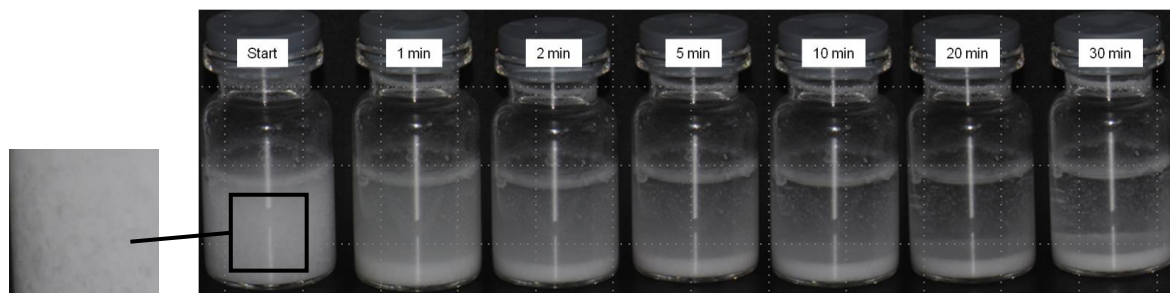


Figure 26: Sedimentation behavior of suspension with 15 mg/mL API at different time points.

In suspensions with 30 mg/mL the supernatant quickly becomes clear and the sediment height reduces with time. The particles settle rapidly as flocs (Figure 27, 1 and 2 min). Only few separated, smaller particles sediment more slowly resulting in supernatant clarification with time.

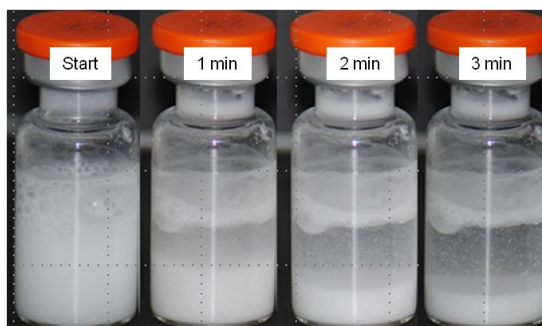


Figure 27: Sedimentation behavior of suspension with 30 mg/mL API at different time points.

The sedimentation of the higher concentrated samples (100 mg/mL) is hindered due to the higher solid fraction. Only a small supernatant becomes visible after 5 minutes. After one hour, the sediment volume is marginally decreased and a loosely packed sediment is observed.



Figure 28: Sedimentation behavior of suspensions with 100 mg/mL API at different time points.

The 300 mg/mL samples only show a minimal supernatant formation after 12 weeks of storage.



Figure 29: Sedimentation behavior of suspension with 300 mg/mL API at different time points.

The calculation of the sedimentation degree (ratio sediment height / total suspension height) of the 300 mg/mL suspension during storage confirms the decreasing sedimentation rate with concentration increase. The graph shows a high, more or less constant sedimentation degree during storage. Over 8 weeks of storage no sedimentation occurs (sedimentation degree of 1.00 ± 0.01). After 12 weeks, a supernatant becomes visible and a sedimentation degree of 0.95 ± 0.01 was seen. After one year the sedimentation degree yields 0.86 ± 0.03 . Thus, regarding the sedimentation rate there is no need for optimization. The sedimentation of the 100 and 300 mg/mL Cilengitide suspension is very slow so that an adequate withdrawal of the required dose is ensured during handling. The particles settle as flocs, building a loose sediment.

Additionally, the time needed to resuspend the Cilengitide suspensions with 30, 100 and 300 mg/mL is analyzed during storage over one year (2 - 8 °C). The low concentrated

suspensions with 30 mg/mL require approximately 10 ± 2 min for resuspension already after 1 week storage (Figure 30). With longer storage this time varies slightly but remains high and reaches approximately 13 minutes after 52 weeks. The long resuspension is due to a fast sedimentation of the particles building a compact cake. Suspensions with 100 mg/mL API need approximately 6 ± 1.3 min for resuspension after 1 week. Storage time does not affect the required time. Resuspension time of 300 mg/mL formulations stays below 5 minutes for up to 8 weeks storage due to the slow sedimentation. Subsequently, the time increases up to approximately 15 minutes after 52 weeks of storage. This significant increase is due to the more compact sediment described above and the resuspension of the highly concentrated aqueous suspension is affected by the high viscosity which increases the required time.

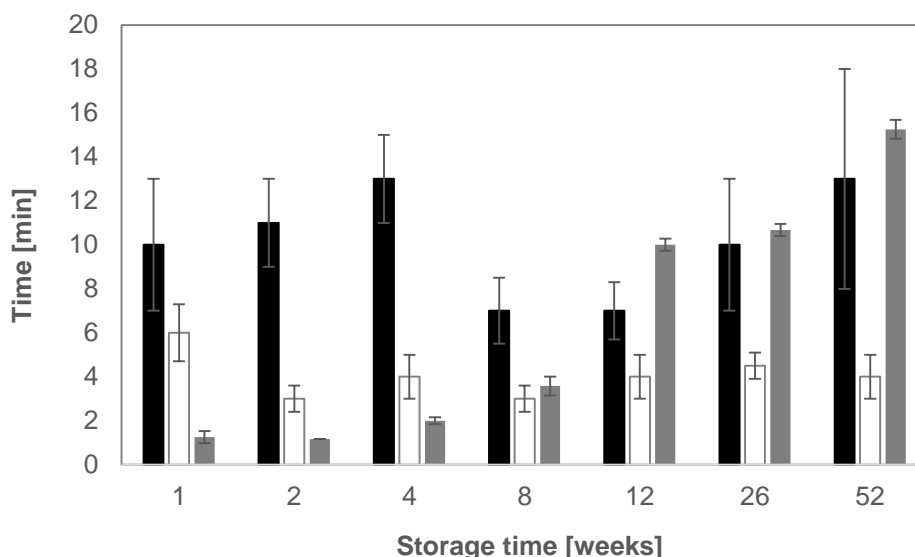


Figure 30: Time needed for resuspension of suspensions with 30 mg/mL (black), 100 mg/mL (white) and 300 mg/mL (grey) API as a function of storage time.

5.4 Rheological characterization

The before mentioned results indicate a good physical stability of the particles in water, even at 300 mg/mL API. But the highest concentrated suspension of micronized particles is a very viscous, paste-like system. As a result, difficulties with resuspendability and syringeability can occur. For this purpose, the rheological properties are determined over a shear range of $\dot{\gamma} = 0.1 - 1000$ 1/s at the different API concentrations. It is expected to observe a viscosity increase with higher solid fraction. Highly concentrated suspensions usually behave as non-Newtonian fluid, offering shear-thinning or shear-thickening characteristics. It is analyzed if a yield point exists for the suspensions. The thixotropy is quantified by calculating the area

between the for- and back-curve (hysteresis area). Finally, the viscosity results are translated into the formulation performance in terms of syringeability, injectability and resuspendability. For this purpose, shear rates have to be defined which represent the above mentioned performance parameter as the viscosity depends on the applied shear rate (non-Newtonian behavior). The shear rate $\dot{\gamma}$ can be calculated by using the following approximation [4] where Q is the volumetric flow rate and R the inner radius of the needle [Eq. 11].

$$\dot{\gamma} = 4 Q / \pi R^3 \quad \text{[Eq. 11]}$$

A 25 Gauge needle is used for drawing up and injecting the suspension. The passage of the 300 mg/mL suspension through a 25 Gauge needle is not an issue as the particles are small enough and the required force during injection low. However, the flow of the suspension down the vial into the cannula is limited due to the high viscosity. For an acceptable syringeability a volume stream of $Q = 0.05$ mL/s (1 mL volume within 20 s) is required [4]. By flowing down the vial ($r = 6.5$ mm) with the required volume stream of 0.05 mL/s a shear rate of $\dot{\gamma} = 0.23$ s⁻¹ is applied to the formulation according to the above mentioned equation. For further discussion of the viscosity, special attention is paid to this shear rate of $\dot{\gamma} = 0.23$ s⁻¹. As the characterization at low shear rates is difficult due to the heterogeneous nature of the suspension and possible slip, higher shear rates, such as $\dot{\gamma} > 5$ 1/s are recommended [28]. Consequently, the viscosity value at $\dot{\gamma} = 12.6$ s⁻¹ is also used to assess the syringeability ensuring the required measurement quality for all samples. Additionally, the data variability is low for all the mentioned samples at $\dot{\gamma} = 12.6$ s⁻¹. Regarding the injectability with a 25 Gauge needle (0.318 mm diameter) or smaller when forcing the suspension through the needle, shear rates higher than 1000 s⁻¹ are applied to the systems according by the calculation and confirmed by Miller et. al [4].

5.4.1 Influence of concentration on rheological properties

The analyses of the suspensions viscosity at $\dot{\gamma} = 0.1 - 1000$ 1/s containing 30, 100, 200 and 300 mg/mL of micronized raw material demonstrates the expected viscosity increase with higher API content (Figure 31).

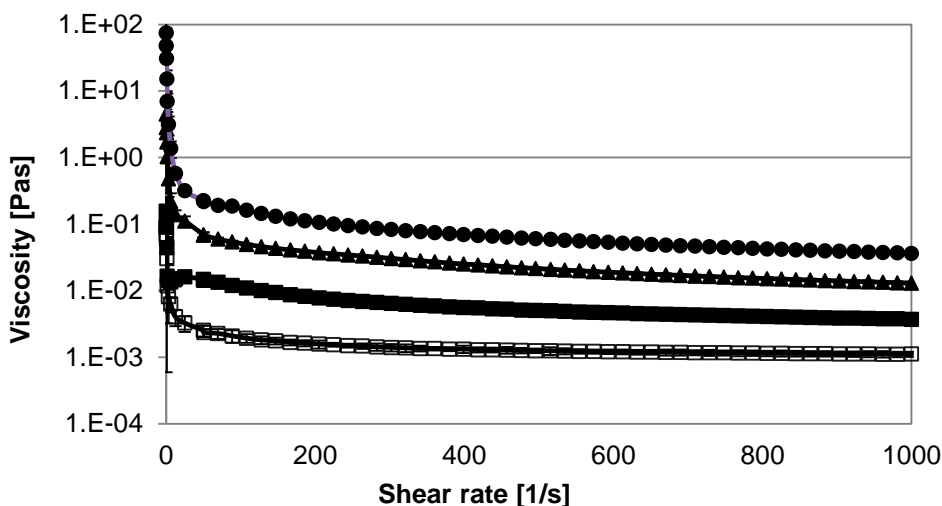


Figure 31: Viscosity of suspensions containing 30 mg/mL (□), 100 mg/mL (■), 200 mg/mL (▲) and 300 mg/mL (●) micronized API as a function of shear rate. Error bars represent standard deviations from triplicate measurements.

Regarding the lowest concentrated formulations (30 mg/mL) the flow behavior corresponds to Newtonian fluid over a broad shear range ($300 < \dot{\gamma} < 1000$ 1/s). Shear-thinning characteristics are only observed at shear rates lower than 300 1/s. The samples are comparable to water with a viscosity of 1 mPas at $\dot{\gamma} > 100$ 1/s. Increasing the concentration to 100 mg/mL, the viscosity increases and the formulations show pseudoplastic flow. At shear rates higher than 400 1/s, the viscosity is almost independent of the shear rate at approximately 4 mPas. It is conspicuous that the suspensions with 100 mg/mL API exhibit a viscosity maximum at about 25 1/s (increasing shear rates) or 50 1/s (decreasing shear rates), respectively (Figure 32). This maximum might be caused by an initial shear thinning with the particles orientating in the shear plane [77]. Subsequently the particle-particle interaction becomes a dominating factor, increasing the viscosity.

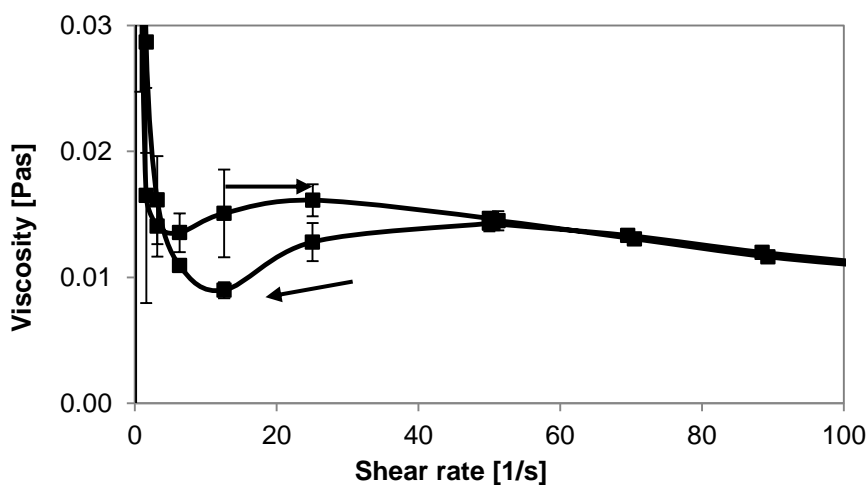


Figure 32: Viscosity of suspensions with 100 mg/mL micronized API as a function of shear rate. Error bars represent standard deviations from triplicate measurements.

When the API concentration is increased to 200 or 300 mg/mL, the viscosity is significantly increased. At lower shear rates, the viscosity strongly increases pointing to the formation of a yield point and a solid like behavior in quiescent conditions. At $\dot{\gamma} = 0.23$ 1/s the 300 mg/mL formulations yield a viscosity of 48.1 ± 39.9 Pas. In comparison, the 200 mg/mL suspensions exhibit a value of 2.80 ± 2.53 Pas, 0.155 ± 0.09 Pas is detected for 100 mg/mL formulations and 0.094 ± 0.10 Pas for 30 mg/mL samples. This is confirmed by the observation that the 300 mg/mL formulation does not flow when the vial is turned upside down (Figure 33). The 200 and 300 mg/mL formulations show typical non-Newtonian behavior with remarkable shear-thinning characteristics. Already at $\dot{\gamma} = 12.6$ 1/s the viscosity is significantly reduced to 0.58 ± 0.08 Pas for the 300 mg/mL and 0.14 ± 0.02 Pas for the 200 mg/mL suspensions. Shear-thickening or a viscosity maximum is not observed in contrast to the 100 mg/mL formulation. This could be due to a lower interparticle distance and a continuous inner structure at 200 mg/mL and more already at the start. The inner structure is destroyed by shearing, resulting in the observed shear-thinning characteristics over the whole shear rate range. At a shear rate of $\dot{\gamma} = 1000$ 1/s, which represents the injection with a cannula, the 200 and the 300 mg/mL samples show a viscosity value of 0.01 ± 0.001 Pas and 0.04 ± 0.004 Pas, respectively.



Figure 33: Flow behavior of a suspension with 300 mg/mL micronized API when vial is turned upside down.

Regarding the shear stress, the 30 and 100 mg/mL concentrated suspensions do not exhibit a relevant yield point (30 mg/mL: $T_0 = 0.025$ Pa, $r = 0.9994$; 100 mg/mL: $T_0 = 0.404$ Pa, $r = 0.9903$, fitted to the Casson model). Also for 200 mg/mL containing suspension, a possible apparent yield point is low ($T_0 = 2.50$ Pa, $r = 0.9655$). For suspension with the highest amount of API, the calculated yield point is 9.92 Pa ($r = 0.9680$). However, the calculation might depend on the used model and it is usually required to confirm the calculations using alternative measurement methods such as measurements of creep.

Finally, the thixotropic behavior is evaluated by calculation of the hysteresis areas (Table 9). The hysteresis area increases with increasing API concentration. Overall, the hysteresis effect is small despite a pronounced shear thinning. In practice this means that the viscosity is temporarily lowered by shaking, but the suspensions return to a higher viscous system during drawing out the suspension from the vial.

| API-concentration | 30 mg/mL | 100 mg/mL | 200 mg/mL | 300 mg/mL |
|------------------------|-------------|--------------|--------------|--------------|
| Hysteresis area [Pa/s] | 46.8 ± 15.1 | 224.5 ± 49.4 | 672.4 ± 76.5 | 2406 ± 819.9 |

Table 9: Calculated hysteresis area of suspensions with 30 mg/mL, 100 mg/mL, 200 mg/mL and 300 mg/mL micronized API.

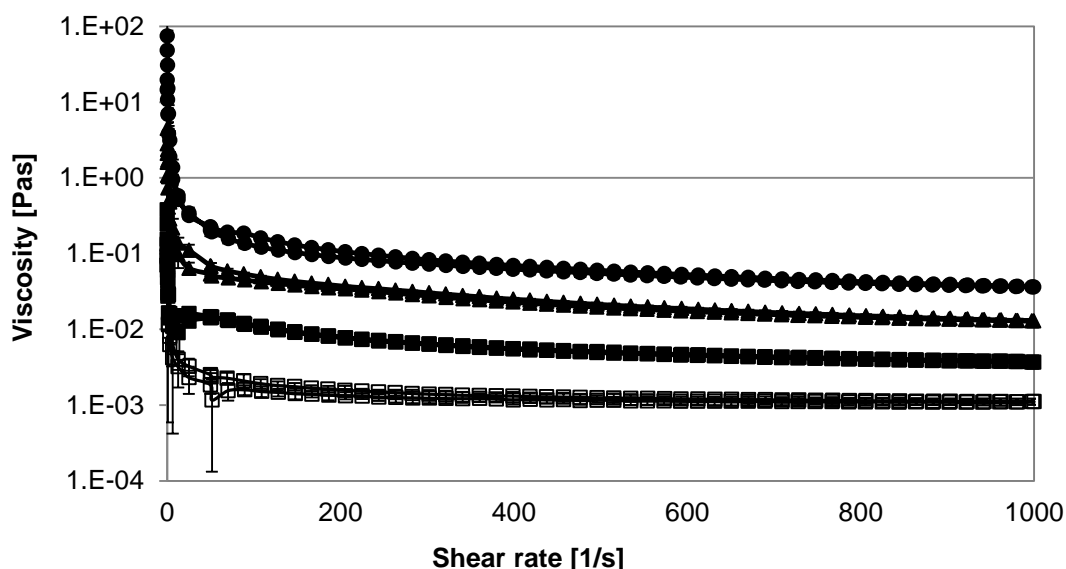


Figure 34: Viscosity of suspensions containing 30 mg/mL (\square), 100 mg/mL (\blacksquare), 200 mg/mL (\blacktriangle) and 300 mg/mL (\bullet) micronized API as a function of shear (forward and backward shearing). Error bars represent standard deviations from triplicate measurements.

5.5 Injectability of different concentrated formulations

The injectability was investigated using a texture analyzer set up. The force needed for the injection of the formulation via a 25, 26 or 27 Gauge needle, respectively, is quantified. The results demonstrate that all the concentrations can be injected at acceptable forces using a 27 G needle or larger (Figure 35). The required force increases with increasing API concentrations up to 2.72 ± 0.14 N (25 G needle). The force measured for the injection of the 300 mg/mL suspension via the smaller 27 Gauge needle is higher (4.8 N), but still acceptable. But needle blockage occurred for one sample with a 27 Gauge needle.

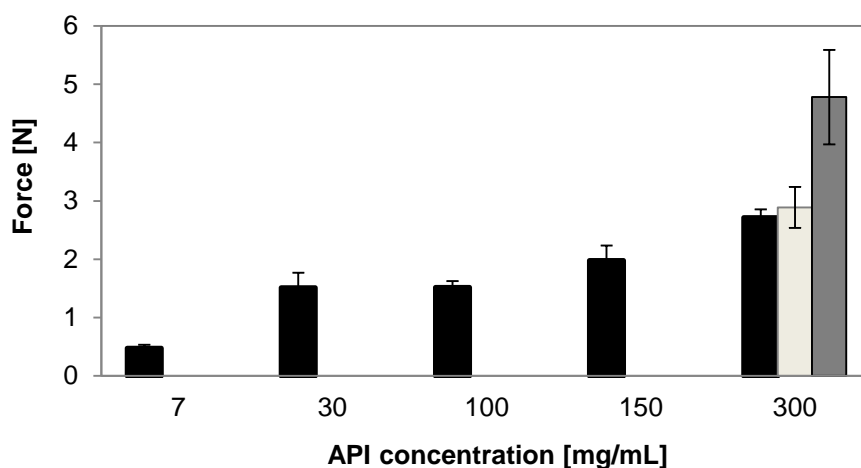


Figure 35: Injection force required for suspensions containing 7 mg/mL, 30 mg/mL, 100 mg/mL, 150 mg/mL or 300 mg/mL micronized API using a 25 (black), 26 (white) and 27 Gauge (grey) needle, a volume of 1 mL and a speed of 10 mm/s. Error bars represent standard deviations from triplicate measurements.

The mentioned injectability results correspond to viscosity measurements demonstrating the extreme shear-thinning character of the suspensions. The shear rates during injection are higher than 1000 1/s as discussed before. In this high shear range even the highly concentrated suspensions offer an acceptable low viscosity (about 40 mPas) and thus, a low force is needed for injection. In literature, a viscosity lower than 50 mPas is required to apply a formulation subcutaneously with a 25 to 27 Gauge needle [4].

5.6 Conclusion

Summing up, the viscosity at low shear rates is significantly higher for suspensions with 300 mg/mL than for formulations of 30, 100 or 200 mg/mL Cilengitide. The 200 and 300 mg/mL formulations show a yield point and behave like a solid with poor flow. Consequently, the syringeability is hindered as the 300 mg/mL suspension does not flow into the cannula. Suspensions with 200 and 300 mg/mL API are remarkable shear-thinning systems offering a significantly lowered viscosity at high shear rates so that injection via a needle is feasible. The suspended Cilengitide particles interact with each other, as seen by micrographs, building a continuous, scaffold-like structure that increases the viscosity. A very low sedimentation rate is observed for the 300 mg/mL suspensions and marginal supernatant quantities are seen only after 12 weeks of storage. Stability problems in the form of caking did not occur due to the high sedimentation degree. Also the particle size distribution was stable during storage for 1 year. Particle sizes comparable to the micronized raw material are obtained when non-micronized material is stirred in suspension for 2 days. Micronized material is used for further formulation

development to reduce manufacturing time and to ensure consistent particle size distributions of the product.

6 Formulation development for 300 mg/mL Cilengitide suspensions

6.1 Parameters influencing the suspension viscosity

As previously outlined, the viscosity of a suspension can be influenced by several parameters including pH, ions, particle size and the addition of surfactants. The potential of these formulation approaches to reduce the viscosity of a 300 mg/mL Cilengitide suspension is analyzed and discussed in the following chapters.

6.1.1 Effect of varying pH on viscosity of 300 mg/mL API suspension

The variation of pH can influence the viscosity by changing the repulsive electrostatic forces while attractive Van der Waals forces remain constant. Therefore, it is expected to detect the highest viscosity around the isoelectric point where repulsive forces are minimal and the hydrophobic forces dominate, whereas the viscosity should be reduced by electrostatic forces at higher and lower pH values. A pH range from 4 to 9 is considered which is physiologically acceptable for a subcutaneous injection [78] and feasible with respect to the API chemical stability [79, 80].

The result at $\dot{\gamma} = 0.2$ 1/s shows that the viscosity is influenced by pH variation (Figure 36). At pH 5.5 the suspension tends to exhibit the highest viscosity. This difference is significant when compared to pH 7.5 and higher and insignificant when compared to pH 4 and 5 due to the high standard deviations at these low pH values ($p < 0.05$).

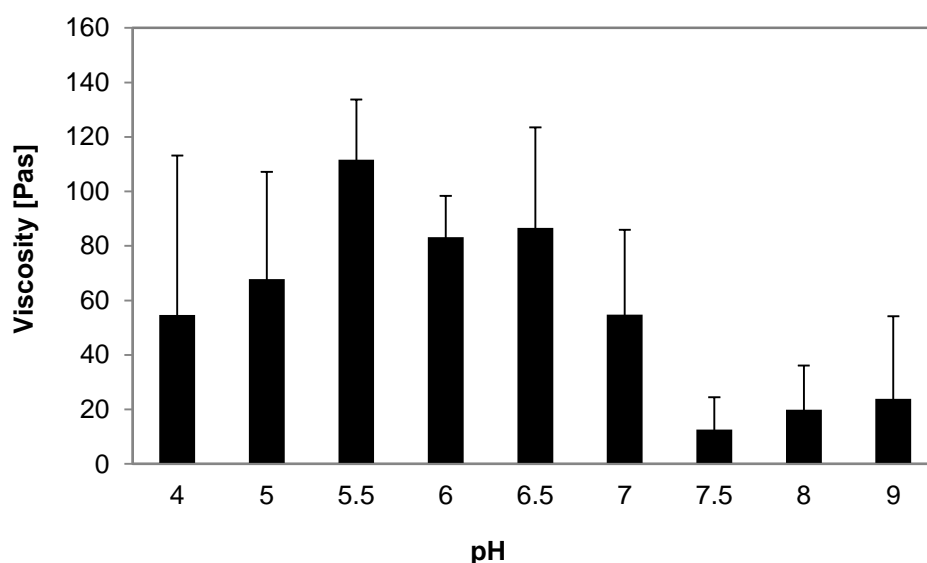


Figure 36: Influence of pH on viscosity of 300 mg/mL API in Wfl at $\dot{\gamma} = 0.2$ 1/s. Error bars represent standard deviations from triplicate measurements.

The same trend is observed at a higher shear rate of $\dot{\gamma} = 12.6 \text{ 1/s}$ with significant differences ($p < 0.05$) between suspensions with pH 5.5, 6 and 6.5 on the one hand and suspensions with 7.5 and higher on the other hand (Figure 37).

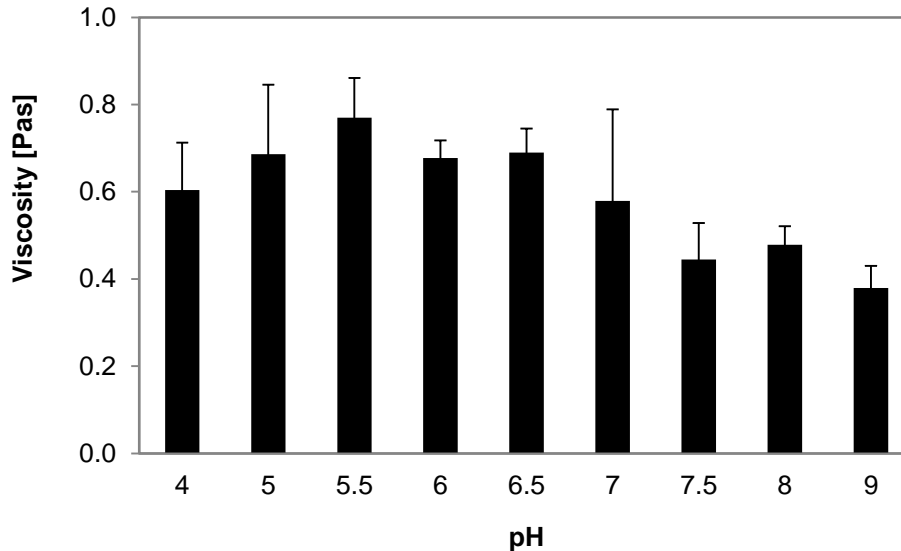


Figure 37: Influence of pH on viscosity of 300 mg/mL API in Wfl at $\dot{\gamma} = 12.6 \text{ 1/s}$. Error bars represent standard deviations from triplicate measurements.

From Zeta potential measurements it is known that the IEP of Cilengitide particles suspended in water is around pH 5.5 (Figure 38). It is conspicuous that the isoelectric point of the suspended particles is lower compared to the calculated IEP ($\text{IEP}_{\text{calculated}} \sim 7$). As demonstrated in chapter 4.2 the arginine group is involved in intermolecular hydrogen bonds, and may therefore not be freely accessible for ionization. Increasing the pH, the particles surface potential becomes negatively charged and exhibits a constant, slightly negative potential value of approximately $-17.4 \pm 1.6 \text{ mV}$ at pH 6.5 and higher. Below pH 5.5 the Zeta potential changes to positive values of $+8.4 \text{ mV}$ at pH 5.0 and $+16.8 \text{ mV}$ at pH 4.0.

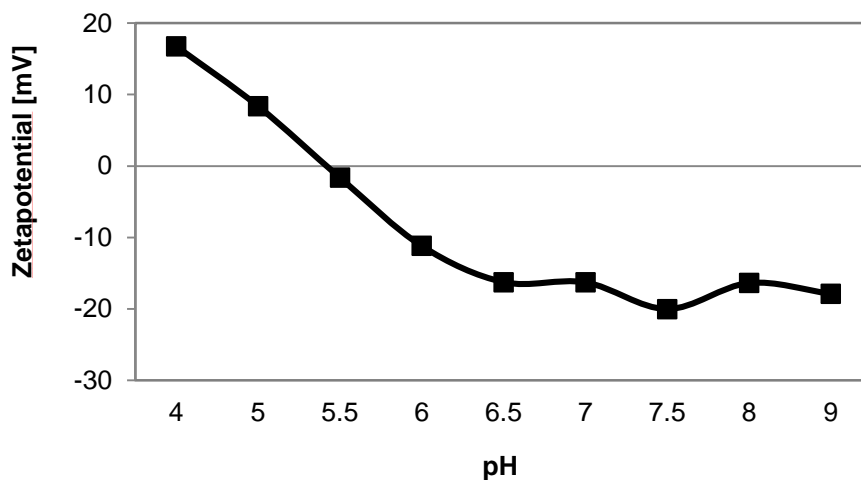


Figure 38: Influence of pH on Zeta potential of suspensions with 15 mg/mL API in Wfl. Error bars represent standard deviations from triplicate measurements.

In summary, the observed viscosity results are in line with the expectations from Zeta potential measurements. The higher viscosity as detected around the IEP correlates with a lack of electrostatic repulsive forces and hence strongest interparticulate interaction. Considering the calculated yield points fitted by the Casson model, the results are comparable high (Figure 39, correlation coefficients between 0.8967 at pH 4 and 0.9772 at pH 7.5).

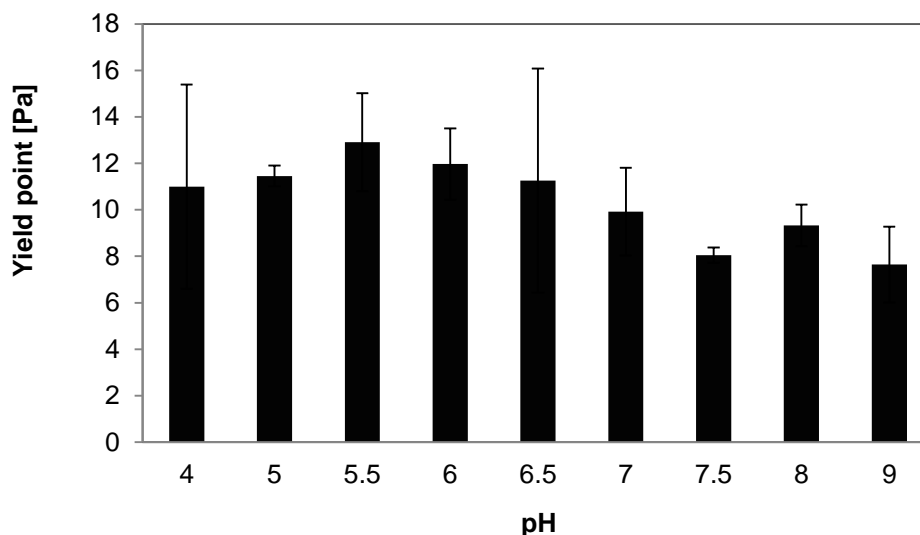


Figure 39: Influence of pH on yield point (calculated by the Casson model) of suspensions with 300 mg/mL API in Wfl. Error bars represent standard deviations from triplicate measurements.

The thixotropic behavior as the hysteresis area between the curves of the up and the down shearing is shown in Figure 40. The hysteresis area varies less at pH 7 and higher, but there is no effect of pH on thixotropy. In conclusion, the variation of the pH influences the viscosity of the suspension, but not to a sufficient extent to enable syringeability of the formulation.

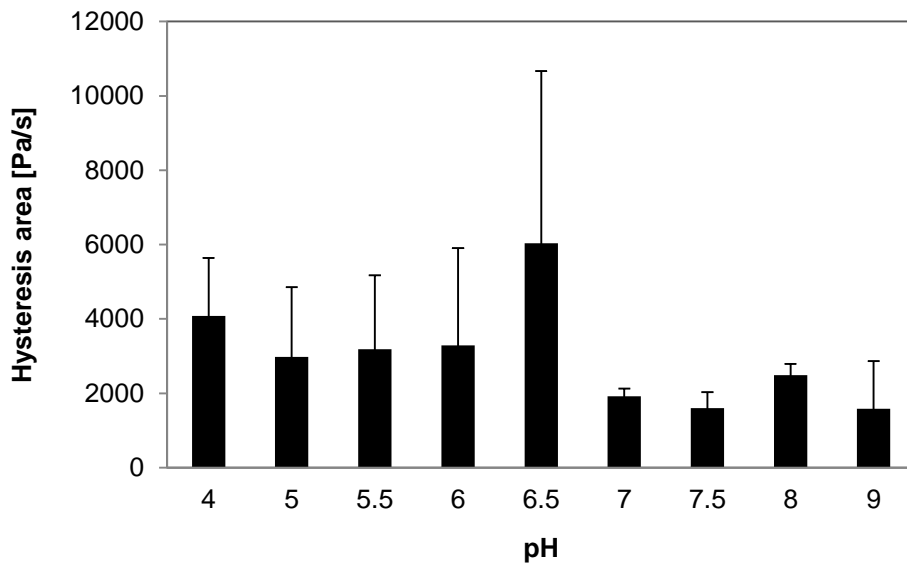


Figure 40: Influence of pH on hysteresis area of the rheometric analysis of suspensions with 300 mg/mL API in Wfl. Error bars represent standard deviations from triplicate measurements.

Additionally, the viscosity of less concentrated suspension with 30, 100 and 200 mg/mL API at pH 4, 5.5, 7 and 9 is determined (Figure 41). The viscosity differences dependent on pH are small at all concentrations. Suspensions at pH 7 and pH 9 tend to be less viscous compared to pH 5.5. Further decrease to pH 4 does not change the viscosity. There is also no effect dependent on concentration.

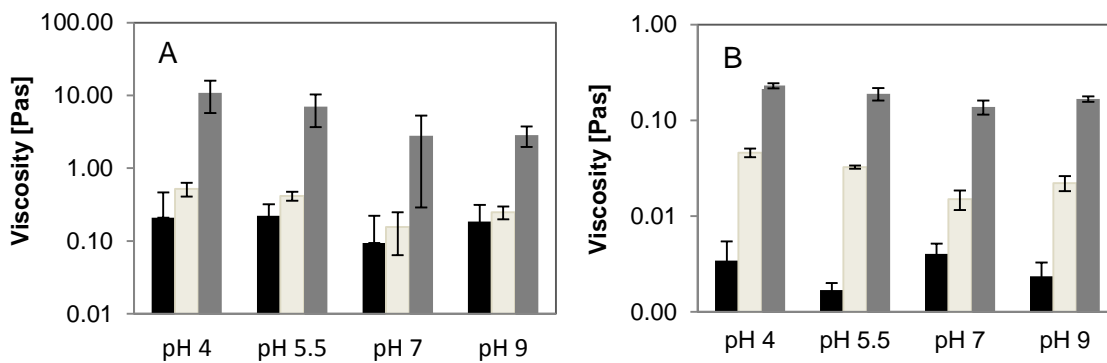


Figure 41: Influence of pH on viscosity of suspension with 30 mg/mL (black bars), 100 mg/mL (white bars) and 300 mg/mL (grey bars) API at $\dot{\gamma} = 0.2$ 1/s (A) and $\dot{\gamma} = 12.6$ 1/s (B). Error bars represent standard deviations from triplicate measurements.

Overall, it can be concluded that the viscosity is only slightly affected by the pH. The viscosity does not generally decrease with increasing Zeta potential.

6.1.2 Influence of ions on viscosity of 300 mg/mL API suspension

The addition of ions may lower the viscosity by reducing the effective volume fraction of the dispersed phase due to a compressed double layer and by affecting the repulsive forces. These effects are dependent on the ion concentration. The influence of NaCl (50 mM, 100 mM, 150 mM) and 150 mM KCl on the viscosity of suspensions with 300 mg/mL API at pH 7 is determined. CaCl₂ was not further analyzed as no effect was seen in preliminary tests. Beside the addition of ions, also glucose with a concentration of 300 mM was tested for a viscosity decrease. Li et al. [81] found a viscosity decrease of nanometric alumina suspensions due to the addition of fructose. This was attributed to the adsorption of fructose on the particle surface and water displacement. Thus, the bulk water is increased and the viscosity becomes lower. Also several other monosaccharides are able to reduce the viscosity of different dispersed systems [82, 83].

Figure 42 shows the effect of salt and glucose addition on viscosity as a function of the shear rate. The viscosity of the 300 mg/mL API suspensions containing ions or glucose is independent from the ion concentration or the addition of monosaccharide. Regarding the viscosity values at low shear rates ($\dot{\gamma} = 0.2$ and $\dot{\gamma} = 12.6$ 1/s), there is also no noticeable difference (Figure 43). The thixotropic behavior of the suspensions is shown in Figure 44. The suspensions with 150 mM NaCl and 300 mM glucose tend to a slightly less thixotropic behavior than the samples without ions and with 150 mM KCl but the differences are insignificant.

In all cases, the paste-like character of the suspension remains unchanged and the suspensions are too viscous for the withdrawal out of the vial.

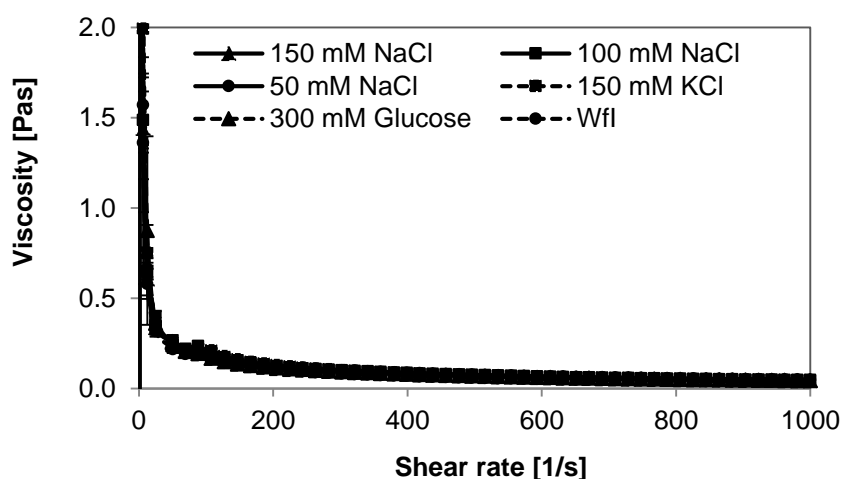


Figure 42: Influence of ions and glucose on viscosity of suspension with 300 mg/mL API (pH 7). Error bars represent standard deviations from triplicate measurements.

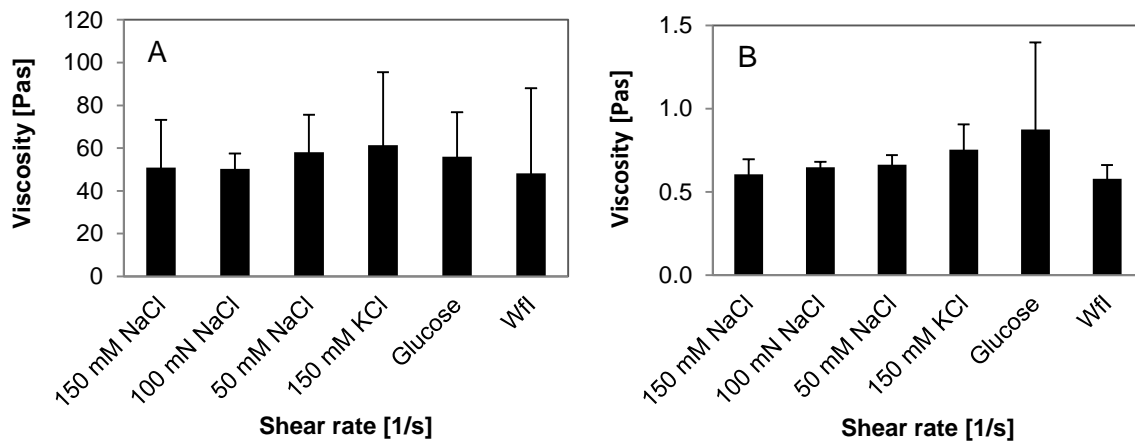


Figure 43: Influence of ions and glucose on viscosity of suspension with 300 mg/mL API (pH 7) at $\dot{\gamma} = 0.2$ 1/s (A) and $\dot{\gamma} = 12.6$ 1/s (B). Error bars represent standard deviations from triplicate measurements.

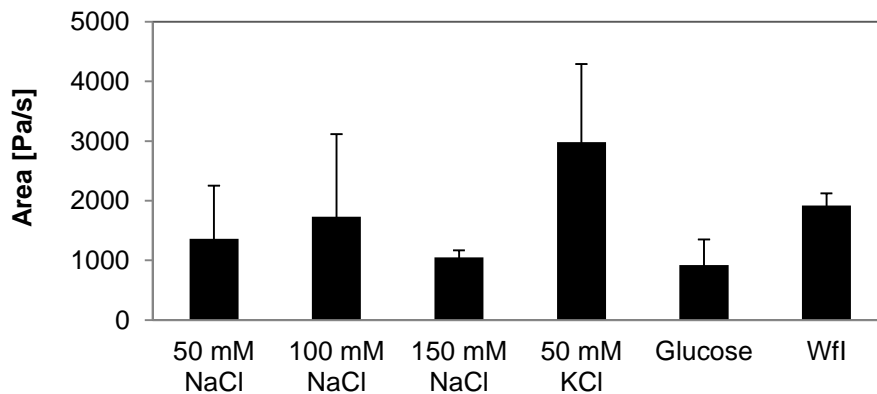


Figure 44: Influence of ions and glucose on thixotropic behavior of suspension with 300 mg/mL API (pH 7). Error bars represent standard deviations from triplicate measurements.

6.1.3 Effect of particle size on viscosity of 300 mg/mL API suspension

The particle size can influence the viscosity of concentrated suspensions. More viscous systems are expected with small particle sizes due to an increase in the effective volume of the dispersed phase and interparticulate contact density [28]. Consequently, the viscosity of suspensions containing 300 mg/mL API of different particle size is analyzed (Figure 45). The smallest particles $D(0.05)$ of all suspensions are comparable in size. The non-micronized suspensions stirred for 48 hours offer larger particles than the micronized ones indicated by the higher values for $D(0.10)$, $D(0.50)$, $D(0.90)$ and $D(0.95)$. The suspensions with additionally milled micronized raw material (1 mm beads, 10 min) contain the smallest particles with a $D(0.95)$ of 22.85 μm .

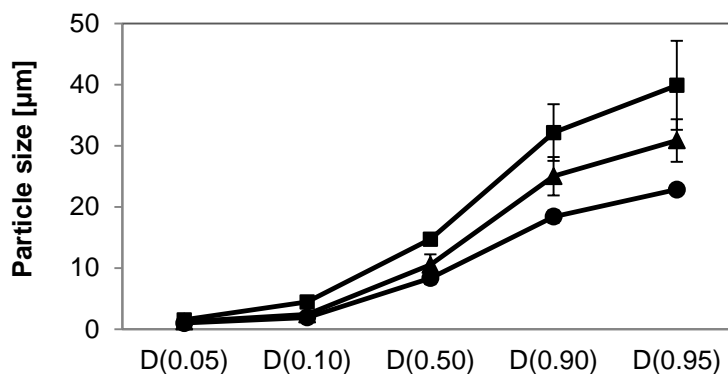


Figure 45: Particle size distribution of suspensions with 300 mg/mL non-micronized API (■), 300 mg/mL micronized API (▲) and 300 mg/mL micronized API additionally milled (●) used for viscosity determination. Error bars represent standard deviations from triplicate measurements.

The viscosity values of the different suspensions are presented in Figure 46. It can be demonstrated that the particle size has a significant influence on the viscosity. A decrease in particle size leads to significantly higher viscosity values of the suspensions. At $\dot{\gamma} = 0.2$ 1/s the viscosity of the suspensions with small and medium particle sizes does not differ significantly. At $\dot{\gamma} = 12.6$ 1/s there is a significant difference between all particle sizes.

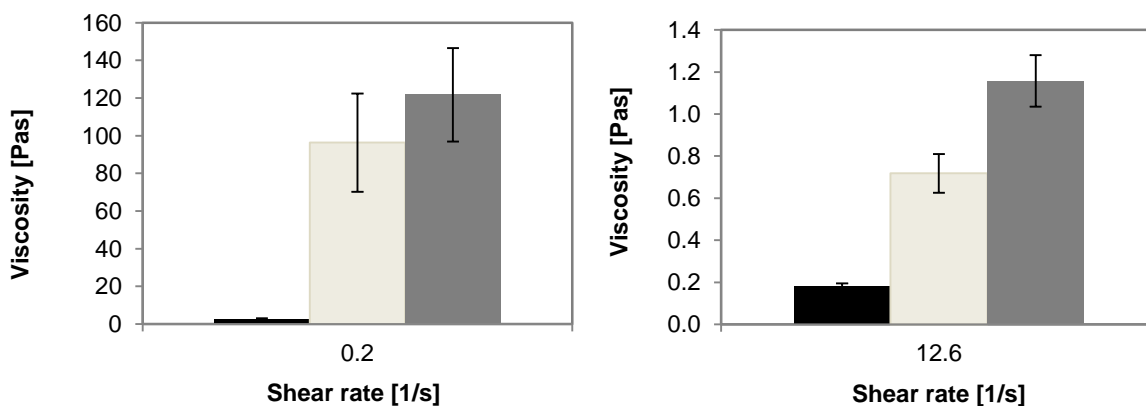


Figure 46: Viscosity of suspensions with 300 mg/mL non-micronized API (black), 300 mg/mL micronized API (white) and 300 mg/mL micronized API additionally milled (grey) at $\dot{\gamma} = 0.2$ 1/s and $\dot{\gamma} = 12.6$ 1/s. Error bars represent standard deviations from triplicate measurements.

However, a decrease in suspension viscosity by using large particles appears not to be suitable. Despite a D(0.95) value of about 40 µm, needle shaped particles longer than 120 µm are detected by microscopy. These particles may block the 25 Gauge needle and would need to be completely rouled out.

6.1.4 Effect of phospholipids on suspension viscosity

Dimyristoylphosphoglycerol (DMPG)

For further formulation development, different excipients are tested with the objective to reduce the viscosity at low shear rates and to improve syringeability. From literature it is known that surfactants can reduce the viscosity by introducing steric or static repulsive forces [61, 62, 64] and by reducing particle interaction [24, 48]. Therefore, different phospholipids are chosen, mainly dimyristoylphosphoglycerol (DMPG), as well as the commonly used polysorbate 80 (PS 80) and mixtures containing polysorbate 80 and sorbitan monooleate (SO). The possible interaction of DMPG with Cilengitide is studied in more detail to get an understanding of the mechanisms of viscosity reduction.

First experiments at shear rates of 100 1/s and higher show a viscosity reduction of suspensions containing DMPG (Figure 47). The most pronounced reduction is achieved by the addition of 2 mg/mL DMPG which was hence selected as phospholipid concentration for further development. DMPG alone dispersed in water leads to a marginal viscosity increase (Figure 48).

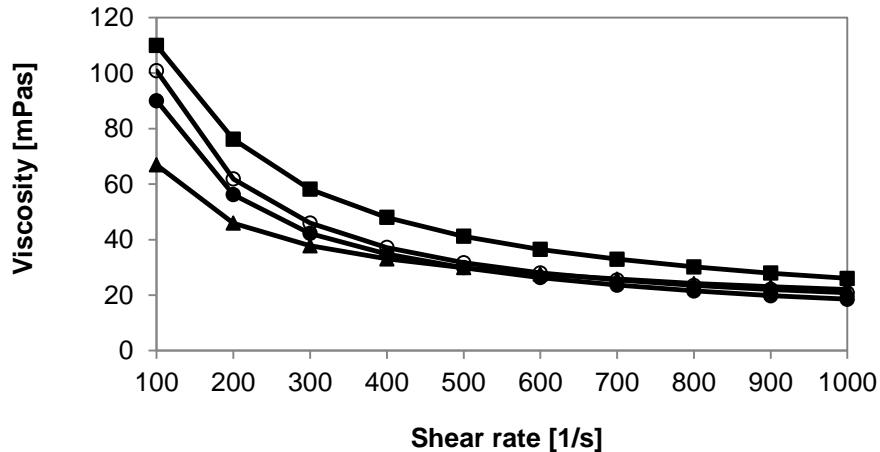


Figure 47: Viscosity of suspensions with 300 mg/mL API (■) and with 1 mg/mL (●), 2 mg/mL (▲) and 5 mg/mL (○) DMPG.

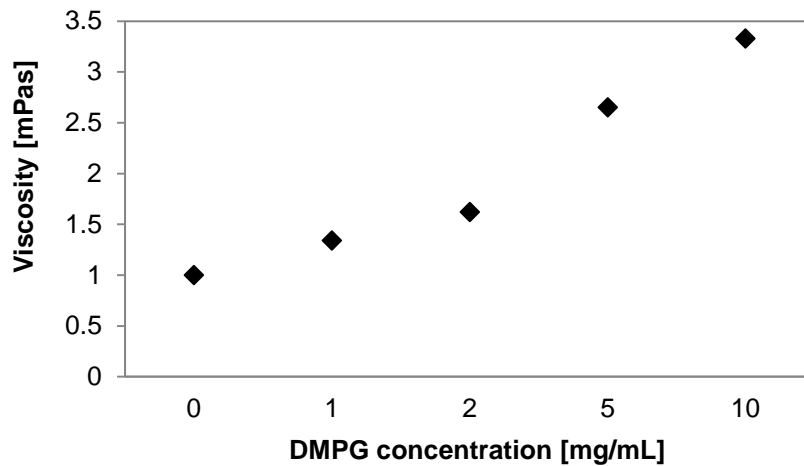


Figure 48: Viscosity of DMPG dispersions as a function of the concentration (without API).

Whether the higher viscosity in water for the 5 mg/mL DMPG dispersion is related to the higher viscosity of the API suspension is unclear. The fact that the beneficial effect of 1 mg/mL DMPG on suspension viscosity is less might be explained by an incomplete surface coverage. 1 mg DMPG (8.75×10^{17} molecules) theoretically cover 1.05 m^2 , assuming that one DMPG molecule occupies an area of 1.2 nm^2 [84]. The surface area of 300 mg Cilengitide is approximately 1.06 m^2 determined by gas adsorption method.

The viscosity of the DMPG-containing suspension compared to the aqueous suspension at low shear rates of 0 - 100 $1/\text{s}$ is shown in Figure 49. Suspensions with DMPG are remarkably reduced in viscosity in the low shear rate range. At $\dot{\gamma} = 0.2 \text{ 1/s}$ the suspension in Wfl exhibits 48.1 Pas with high variability (SD = 40 Pas, $n = 3$) whereas the 2 mg/mL DMPG containing system features $7.7 \pm 0.7 \text{ Pas}$.

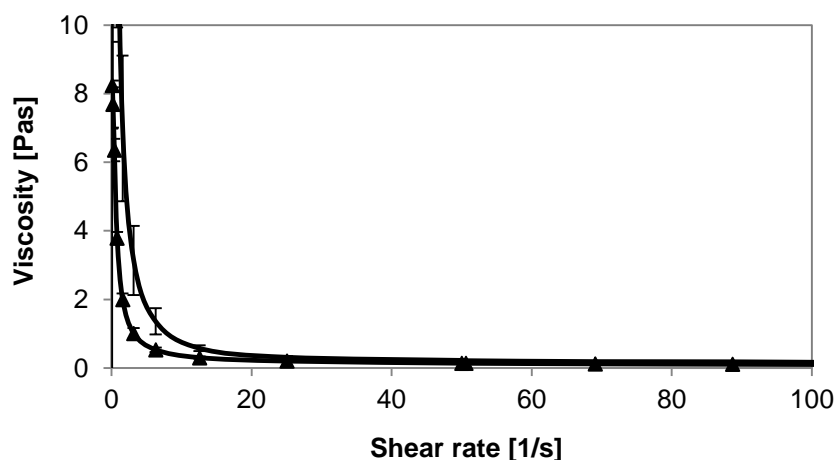


Figure 49: Viscosity of 300 mg/mL Cilengitide in Wfl (■) and with 2 mg/mL DMPG added (▲) at pH 7. Error bars represent standard deviations from triplicate measurements.

Fitting the curves to the Casson model gives an average yield point of 4.9 ± 2.4 Pa ($r = 0.9640$) for the 2 mg/mL DMPG suspensions compared to 9.9 ± 1.9 Pa ($r = 0.9681$) for the WFI suspension. The thixotropic behavior is not changed with the addition of 2 mg/mL DMPG (1918.7 ± 207.6 Pa/s for suspension in WFI, 2277.0 ± 380.6 Pa/s for suspension with 2 mg/mL DMPG).

It can be concluded that the addition of the DMPG strongly impacts the viscosity. The viscosity reduction is most pronounced with 2 mg/mL DMPG. The suspensions exhibit a lower yield point and the flow behavior of the different samples is less variable when compared to a suspension in WFI. With addition of 2 mg/mL DMPG the suspension becomes syringeable as it is possible to extract 1.0 mL from the vial within 17 ± 1 s using a 25 G needle (discussed in Chapter 6.2.5, Figure 83).

Characterization of the DMPG structure in presence of Cilengitide

From literature it is known that DMPG may build a variety of lamellar structures in water. The size and shape of the bilayers depend on the pH and the ionic strength of the dispersion, the kind of added ions, the temperature and the storage time. Aqueous dispersions of DMPG form polyanionic unilamellar vesicles [85] or bilayer fragments and bilayered micelles (bicelles) [86]. Fernandez [87] observed submicroscopic vesicles in presence of up to 20 mM NaCl. With 50 mM NaCl most molecules are arranged in small vesicles and giant (loose) multilamellar vesicles (MLVs) start to appear [87]. A further increase of the ionic strength leads to denser and more MLVs. MLVs are the prevailing structures when 500 mM NaCl is added. Giant DMPG vesicles were found in 10 mM Hepes buffer at pH 7.4 with 2 mM NaCl at different temperatures by Riske et al. [88]. Epand [89] showed that flat sheets exist for aged DMPG at low temperature. At 50 °C, the lipid spontaneously vesiculates. The vesicle size is not uniform but they are generally larger (100-300 nm) than some of the vesicles and fragments formed at low ionic strength (20-30 nm, Epand and Hui, [90]). Spinozzi et al. [91] confirm the existence of pores in DMPG bilayers at higher DMPG concentrations (300 mM) which were already proposed for 70 mM DMPG in water [92]. Leaky DMPG vesicles were found by Barroso [93] at low ionic strength (10 mM Hepes buffer). The structural changes of DMPG dispersed in water during storage were investigated by Garidel [94]. Besides small vesicles, flat or slightly curved multilayered lamellae or cochleate cylinders are found at low temperatures (4 °C). The film expanded when the NaCl amount is increased caused by ionization of the DMPG headgroup. A more condensed film is achieved with increasing the NaCl concentration and lowering the pH-value due to the reduction of the electrostatic repulsion and the possibility for

the formation of a hydrogen bonding network. Beside electrostatic effects, site-specific binding was found for Ca^{2+} , Mg^{2+} and Sr^{2+} .

Consequently, DMPG structures are analyzed when dispersed in water in presence of dissolved Cilengitide, NaCl or glucose. Turbidity measurements are performed to detect structural changes when other components are added to the DMPG dispersion. Cryo-TEM micrographs and DLS measurements are taken to show whether bilayer structures are built. If they are consistent in presence of API and NaCl, the viscosity reduction may be caused by the bilayer structures acting as a kind of ball bearing between suspended API particles. More information about the potential interaction should be received from NMR spectroscopy. Ionic interaction may take place between the negatively charged headgroup of the DMPG and the positively charged arginine of the Cilengitide molecule. Furthermore, the hydrophobic carbon chain of the phospholipid may interact with the hydrophobic amino acids phenylalanine and valine. The mentioned analytical methods only enable the characterization of the DMPG structures in presence of dissolved API. Interaction between DMPG and suspended API particles are characterized with Zeta potential measurements.

Turbidity and dynamic light scattering measurement of DMPG dispersions

Changes in turbidity and size indicate a potential interaction between dissolved Cilengitide and DMPG. Therefore, samples containing 2 mg/mL DMPG are characterized and compared to samples with 4 mg/mL API, 150 mM NaCl or 300 mM glucose added (pH 7). The turbidity of 2 mg/mL DMPG in water is low (2.1 ± 0.2 NTU) and even less in presence of API (0.7 ± 0.0 NTU). DLS measurements show that DMPG dispersed in water exhibits an average structure size of 37 nm with the built structures being quite polydisperse as indicated by a high polydispersity index (PDI) of 0.7. The samples with API added are too polydisperse to provide a useful average size. The turbidity is higher and the difference more pronounced for NaCl containing DMPG dispersions. Samples with 2 mg/mL DMPG and 150 mM NaCl exhibit 127.3 ± 4.0 NTU and 6.0 ± 0.1 NTU with 4 mg/mL API added. Much larger structures are detected in presence of 150 mM NaCl but without API (140 nm, PDI = 0.17) in contrast to samples with Cilengitide (30 nm, PDI = 0.5). The addition of NaCl induces ionization of the headgroup of DMPG causing expansion of the bilayer structures [84]. In contrast, the turbidity and DLS results seen for samples with 300 mM glucose are comparable to the samples without an isotonic agent. The turbidity is low for samples with 300 mM glucose (2.1 ± 0.2 NTU) and further reduced with 4 mg/mL API added (0.5 ± 0.0 NTU). Structures in the size range of 42 nm and with a PDI of 0.6 are detected without API. The result for the API containing sample are

not useable as they are too polydisperse. In conclusion, the observed changes in turbidity and size point towards potential interaction of DMPG with Cilengitide.

Cryo-TEM images of DMPG dispersions

Cryo-TEM is used to characterize the structures which DMPG builds. DMPG dispersed in water forms bilayered micelles (bicelles or disc micelles) as shown in Figure 50A with a size of around 40 nm diameter. This is in line with the DLS results and literature [86]. In presence of 4 mg/mL API dissolved in water the bicelles are destroyed and spherical micelles are formed (Figure 50 B), which are more variable in size (between 25 to 75 nm).

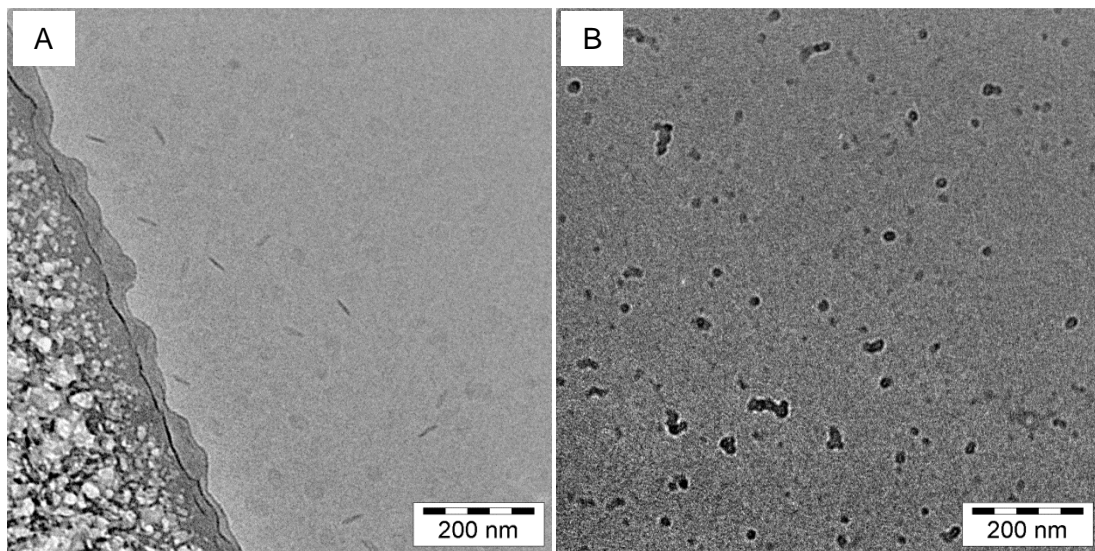


Figure 50: Cryo-TEM pictures of 2 mg/mL DMPG dispersed in water (A) and 4 mg/mL API solution (B).

The corresponding 150 mM NaCl containing samples exhibit larger, spherical vesicles (Figure 51). With 4 mg/mL API the vesicles are again destroyed and irregularly formed micelles are detected. This micellization of phospholipid bilayers was also observed for surface-active peptides like melittin [95, 96].

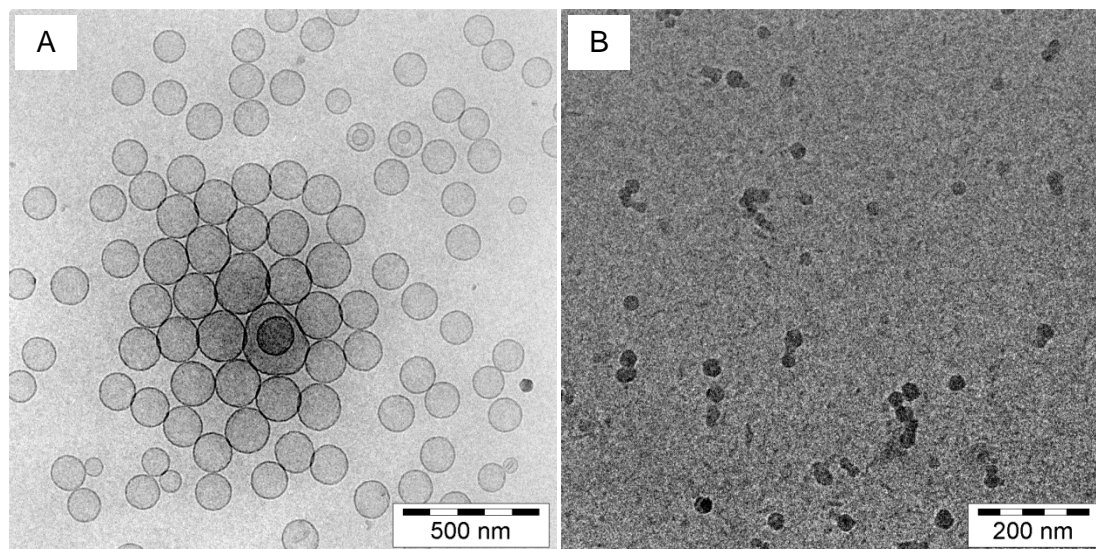


Figure 51: Cryo-TEM pictures of 2 mg/mL DMPG with 150 mM NaCl dispersed in water (A) and 4 mg/mL API solution (B).

Thus, the DMPG-bicelles are not preserved when Cilengitide is added and viscosity reduction by DMPG structures acting as ball bearing is less likely.

NMR-spectroscopy characterizing the interaction between DMPG and Cilengitide

To get a better understanding on the interaction mechanism between dissolved Cilengitide and DMPG molecules, the supernatant of suspensions containing 300 mg/mL API and 2 mg/mL DMPG was investigated by NMR-spectroscopy. The ^1H -NMR stacked plot of the supernatant of Cilengitide suspension (300 mg/mL) and the Cilengitide/DMPG suspension (300 mg/mL API + 2 mg/mL DMPG) in D_2O at pH 6.4 is shown in Figure 52. For the signals marked in red squares, there is no signal overlap of resonances of DMPG with that of Cilengitide allowing the differentiation between inter- and intramolecular interaction. However, the non-overlapping regions belong to hydrophobic groups. The ionic interaction between the negatively charged phosphate group and the positive arginine cannot be detected due to the overlap of the phosphate group signal with the arginine signal of Cilengitide at around 4 ppm.

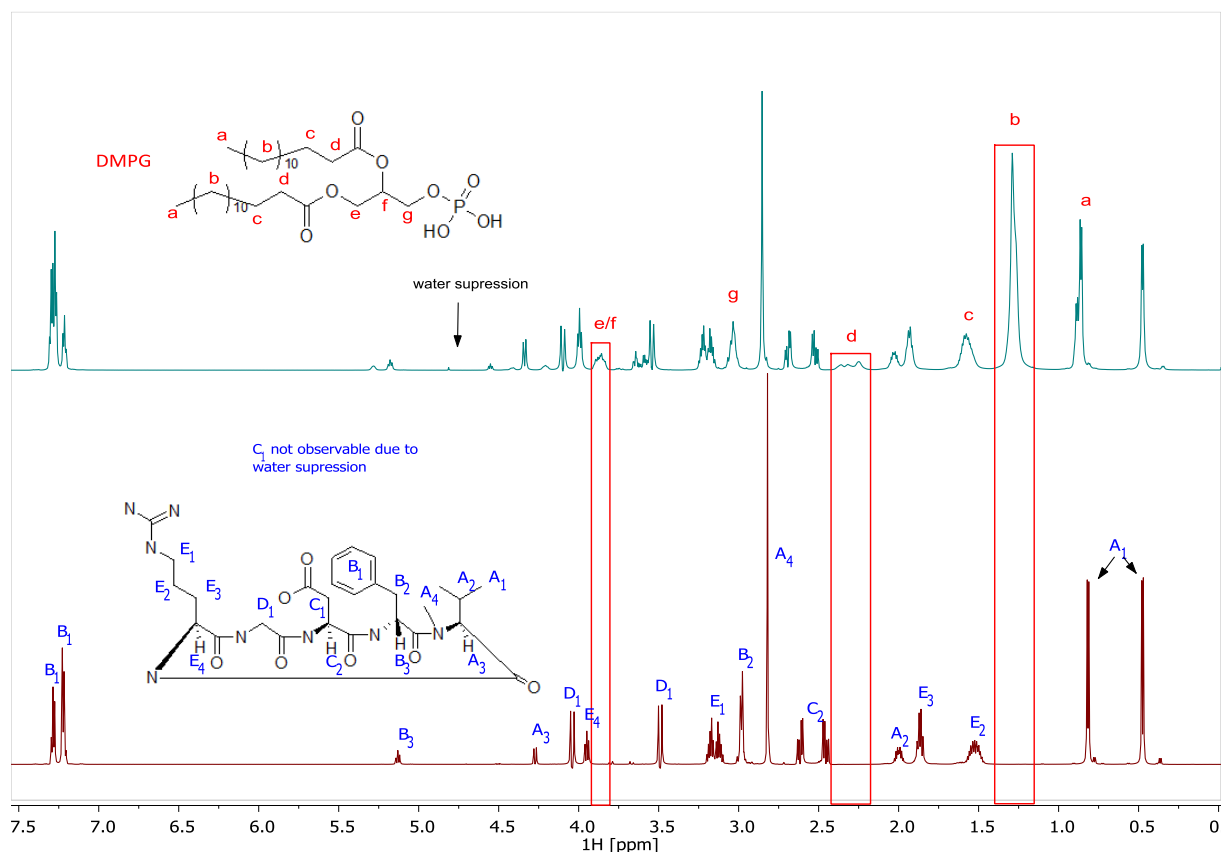


Figure 52: Stacked plot of 4 mg/mL Cilengitide dissolved in D₂O (below) and 2 mg/mL DMPG (above). The letters in the spectra indicate DMPG and Cilengitide resonances assigned to the chemical group in the formula. Group C 1 of Cilengitide is not observable due to water suppression. No spectral overlap of Cilengitide and DMPG is indicated by the red boxes.

In order to probe for intermolecular interactions, a 2D NOESY (Nuclear Overhauser Effect Spectroscopy) NMR spectrum of the supernatant of Cilengitide suspension (300 mg/mL) containing 2 mg/mL DMPG in D₂O was recorded (Figure 53, pH 6.4). The NOESY NMR spectrum allows one to identify spatially proximate groups. If there is a pronounced interaction of DMPG with Cilengitide, the interacting groups will be necessarily close in space to each other and hence give a correlation in a 2D- NOESY NMR spectrum. In Figure 53 unambiguous DMPG/Cilengitide correlations can be seen for the CH₂-group of the myristoyl side chain at 1.3 ppm with both the valine and phenylalanine group of Cilengitide. From this finding a strong hydrophobic interaction can be deduced. The other signals outside the diagonal correspond to intramolecular interactions.

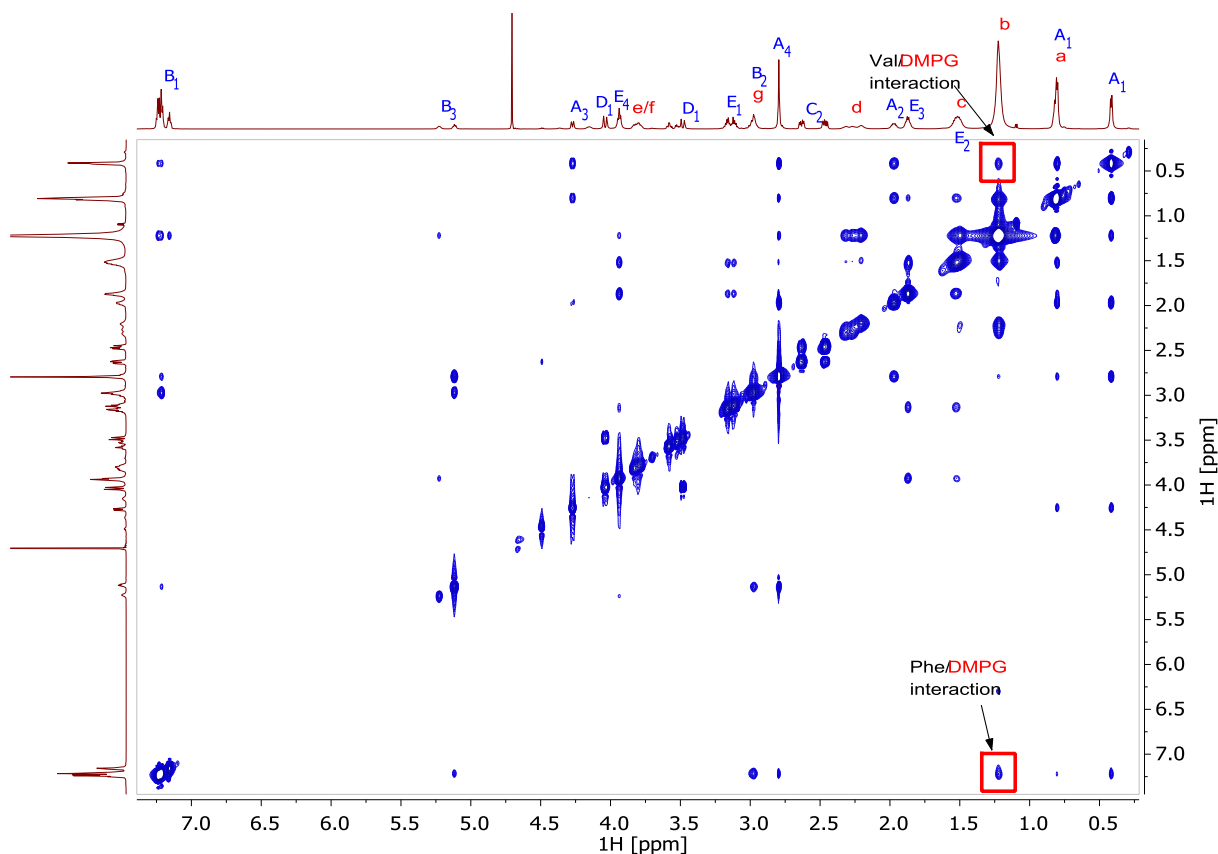


Figure 53: 2D NOESY NMR spectrum of the supernatant of Cilengitide suspension (300 mg/mL) containing DMPG (2 mg/mL) at pH 6.4. All signals outside the diagonal correspond to spatially close ^1H -nuclei.

To get information about the dependency of the observed DMPG / Cilengitide interactions upon molecular charge, 2D NOESY NMR spectra were also recorded for the supernatants of samples with pH 4.2, 5.4 and 6.9 (pD 4.6, 5.8, 7.3) (Figure 54 A-C). In all spectra, the same correlations between the hydrophobic part of DMPG and the phenylalanine and valine groups of Cilengitide as seen in the supernatant of suspension at pH 6.4 are observed, leading to the conclusion that hydrophobic interactions between DMPG and Cilengitide in solution occur at all pH values.

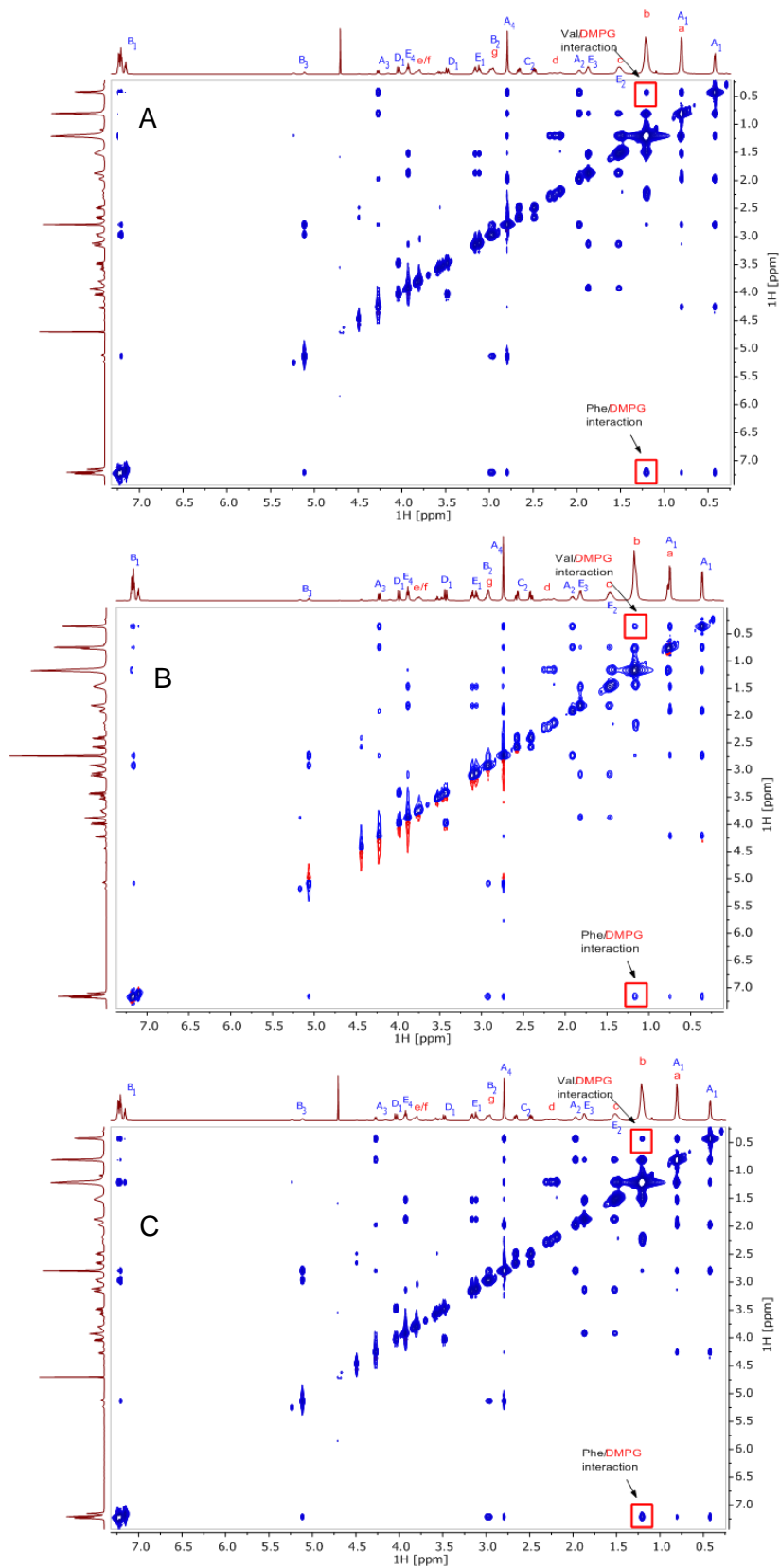


Figure 54: 2D NOESY NMR spectrum of the supernatant of Cilengitide suspension (300 mg/mL) containing DMPG (2 mg/mL) at pH 6.9 (A), pH 5.4 (B) and pH 4.2 (C). All signals outside the diagonal correspond to spatially close ^1H -nuclei.

The results of NMR spectroscopy confirm hydrophobic interaction between the myristoyl side chain of DMPG and phenylalanine and valine of the Cilengitide molecule in solution at all pH values leading to the destruction of bilayer structures seen in Cryo-TEM pictures. However, electrostatic interaction is not proven as the signal for the phosphate group does overlap of the Cilengitide signals.

6.1.5 Effect of varying pH on viscosity of 300 mg/mL Cilengitide suspensions containing 2 mg/mL DMPG

Beside the addition of DMPG, the pH of DMPG containing Cilengitide suspension is varied and the effect on viscosity is studied. A remarkably low viscosity is found at pH 5 and 5.5 over the whole shear range (Figure 55).

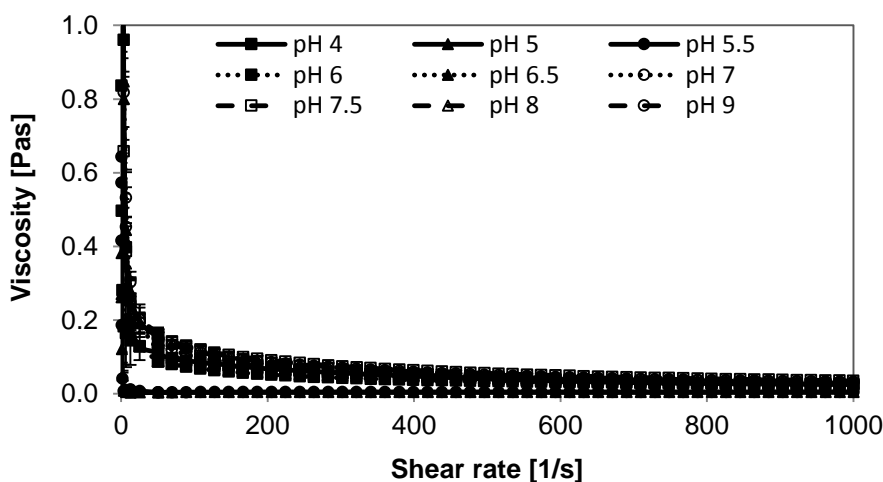


Figure 55: Viscosity of suspensions containing 300 mg/mL API and 2 mg/mL DMPG as a function of pH. Error bars represent standard deviations from triplicate measurements.

Figure 56 shows the viscosity values at the low shear rate of $\dot{\gamma} = 0.2$ 1/s relevant for flow in the vial. Besides the suspensions with pH 5 and 5.5, the suspensions at pH 6 also exhibit a minimal viscosity of less than 1.2 Pas at this shear rate. At $\dot{\gamma} = 12.6$ 1/s a significantly lower viscosity is found for suspensions with pH 5 and 5.5 as compared to suspensions with other pH value (Figure 57). Further increase in the shear rate leads to a constant viscosity of 30 mPas at pH 6 or approximately 4 mPas at pH 5 and 5.5, respectively.

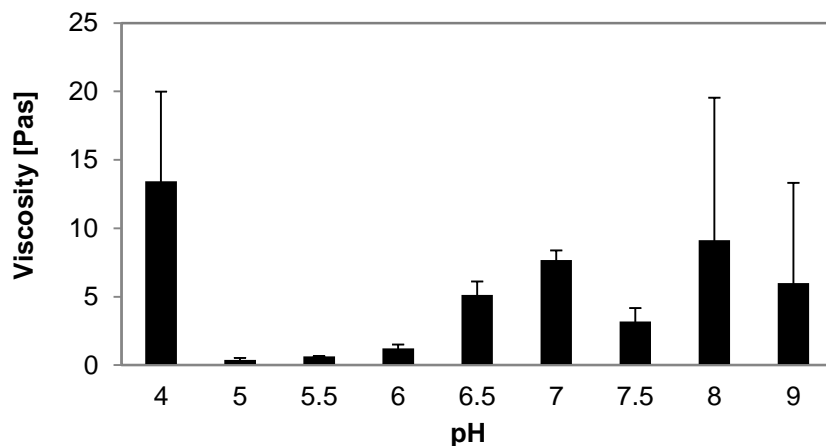


Figure 56: Viscosity of suspensions containing 300 mg/mL API and 2 mg/mL DMPG as a function of pH at $\dot{\gamma} = 0.2$ 1/s. Error bars represent standard deviations from triplicate measurements.

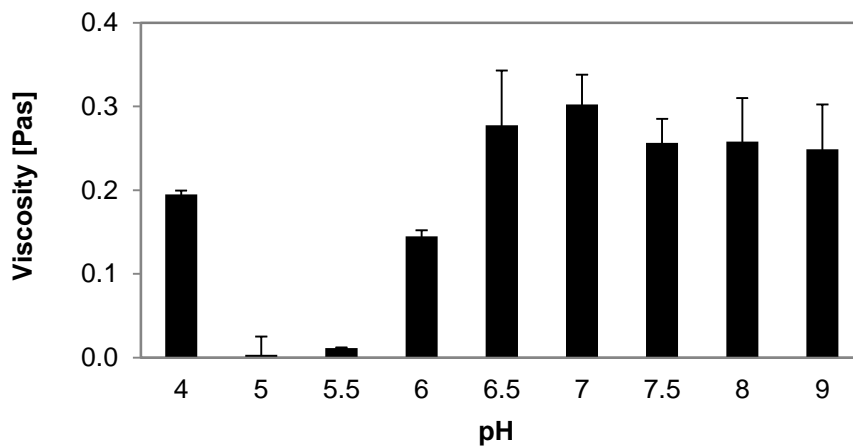


Figure 57: Viscosity of suspensions containing 300 mg/mL API and 2 mg/mL DMPG as a function of pH at $\dot{\gamma} = 12.6$ 1/s. Error bars represent standard deviations from triplicate measurements.

Yield points are generally high for all pH values but suspensions at pH 6 tend to offer a lower yield point (Figure 58). The fitting cannot be performed for pH 5 and 5.5 as these suspensions of low viscosity exhibit not yield point (calculated value is 0).

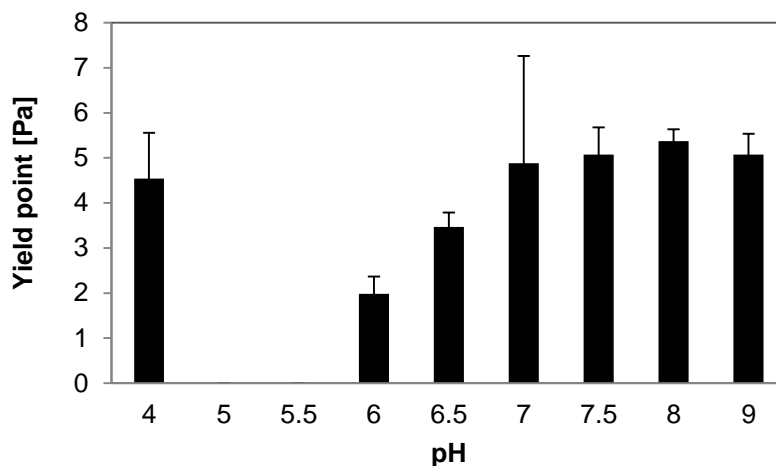


Figure 58: Influence of pH on yield point (calculated by the Casson model) of suspensions with 300 mg/mL API and 2 mg/mL DMPG as a function of pH. Error bars represent standard deviations from triplicate measurements.

When comparing the viscosity results to suspensions in WfI only it can be noted that the viscosity is strongly reduced over the whole pH-range when the phospholipid is added (Figure 59, Figure 60). At pH 5.5, the viscosity of suspensions in WFI tends to be the highest, whereas suspensions with DMPG display a viscosity minimum at this pH.

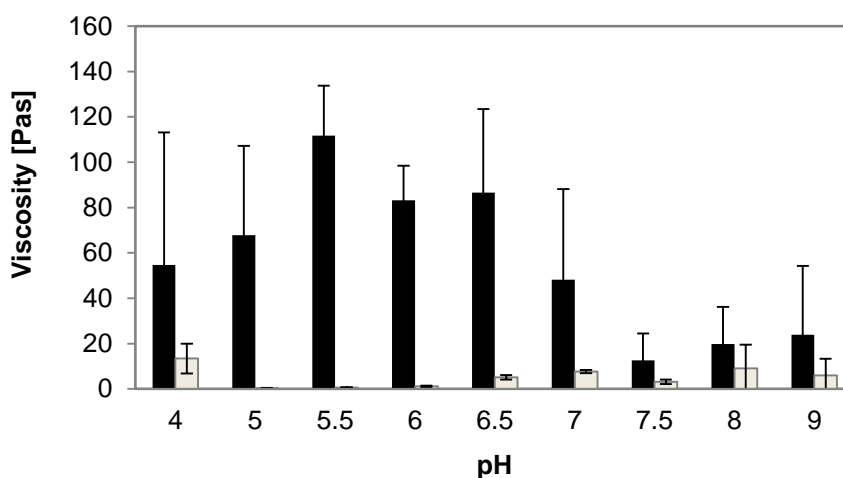


Figure 59: Viscosity of suspensions with 300 mg/mL API (black) and 2 mg/mL DMPG (white) compared to 300 mg/mL suspensions in WfI as a function of pH ($\dot{\gamma} = 0.2 \text{ 1/s}$). Error bars represent standard deviations from triplicate measurements.

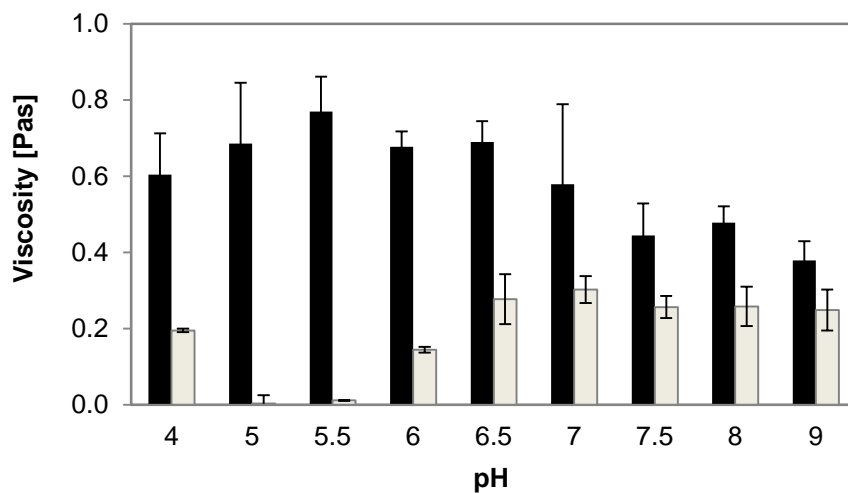


Figure 60: Viscosity of suspensions with 300 mg/mL API (black) and 2 mg/mL DMPG (white) compared to 300 mg/mL suspensions in Wfl as a function of pH ($\dot{\gamma} = 12.6$ 1/s). Error bars represent standard deviations from triplicate measurements.

These low viscous DMPG suspensions at pH 5 - 6 show a very low sediment volume compared to the suspensions at higher pH (Figure 61) with a sedimentation degree F of 0.55 at pH 5.5 compared to 0.99 at pH 7.

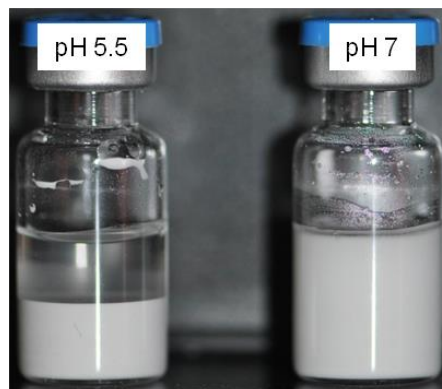


Figure 61: Sediment of suspensions containing 300 mg/mL API and 2 mg/mL DMPG at pH 5.5 (left) and pH 7 (right) after 4 hours.

The micrographs of suspended particles at the lower pH value show separated, individual particles, while suspensions at pH 7 contain agglomerates indicating a flocculated system (Figure 62).

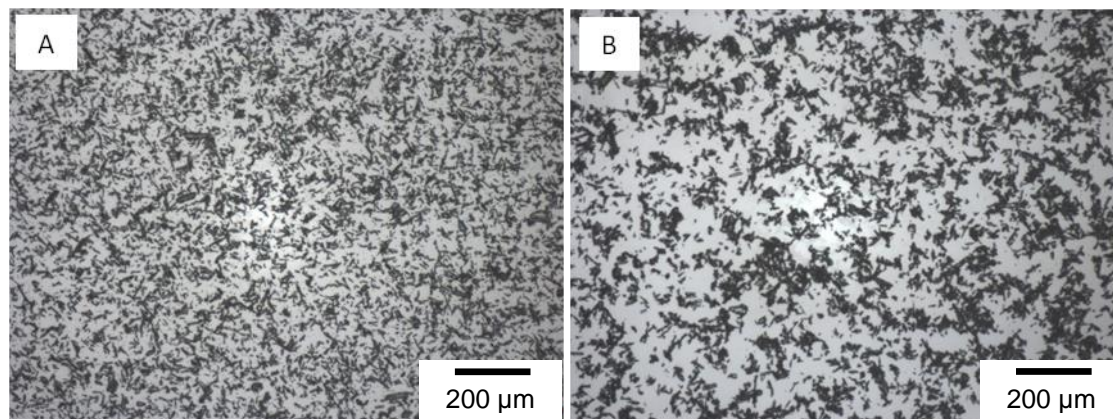


Figure 62: Microscopic pictures of suspensions containing 300 mg/mL API and 2 mg/mL DMPG at pH 5.5 (A) and pH 7 (B) after 1:10 dilution. Bar corresponds to 200 μm .

This result gives rise to the conclusion that the suspensions at pH 5.5 are deflocculated systems that are characterized by non-agglomerated particles which usually settle more slowly compared to flocculated particles. Nevertheless, the sedimentation velocity depends on the particle size and concentration. In case for suspensions at pH 7 particles agglomerate and built an inner, scaffold-like structure leading to a complete hindrance of sedimentation and high viscosity in combination with the high concentration. In case for suspensions at pH 5.5 no inner structure is built and thus, particles settle.

The corresponding Zeta potential results of suspensions containing 15 mg/mL API and 2 mg/mL DMPG dependent on pH are shown in Figure 63 in comparison to the suspensions in WfI and 2 mg/mL DMPG dispersions. The Cilengitide concentration was limited to 15 mg/mL as higher concentrations did not show an evaluable signal. But comparable Zeta potential results are found for the low-concentrated suspension (-67.6 ± 1.5 mV) and saturated solution (-73.4 ± 7.6 mV) at pH 6 indicating that similar interaction occurs for dissolved or suspended Cilengitide, respectively.

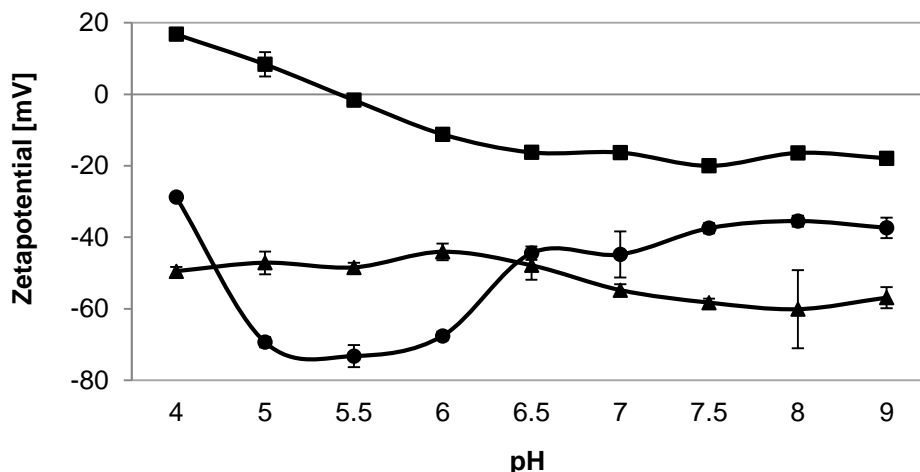


Figure 63: Zeta potential of 2 mg/mL DMPG dispersions (▲), suspensions with 15 mg/mL in WfI (■) and with 2 mg/mL DMPG (●) as a function of pH. Error bars represent standard deviations from triplicate measurements.

In the considered range, the Zeta potential of the DMPG-containing suspensions is always negative in contrast to the potential of suspensions in WfI. There is a Zeta potential maximum observed at pH 5 - 6, the same pH range the 300 mg/mL in which suspensions exhibit the lowest viscosity and the Cilengitide suspended in water exhibit its isoelectric point (pH 5.5). The Zeta potential at this maximum is even higher than the Zeta potential of the dispersed DMPG vesicles at this pH. Above pH 6.5, the Zeta potential of suspensions with 2 mg/mL DMPG increases and becomes less negative, whereas suspensions in WfI show a constant potential. The DMPG vesicles exhibit a more or less constant potential from pH 4 to 6.5. Above pH 6.5, they tend to become more negatively charged and the observed potential becomes even more negative than the API particles suspended in 2 mg/mL DMPG. At pH 6.5, the suspended particles and the DMPG vesicles exhibit a similar potential.

To observe the effect of the DMPG concentration on the Zeta potential as well as to confirm the interaction between the Cilengitide and the phospholipid, the DMPG concentration is varied (Figure 64) and later on, the supernatant of the samples is replaced by saturated API solution (Figure 65). The results for suspensions show a comparable Zeta potential for different DMPG concentrations between 0.05 and 2 mg/mL. A difference dependent on the DMPG amount is detected at pH 6, where the Zeta potential becomes less negative with decreasing amount of DMPG. The constant Zeta potential shows that the maximum amount of DMPG is attached to the particles by adding 0.05 mg/mL of the phospholipid. In contrast, the absolute value of the Zeta potential of the suspended particles with 0.01 mg/mL DMPG is lower in a wide pH range of 4 – 7 leading to the conclusion that the particle surface is not completely covered with DMPG molecules. However, the Zeta potential is constant for all suspensions with 0.01 to 2 mg/mL

DMPG added at pH 7.5 – 9 suggesting that the maximum interaction potential of DMPG with negatively charged Cilengitide particles is less and is already reached with the lowest DMPG concentration.

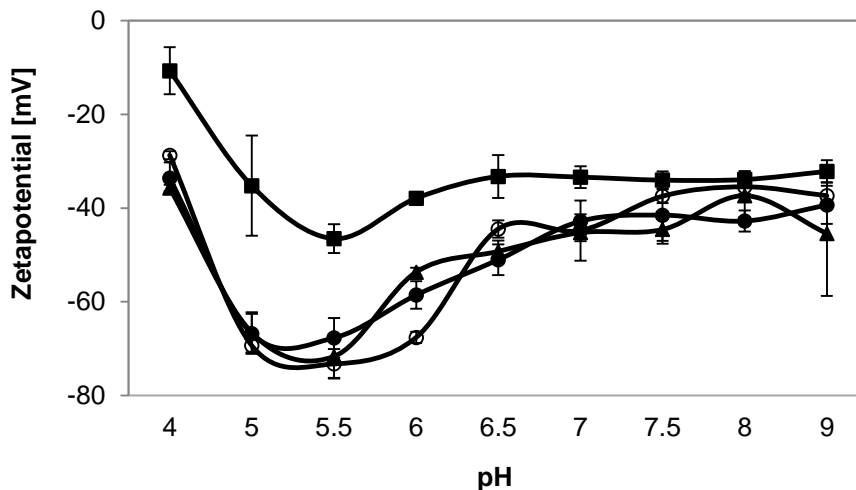


Figure 64: Zeta potential of suspensions with 15 mg/mL API and 0.01 mg/mL (■), 0.05 mg/mL (▲), 0.1 mg/mL (●) and 2 mg/mL (○) DMPG as a function of pH. Error bars represent standard deviations from triplicate measurements.

The Zeta potential becomes less negative when the supernatant is replaced (Figure 65). At pH 4 and above 7 the Zeta potential is constant after the first replacement. In the range of pH 5 to 6.5 the Zeta potential further decreases with the second replacement indicating that loosely bound or unbound DMPG molecules are present. In general, this result confirms that API particles are detected and not DMPG structures.

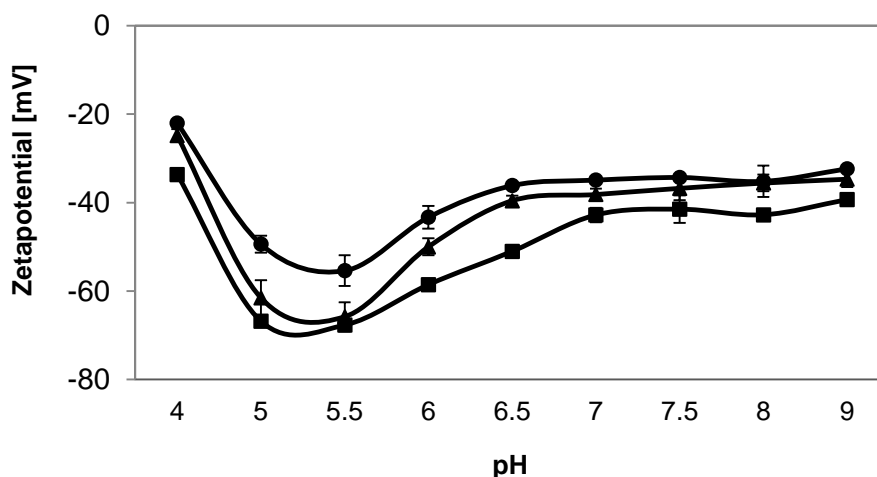


Figure 65: Zeta potential of suspensions containing 15 mg/mL API (■) and with supernatant replaced once (▲) and twice (●) as a function of pH. Error bars represent standard deviations from triplicate measurements.

The Zeta potential results of suspensions containing DMPG in different concentrations and with replaced supernatants lead to the conclusion that the interaction between DMPG and Cilengitide depend on the pH of the suspensions. The most pronounced interaction seems to occur around the isoelectric point (pH 5 - 6), where the pure Cilengitide particles suspended in water are overall uncharged but exhibit a highly negative potential in suspensions with DMPG. The extent of interaction seems to be less at pH values above pH 6.5 and at pH 4 compared to pH 5 - 6. At pH 4, the absolute value of Zeta potential is generally the lowest. Additionally, suspensions at pH 4 and 6 show a concentration dependent Zeta potential. The potential is constant for suspensions from pH 7 - 9 and almost independent from the amount of DMPG added. The supernatant replacement steps lower the potential value, but only marginally. Zeta potential measurements of 15 mg/mL Cilengitide suspensions with 150 mM NaCl added show a shift of the isoelectric point of Cilengitide particles to approximately pH 4 (Figure 66). The NaCl-containing suspensions with 2 mg/mL DMPG offer deflocculation at pH 4 confirming the stronger interaction between DMPG and API around the isoelectric point as shown for suspensions without NaCl. However, the suspensions with 15 mg/mL Cilengitide, 2 mg/mL DMPG and 150 mM NaCl do not show a Zeta potential maximum. The Zeta potential remains fairly constant at around -40 mV for pH 5.5 to pH 9 and decreases to -36 mV at pH 5 or -24 mV at pH 4, respectively. The addition of 150 mM NaCl seems to quench the Zeta potential differences due to the strong compression of the double layer.

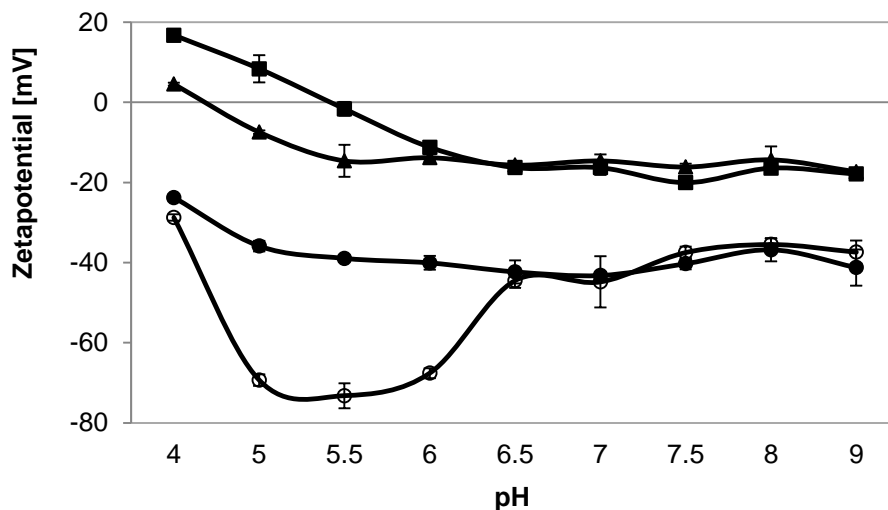


Figure 66: Zetapotential of suspensions with 15 mg/mL API in Wfl (■), with 9 mg/mL NaCl (▲), 2 mg/mL DMPG (○) and with 2 mg/mL DMPG and 9 mg/mL NaCl (●). Error bars represent standard deviations from triplicate measurements.

In summary, turbidity, DLS, Cryo-TEM and NMR analysis results confirm the interactions between dissolved Cilengitide and DMPG molecules. The addition of Cilengitide to the DMPG dispersion leads to the destruction of bilayer structures seen in Cryo-TEM pictures due to

interactions with Cilengitide as demonstrated by NMR. Electrostatic interactions between the negatively charged phosphate groups and the positively charged Cilengitide particles at pH 4 could not be detected due to the overlap of the phosphate group signal with the Cilengitide arginine signal around 4 ppm. Interaction between suspended Cilengitide particles and dispersed DMPG molecules are confirmed by Zeta potential measurements. Most pronounced interaction between Cilengitide and DMPG is seen around the isoelectric point. Comparable Zeta potential results of the low-concentrated suspensions and the saturated solution (-73.4 ± 7.6 mV) indicate that observed interaction mechanisms in solution are also present for suspensions.

6.1.6 Interaction model for Cilengitide and DMPG at varying pH values

Based on the measured results an interaction model explaining the varying fluidity of suspensions at pH 4, 5.5 and 7 is conceived (Figure 67 a - c). The Cilengitide particles in water are positively charged at pH 4, in total neutral at pH 5.5 and negatively charged at pH 7. Generally, the hydrophobic amino acids are orientated outwardly as known from single-crystal structure analysis (see chapter 4.1). Furthermore, dissolved API has to be taken into account since more dissolved API molecules are in the environment of a solid particle than DMPG molecules (API solubility 6 mg/mL).

At pH 4 (Figure 67 a), the Zeta potential of the Cilengitide particles is positive, whereas DMPG molecules are negatively charged (pKs ~ 3). In solution DMPG and Cilengitide interact leading to a negative Zeta potential by DMPG phosphate groups. Electrostatic interactions are also expected between the negatively charged phospholipid and positively charged protein. The dissolved API molecules may additionally interact with the negatively charged head group of DMPG as well as with the particle surface due to their surface-active properties (surface tension of a saturated API-solution 54.70 ± 1.38 mN/m). Agglomerates as observed by microscopy are due to physical particle interaction. The absolute value of the Zeta potential is lower compared to other pH-values, leading to the conclusion that the surface of the particle is not fully covered with negative DMPG molecules. Thus, the particles are enabled to network which causes the higher viscosity compared to pH 5.5.

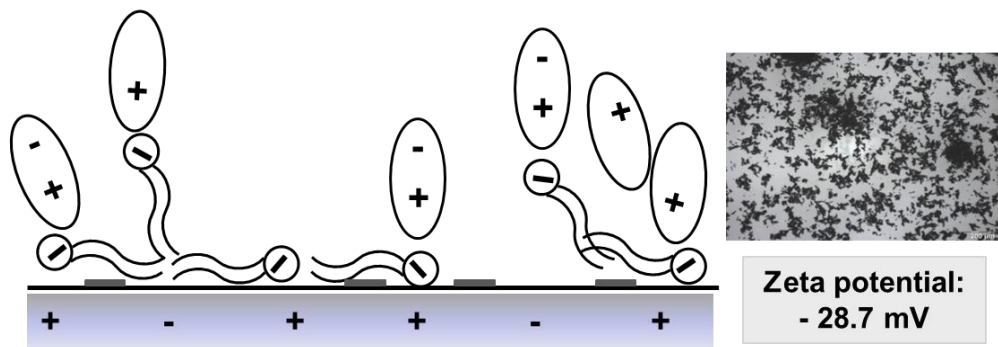


Figure 67 a: Interaction model at pH 4 demonstrating the interaction between a suspended API particle () with its hydrophobic sides (), DMPG () and dissolved API molecules ().

Figure 67 b shows the interactions model at pH 5.5 at which the API particles exhibit their isoelectric point in water. The hydrophobic interaction between the DMPG molecules and the net uncharged particle surface is strongest while electrostatic interaction between particle surface and DMPG is at a minimum. A very close packing of the DMPG molecules on the particle surface is enabled by the dissolved, zwitter-ionic API molecules which reduce the electrostatic repulsion between the negatively charged head groups of DMPG. Thus, a highly negative Zeta potential results. The high surface coverage with negatively charged molecules leads to separated suspended particles with minimal interparticle interaction and without agglomeration (see micrograph, Figure 67 b). This absence of a particle network leads to a low suspension viscosity. The separated particles sediment quite fast and build a closely packed sediment which has a high caking potential. Usually, deflocculated systems exhibit a slow sedimentation rate due to the smaller size of separated particles. In this case, the separated particles are large enough for a fast sedimentation. Additionally, due to the sedimentation the stabilizing potential barrier (repulsive forces) is overcome and a compact, hardly redispersible sediment is built.

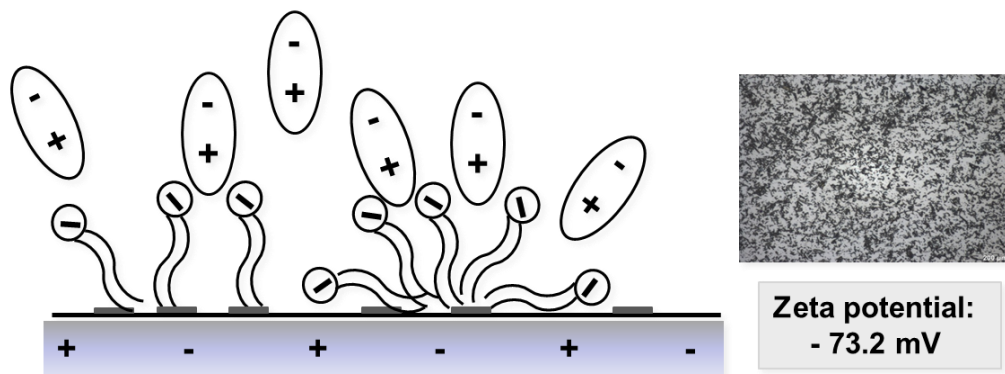


Figure 67 b: Interaction model at pH 5.5 demonstrating the interaction between a suspended API particle () with its hydrophobic sides (), DMPG () and dissolved API molecules ().

The zeta potential of particles at pH 7 is negative resulting in repulsive forces between suspended API and the negatively charged phospholipid (Figure 67 c). Nevertheless, some DMPG molecules are attached via hydrophobic interactions on the particle surface and potentially localized charge interaction, leading to a higher absolute zeta potential than pure API. Nevertheless, due to incomplete surface coverage, particles interact with each other and agglomerates are built. A flocculated structure is observed. This result in a higher viscosity of suspensions at pH 7 compared to pH 5.5.

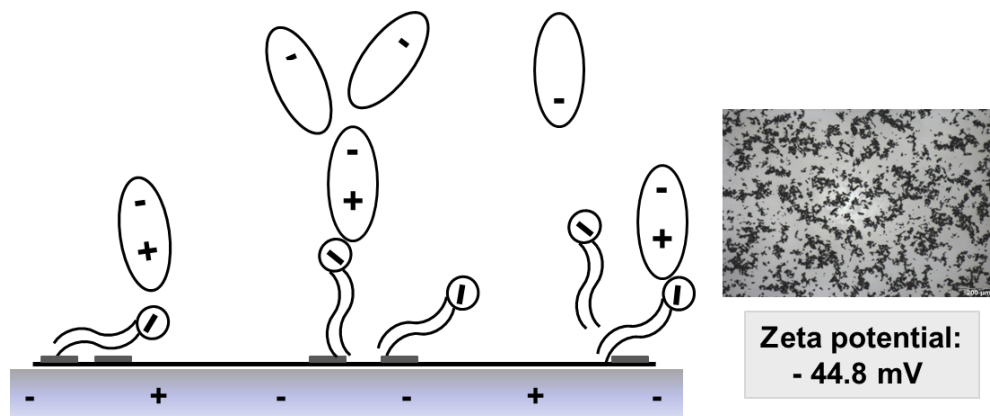


Figure 67 c: Interaction model at pH 7 demonstrating the interaction between a suspended API particle () with its hydrophobic sides (), DMPG () and dissolved API molecules ().

Overall, the viscosity at different pH-values correlates with the varying adsorbed amount of DMPG on the particle surface. A higher surface coverage increases electrostatic repulsions and decreases the interparticle attraction which have a significant impact at high concentrations.

6.1.7 Addition of phospholipids with alternative chain length to confirm the interaction model

In order to confirm the interaction model, DMPG is replaced by other phospholipids which differ in the length of the fatty acid moiety (C10: Didecanoylphosphoglycerol (DDPG), C12: Dilauroylphosphoglycerol (DLPG), C16: Dipalmitoylphosphoglycerol (DPPG), C18: Distearoylphosphoglycerol (DSPG)). The interaction of the phospholipid with the Cilengitide particle may depend on the length of the fatty acid, meaning the hydrophobicity and the size of the phospholipid. On the one hand side, the more hydrophobic phospholipids might interact stronger with the Cilengitide particles resulting in a higher viscosity reduction as compared to hydrophilic phospholipids with short fatty acid chain length. On the other hand side, smaller phospholipids with shorter fatty acid moieties might cover the surface more densely, leading to a more pronounced charge based repulsion and higher viscosity reduction. It is reported that phosphoglycerols with fatty acids longer than C11 or C12 support bilayer structures in water [97]. Whereas phosphoglycerols with shorter fatty acids form micelles in water due to their geometric constraints [97]. The zeta potential of suspensions containing 15 mg/mL API and 0.1 mg/mL phospholipids at pH 4, 5.5 and 7 as well as the viscosity of suspensions with 300 mg/mL API and 2 mg/mL phospholipid at the mentioned pH-values are determined.

Figure 68 A shows the viscosity at $\dot{\gamma} = 0.2 \text{ 1/s}$ for suspensions containing the selected phospholipids at pH 4, 5.5 and 7. The viscosity of all suspensions is reduced at pH 5.5 compared to the other pH-values. The respective samples show a higher absolute zeta potential (Figure 69), leading to the conclusion that the surface is more covered with phospholipid molecules and thus, the attractive interaction between the Cilengitide particles is reduced resulting in a lower viscosity. Considering the influence of the fatty acid chains on the viscosity, no continuous trend is observed (Figure 68 A, $\dot{\gamma} = 0.2 \text{ 1/s}$). At pH 4, suspensions with the more hydrophilic DDPG and DLPG seem to have a significantly lower viscosity compared to the DMPG containing samples. The DPPG and DSPG containing samples show a similar viscosity as the DMPG formulation. At pH 5.5, the viscosity of the suspensions containing the alternative phospholipids is similar to the DMPG containing suspension except for DDPG. At pH 7 the DDPG or DLPG containing formulations seems to be less viscous than the DMPG, DPPG and DSPG containing formulations. However, it is seen that the measurement quality for DDPG and DLPG containing samples at pH 4 and 7 is possibly reduced leading to an apparently lower viscosity also indicated by a lower viscosity value detected during back shearing. At a shear rate of $\dot{\gamma} = 12.6 \text{ 1/s}$ all phospholipid containing formulations exhibit a

similar viscosity at pH 4 and 7 of approximately 0.2 Pas (Figure 68 B). At pH 5.5 the viscosity is significantly lower except for the formulation containing the phospholipid DPPG.

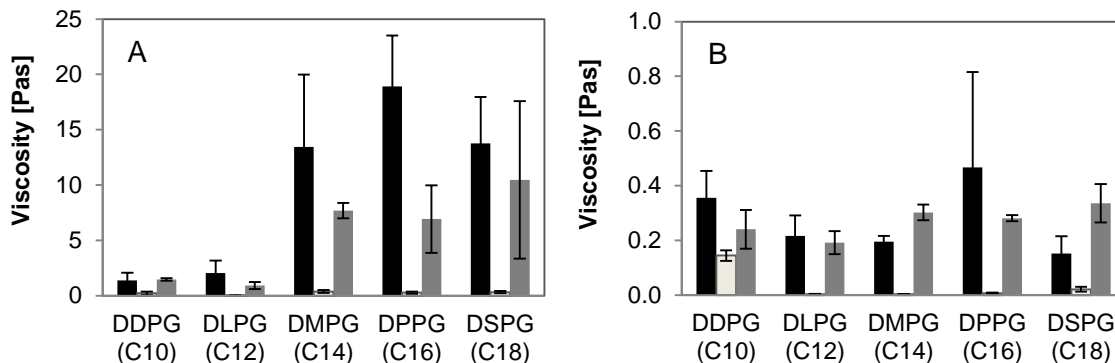


Figure 68: Viscosity of suspensions with 300 mg/mL API and 2 mg/mL alternative phospholipids (DDPG, DLPG, DPPG, DSPG) at pH 4 (black), pH 5.5 (white) and pH 7 (grey) compared with DMPG containing suspension at $\dot{\gamma} = 0.2$ 1/s (A) and $\dot{\gamma} = 12.6$ 1/s (B). Error bars represent standard deviation from triplicate measurements.

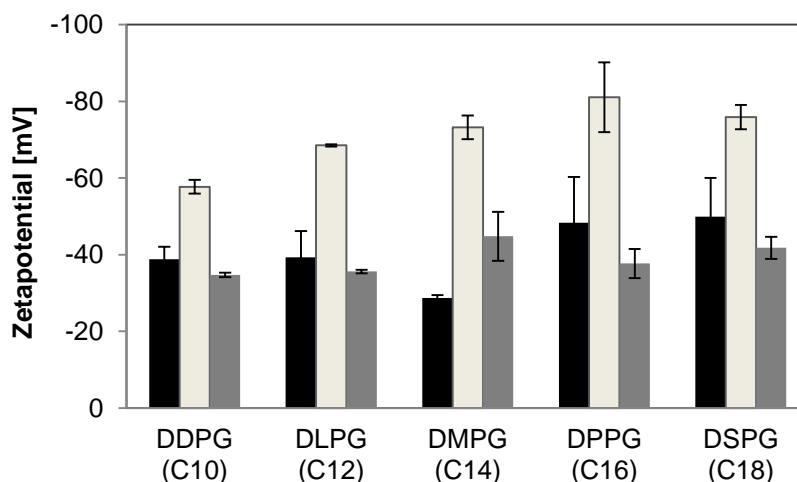


Figure 69: Zeta potential of suspensions with 15 mg/mL API and 2 mg/mL of alternative phospholipids (DDPG, DLPG, DPPG, DSPG) at pH 4 (black), pH 5.5 (white) and pH 7 (grey) compared with DMPG containing suspension. Error bars represent standard deviation from triplicate measurements.

At a typical shear rate applied during injection with a 25 Gauge needle ($\dot{\gamma} = 1000$ 1/s) the samples with the alternative phospholipids tend to be more viscous at pH 7 than the DMPG containing samples (Figure 70). At pH 5.5, the above mentioned higher viscosity of the suspension with DDPG is found again. All the other samples show similar viscosity. At pH 4 the suspension with DMPG tend to be less viscous than samples with the alternative phospholipids.

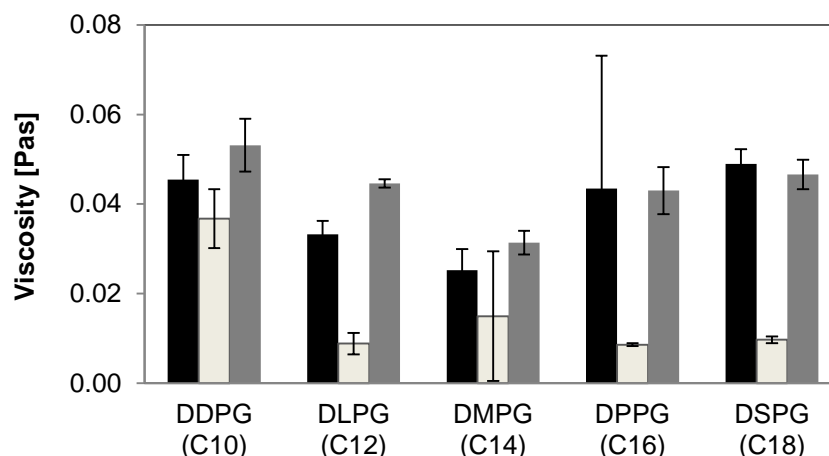


Figure 70: Viscosity of suspensions with 300 mg/mL API and 2 mg/mL of alternative phospholipids (DDPG, DLPG, DPPG, DSPG) at pH 4 (black), pH 5.5 (white) and pH 7 (grey) compared with DMPG containing suspension at $\dot{\gamma} = 1000$ 1/s. Error bars represent standard deviation from triplicate measurements.

In summary the viscosity of all phospholipid containing suspensions is reduced at pH 5.5 compared to pH 4 and 7, confirming the interaction model. However, these formulations are deflocculated systems with a high caking potential and thus, not suitable as final formulation. The viscosity of the suspensions does not depend on the added phospholipid. Only at the highest shear rate a lower viscosity is detected for suspensions containing DMPG. Finally, for stability studies suspensions with 2 mg/mL DMPG at pH 7 are evaluated (see chapter 6.2).

6.1.8 Polysorbate 80 and sorbitan monooleate as alternative surfactants

In addition to the phospholipids as viscosity reducing agent, more commonly used non-ionic surfactants are tested with respect to their influence on the viscosity of the highly concentrated suspension. Polysorbate 80 (PS 80) as well as sorbitan monooleate (SO) were selected as they are acceptable for parenteral use and a wide HLB range can be covered by using mixtures of both components at different ratios. PS 80 itself with a HLB value of 15 and mixtures which cover a HLB range between 11.8 and 7.5 were tested (Table 10). Pure SO with a HLB value of 4.3 could not be used as it cannot be dispersed in water due to its high hydrophobicity. Additionally, the concentration of the added mixtures is varied from 1 to 10 mg/mL.

| PS 80 [%] | SO [%] | HLB value |
|-----------|--------|-----------|
| 100 | 0 | 15 |
| 70 | 30 | 11.8 |
| 60 | 40 | 10.7 |

| | | |
|--------------------------|-----|-----|
| 50 | 50 | 9.7 |
| 40 | 60 | 8.6 |
| 30 | 70 | 7.5 |
| 0 | 100 | 4.3 |
| Not dispersible in water | | |

Table 10: HLB values of different mixture ratio of PS 80 / SO mixtures.

Figure 71 shows the viscosity of suspensions containing 2 mg/mL PS 80/SO mixtures at $\dot{\gamma} = 0.2$ 1/s. The viscosity of the suspension in Wfl is significantly higher than the viscosity of suspensions containing 2 mg/mL surfactant mixtures with a HLB of 11.8 (mixing ratio 70/30) and less. The addition of PS 80 only does not lower the viscosity significantly, possibly due to lower surface interaction and thus, higher particle interaction. This suspension is still too viscous to draw 1 mL out of the vial within 20 s. The suspensions containing different ratios show similar viscosity and are comparable viscous to DMPG containing suspensions.

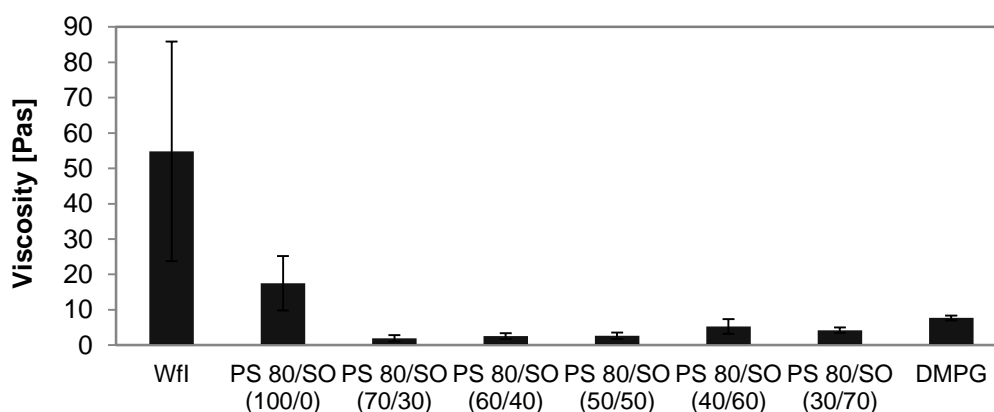


Figure 71: Viscosity of suspensions with 300 mg/mL API and 2 mg/mL PS 80/SO mixtures compared to Wfl and 2 mg/mL DMPG at $\dot{\gamma} = 0.2$ 1/s and pH 7. Error bars represent standard deviation from triplicate measurements.

The Zeta potential of Cilengitide particles is not affected by the addition of the non-ionic surfactant mixtures (Figure 72). Suspensions containing 15 mg/mL Cilengitide and 2 mg/mL PS 80/O mixtures show an absolute value of approximately -19.2 ± 2.4 mV compared to -16.3 ± 1.4 mV for 15 mg/mL Cilengitide in Wfl. A significantly higher potential is seen for suspensions with 0.1 mg/mL DMPG (-44.8 ± 6.4 mV).

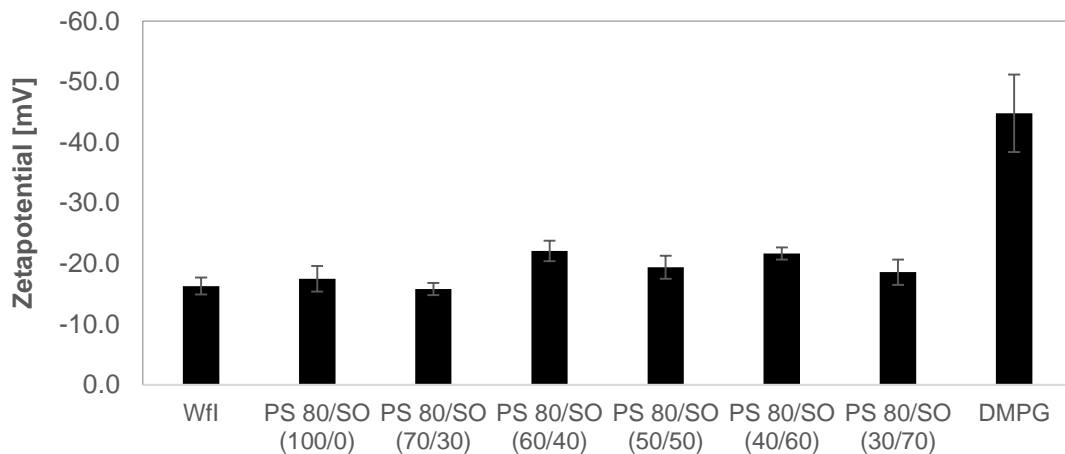


Figure 72: Zeta potential of suspensions with 15 mg/mL API and 2 mg/mL PS 80/SO mixtures compared to Wfl and 0.1 mg/mL DMPG at pH 7. Error bars represent standard deviation from triplicate measurements.

The effect of surfactant concentrations on the viscosity of the suspension is shown in Figure 73 at the lowest shear rate ($\dot{\gamma} = 0.2$ 1/s). The viscosity of suspensions with pure PS 80 depends on the concentration and lower values result with 5 mg/mL PS 80 or more. Nevertheless, the results vary widely and differ not significantly. The viscosity of the suspensions with 70/30 and 60/40 mixtures do not depend on concentration. Suspensions with 50/50 mixtures tend to be less viscous with increasing surfactant concentrations. Considering the more lipophilic mixtures (40/60 and 30/70) the suspensions with 7.5 or 10 mg/mL are more viscous than suspensions with lower concentrations. This might be an effect of the higher viscosity of the surfactant dispersion itself. Figure 74 shows the viscosity of the placebo surfactant mixtures (without API). It is seen that the viscosity of the two most lipophilic mixtures at the highest concentrations (7.5 and 10 mg/mL) is markedly higher compared the other.

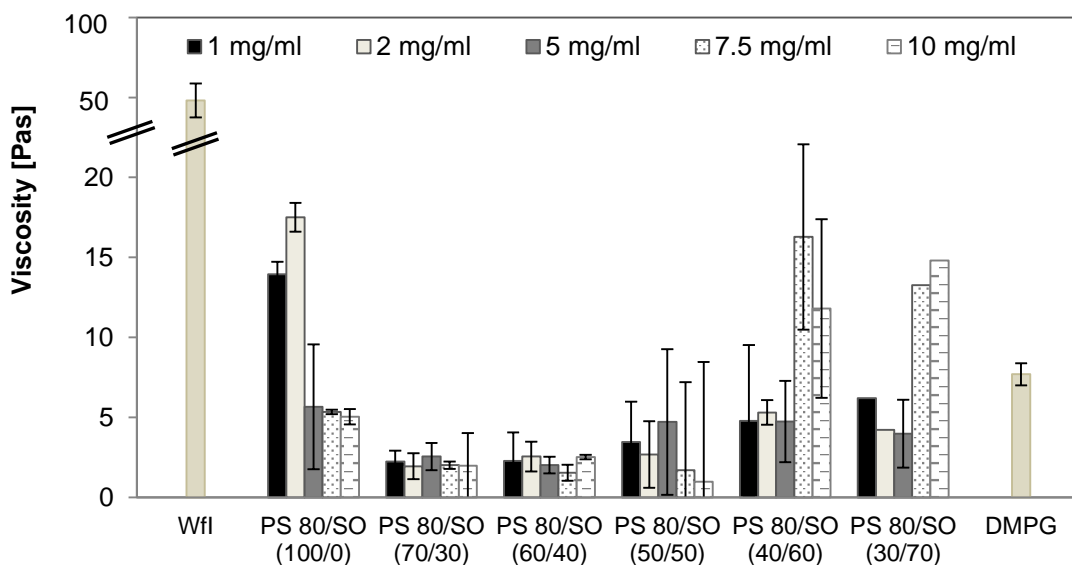


Figure 73: Viscosity of 300 mg/mL API suspensions as a function of mixing ratio and surfactant concentration compared to Wfl and 2 mg/mL DMPG at $\dot{\gamma} = 0.2 \text{ 1/s}$ (pH 7). Error bars represent standard deviation from triplicate measurements.

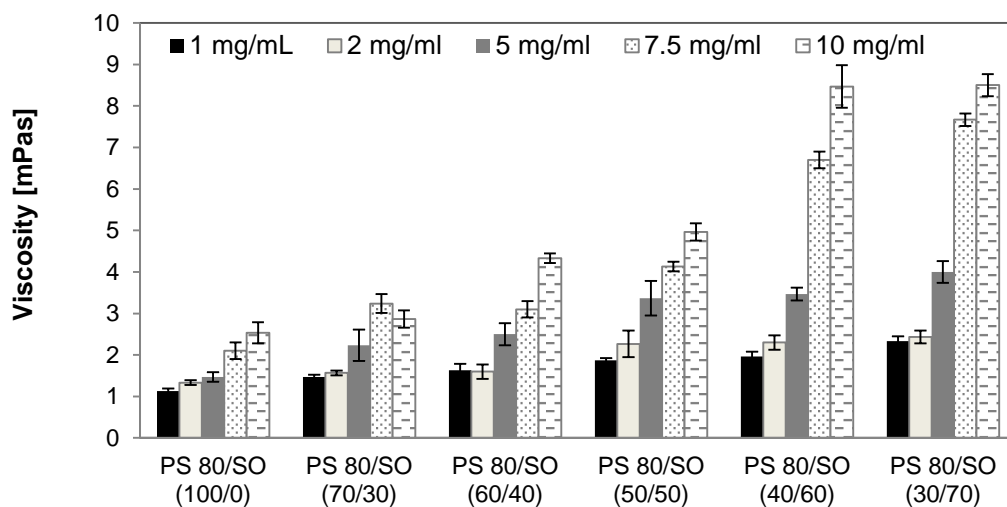


Figure 74: Viscosity of surfactant dispersions (without API) as a function of mixing ratio and surfactant concentration at $\dot{\gamma} = 0.2 \text{ 1/s}$ (pH 7). Error bars represent standard deviation from triplicate measurements.

At medium shear rates no significant differences between DMPG and PS 80/SO mixtures are observed while the aqueous suspension is more viscous. Suspensions with PS 80 only tend to be more viscous than suspensions with SO included, but the differences are not significant. At this medium shear rate, the viscosity is a complex function of solid and liquid properties [40] so that the observed differences at lower shear rates obviously level off.

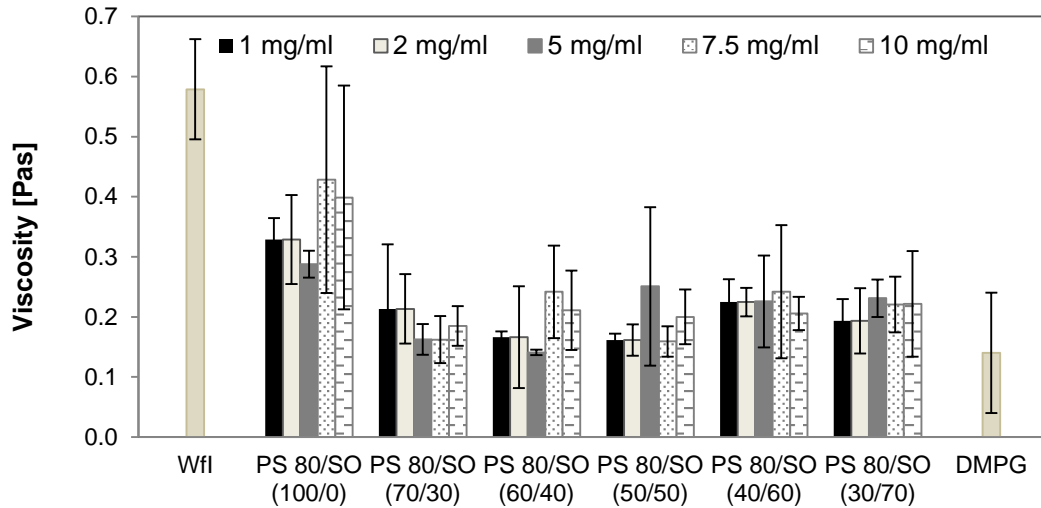


Figure 75: Viscosity of 300 mg/mL API suspensions as a function of mixing ratio and surfactant concentration compared to Wfl and 2 mg/mL DMPG at $\dot{\gamma} = 12.6$ 1/s (pH 7). Error bars represent standard deviation from triplicate measurements.

At the high shear rate $\dot{\gamma} = 1000$ 1/s only suspensions with PS 80/SO mixtures 40/60 and 30/70 at 5 and 10 mg/mL concentrations yield lower viscosity values than the Wfl samples. The viscosity of all the other suspensions is comparable to the Wfl and DMPG suspensions. An influence of surfactant concentration is seen for suspensions with 50/50, 40/60 and 30/70 mixtures. Nevertheless, all of the formulations are suitable with respect to the syringeability as even the Wfl suspension can be injected with a 25 Gauge needle.

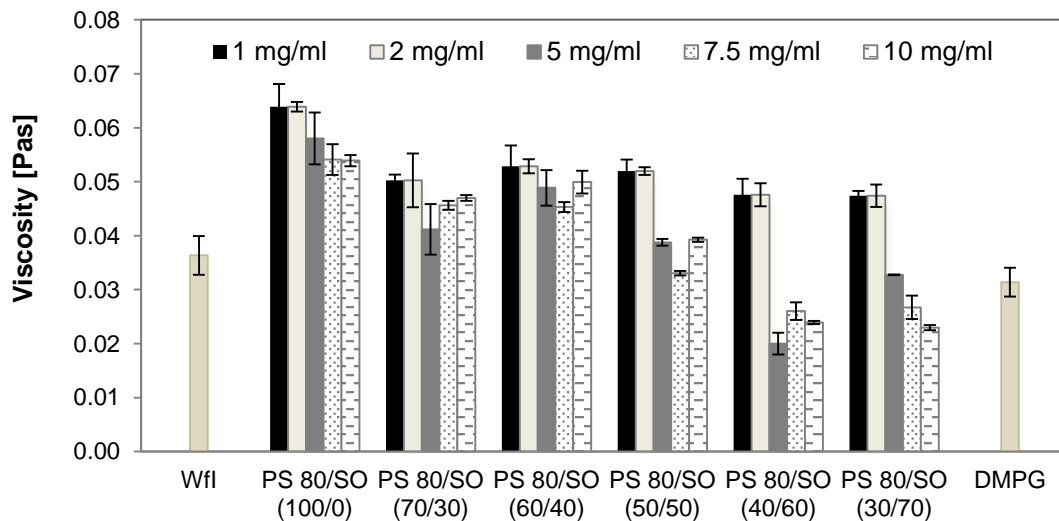


Figure 76: Viscosity of 300 mg/mL API suspensions as a function of mixing ratio and surfactant concentration compared to Wfl and 2 mg/mL DMPG at $\dot{\gamma} = 1000$ 1/s (pH 7). Error bars represent standard deviation from triplicate measurements.

These results lead to the conclusion that the addition of varying amounts of PS 80 does not lower the viscosity sufficiently due to insufficient particle surface interaction. Suspensions with mixtures exhibiting a HLB 11.8 and lower are considerably less viscous in the low shear range than the Wfl and PS 80 samples. No obvious dependency on the HLB value and the added amount can be detected at the lowest shear rate. At the highest shear rate, lower viscosities were observed for suspensions with higher concentrated hydrophobic surfactant mixtures. In conclusion, 5 mg/mL PS 80/SO 40/60 is chosen for further investigations due to the viscosity-reducing efficiency at mainly lower, but also higher shear rates.

6.1.9 Influence of pH on viscosity of suspensions containing 2 mg/mL DMPG or 5 mg/mL PS 80/SO (40/60)

Additionally, it was to be investigated if the viscosity of suspensions with 5 mg/mL of the 40/60 mixture depends on the pH as seen for DMPG containing samples. In contrast to DMPG, PS 80 and SO are nonionic molecules and thus, potentially less sensitive to changes in pH value. Nevertheless, the interaction with the net uncharged API molecule in solution and API particle surface might be stronger at pH 5.5 leading to a lower viscosity. Figure 77 A shows the viscosity of all suspensions dependent on pH at $\dot{\gamma} = 0.2 \text{ 1/s}$. The viscosity of PS 80/SO containing samples is not affected by pH. In contrast to the DMPG containing suspensions the formulations with the surfactant mixture are physical stable, flocculated systems within the investigated pH range, making the suspensions more robust to pH variation. Nevertheless, all PS 80/SO or DMPG containing suspensions have a lower viscosity than the Wfl suspension at the physiologically relevant pH value (pH 7). At a medium shear rate the viscosity of the surfactant mix containing suspensions tends to be even lower (at pH 6.5 and 7) than that of the DMPG containing suspensions (Figure 77 B). The viscosity of suspensions with the surfactant mixtures is also lower than that of the other systems at the highest shear rate ($\dot{\gamma} = 1000 \text{ 1/s}$) for pH 6 – 7 (Figure 77 C).

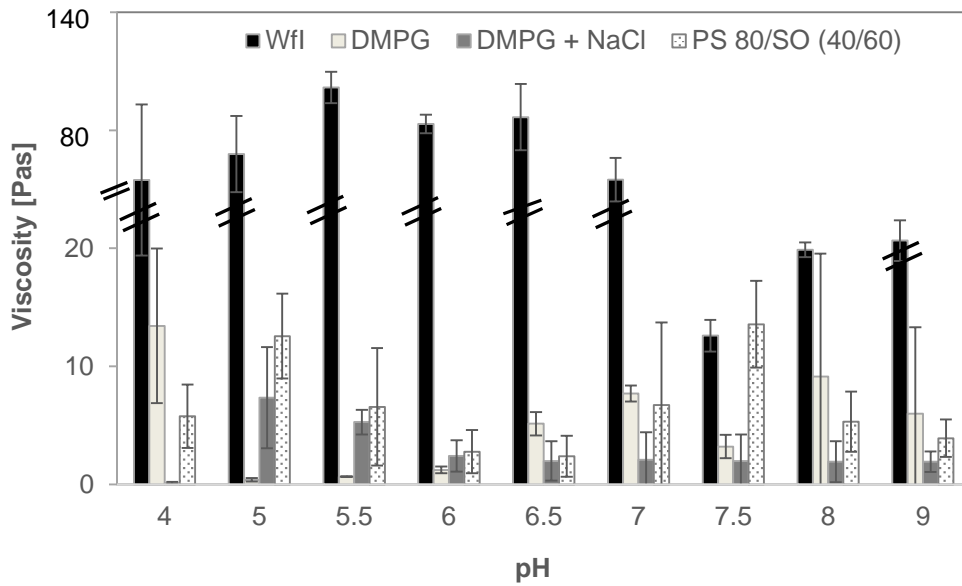


Figure 77 A: Viscosity of 300 mg/mL API suspensions in WfI, with 2 mg/mL DMPG, 2 mg/mL DMPG and 150 mM NaCl or 5 mg/mL PS 80/SO (40/60) as a function of pH at $\dot{\gamma} = 0.2$ 1/s. Error bars represent standard deviation from triplicate measurements.

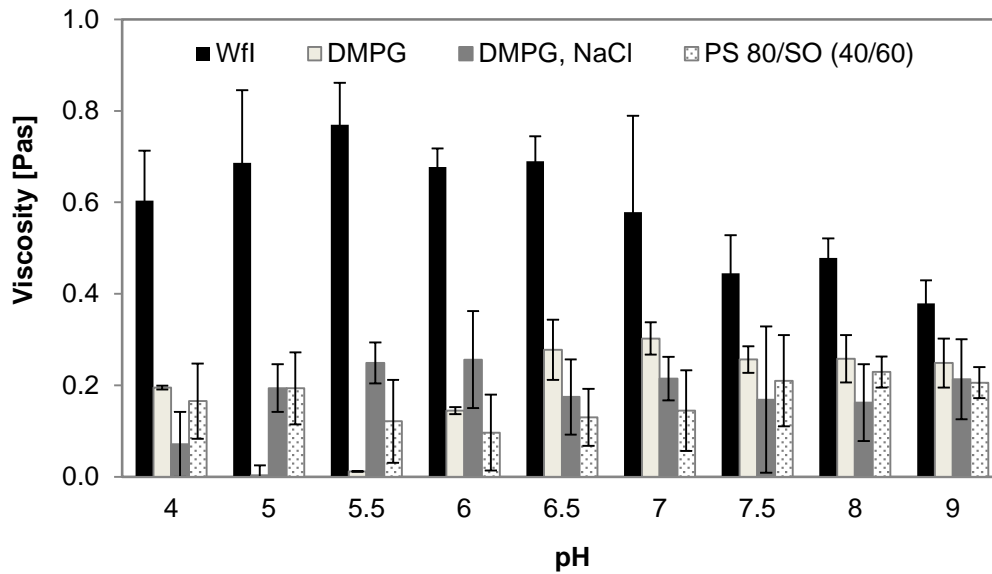


Figure 77 B: Viscosity of 300 mg/mL API suspensions in WfI, with 2 mg/mL DMPG, 2 mg/mL DMPG and 150 mM NaCl or 5 mg/mL PS 80/SO (40/60) as a function of pH at $\dot{\gamma} = 12.6$ 1/s. Error bars represent standard deviation from triplicate measurements.

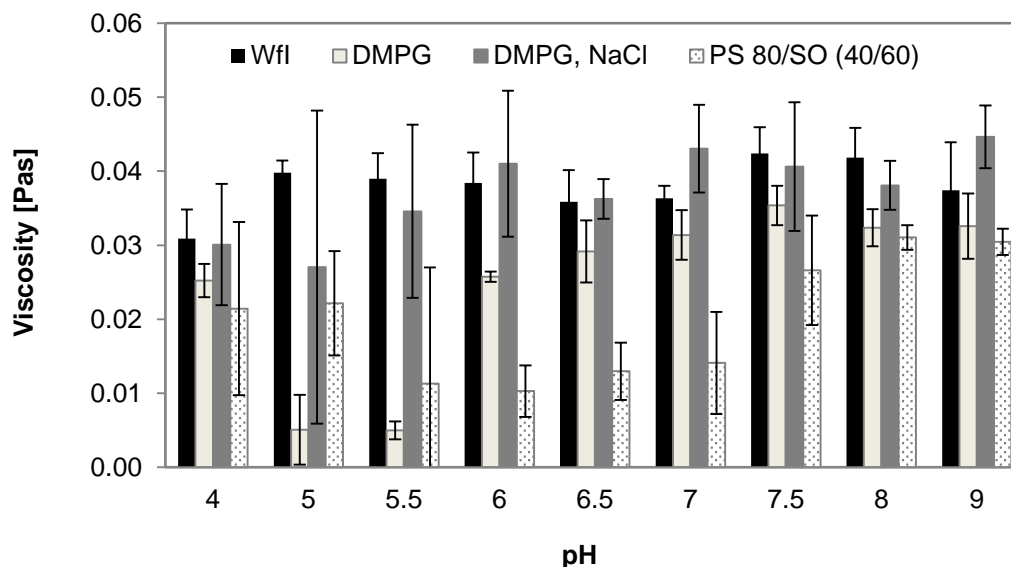


Figure 77 C: Viscosity of 300 mg/mL API suspensions in WfI, with 2 mg/mL DMPG, 2 mg/mL DMPG and 150 mM NaCl or 5 mg/mL PS 80/SO (40/60) as a function of pH at $\dot{\gamma} = 1000$ 1/s. Error bars represent standard deviation from triplicate measurements.

In conclusion, the viscosity of 300 mg/mL Cilengitide suspension could be reduced by the addition of surfactants. The addition of PS 80 only does not lower sufficiently the viscosity in the low shear range. At low and medium shear rates the viscosity of the suspensions does not show any dependency on HLB or surfactant concentration except for 7.5 or 10 mg/mL of PS 80/SO 40/60 and 30/70. These suspensions are more viscous possibly due to the higher viscosity of the surfactant dispersion itself. At the highest shear rate, suspensions with 5 mg/mL PS 80/SO 40/60 exhibit the lowest viscosity. For suspensions with 5 mg/mL PS 80/SO 40/60 no dependency on pH is seen for suspensions containing a surfactant mix. Furthermore, suspensions with 5 mg/mL PS 80/SO 40/60 tend to be less viscous at pH 6.5 and 7 than DMPG containing suspensions at $\dot{\gamma} = 12.6$ 1/s. Thus, the PS 80/SO formulations are robust systems and a suitable alternative to the use of phospholipids.

6.2 Physical stability during storage of suspensions containing 300 mg/mL Cilengitide and 2 mg/mL DMPG or 5 mg/mL PS 80/SO (40/60)

For a suspension with 2 mg/mL DMPG and 5 mg/mL PS 80/SO 40/60, 150 mM NaCl and 300 mM glucose the physical stability over one year storage at 2 – 8 °C was tested. All the suspension had an initial pH of 7.

6.2.1 Initial characteristics

The initial particle size distribution of the different formulations is shown in Figure 78. The smallest particles (D(0.05) and D(0.10)) are comparable in size for all suspensions. The surfactant mix containing formulations exhibit lower (D(0.50), D(0.90) and D(0.95)) values than the DMPG containing samples possibly indicating reduced particle interaction resulting in less or smaller agglomerates. This may correspond to lower viscosity values for the PS 80/SO containing suspensions at high shear rates (Figure 77 C). However, the microscopic pictures show comparable structures for the PS80/SO and phospholipid suspensions (Figure 79). The addition of NaCl or glucose does not affect the particle size of the suspensions.

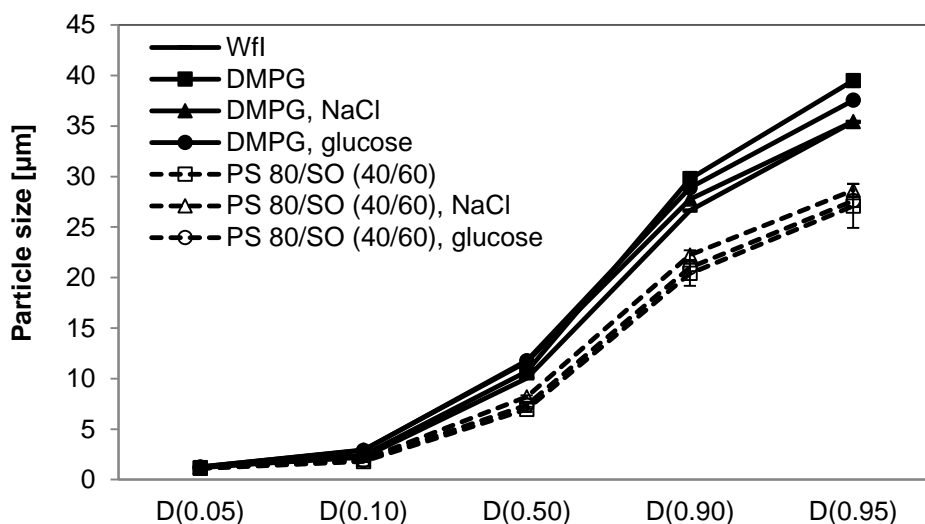


Figure 78: Particle size distribution of suspensions containing 300 mg/mL API in WfI, with 2 mg/mL DMPG or 5 mg/mL PS 80/SO (40/60) and 150 mM NaCl or 300 mM glucose after production.

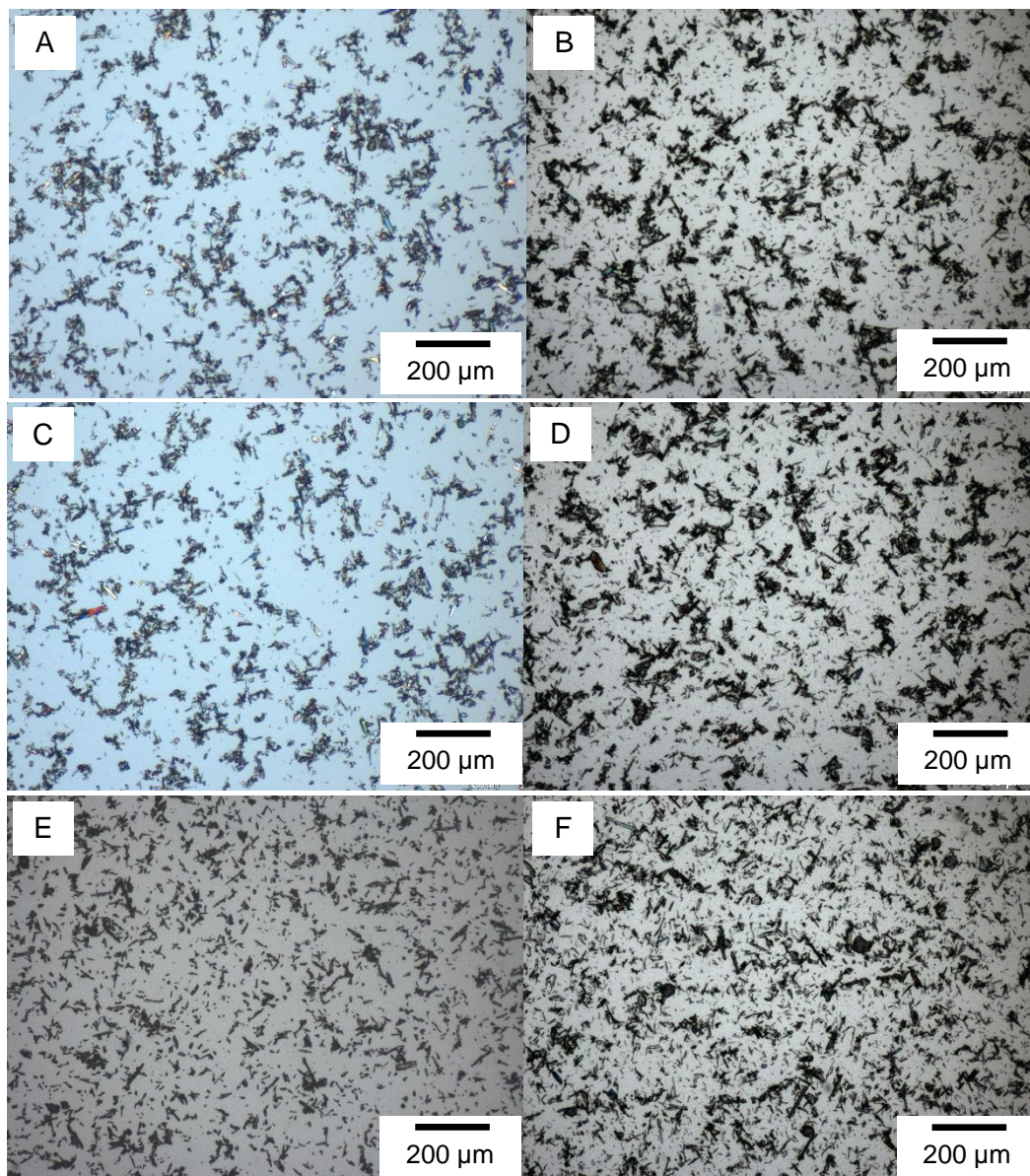


Figure 79: Microscopic pictures of suspensions with 300 mg/mL API and 2 mg/mL DMPG (A) and 150 mM NaCl (C) or 300 mM glucose (E) or 5 mg/mL PS 80/SO (40/60) (B) and 150 mM NaCl (D) or 300 mM glucose (F) diluted 1:10. Bar corresponds to 200 μm.

6.2.2 Particle size stability

Table 11 shows the result of the particle size stability. For a better overview only the values for D(0.05), D(0.50) and D(0.95) at the beginning and the end of storage are presented. All the suspensions show acceptable particle size stability for one year at 2 – 8 °C as particle size remains in the acceptable range.

Formulation development for 300 mg/mL Cilengitide suspensions

| Formulation | | D(0.05) [μm] | D(0.50) [μm] | D(0.95) [μm] |
|--|----------|---------------------------|---------------------------|---------------------------|
| Wfl | start | 1.22 | 10.03 | 35.42 |
| | 52 weeks | 1.39 | 13.31 | 44.79 |
| Relative increase [%] | | 13.9 | 32.7 | 26.5 |
| 2 mg/mL DMPG | start | 1.18 | 10.69 | 39.50 |
| | 52 weeks | 1.37 | 13.99 | 43.88 |
| Relative increase [%] | | 16.1 | 30.9 | 11.1 |
| 2 mg/mL DMPG, 9 mg/mL NaCl | start | 1.25 | 11.65 | 35.44 |
| | 52 weeks | 1.42 | 14.54 | 41.95 |
| Relative increase [%] | | 13.6 | 24.8 | 18.4 |
| 2 mg/mL DMPG, 50 mg/mL glucose | start | 1.25 | 11.78 | 37.55 |
| | 52 weeks | 1.54 | 13.78 | 42.69 |
| Relative increase [%] | | 23.2 | 17.0 | 13.7 |
| 5 mg/mL PS 80/SO (40/60) | start | 1.11 | 6.96 | 27.09 |
| | 52 weeks | 1.14 | 8.70 | 31.71 |
| Relative increase [%] | | 2.7 | 25.0 | 17.1 |
| 5 mg/mL PS 80/SO (40/60), 9 mg/mL NaCl | start | 1.16 | 8.11 | 35.08 |
| | 52 weeks | 1.17 | 9.34 | 38.52 |
| Relative increase [%] | | 0.9 | 15.2 | 9.8 |
| 5 mg/mL PS 80/SO (40/60), 50 mg/mL glucose | start | 1.15 | 7.37 | 27.60 |
| | 52 weeks | 1.15 | 8.74 | 30.84 |
| Relative increase [%] | | 0 | 18.6 | 11.7 |

Table 11: Particle size stability of suspensions with 300 mg/mL API and 2 mg/mL DMPG or 5 mg/mL PS 80/SO (40/60) and 150 mM NaCl or 300 mM glucose stored at 2-8 °C for one year.

For comparison, a formulation containing 2 mg/mL of the more hydrophilic phospholipid DSPE-PEG 2000 was evaluated. This formulation showed a more pronounced particle size increase as compared to the tested formulations (Table 12). The observed particle size increase correlates with solubility changes during storage. The solubility increases to 8.4 ± 0.4 mg/mL within 48 h and decreases again to 6.1 ± 0.2 mg/mL after 10 days. In contrast, the solubility for Cilengitide in Wfl or 2 mg/mL DMPG remains at 5 or 6 mg/mL during storage.

| Formulation | | D(0.05) [μm] | D(0.50) [μm] | D(0.95) [μm] |
|---------------------------|----------------------------------|---------------------------|---------------------------|---------------------------|
| 2 mg/mL DSPE- PEG 2000 | start | 1.28 | 11.94 | 37.09 |
| | 52 weeks | 2.53 | 18.57 | 52.59 |
| | Relative increase [%] | 50.6 | 64.3 | 70.5 |

Table 12: Particle size stability of suspensions with 300 mg/mL API and 2 mg/mL DSPE-PEG 2000 stored at 2 – 8 °C for one year.

6.2.3 Sedimentation rate of DMPG and PS 80/SO containing suspensions

Particles suspended in water build a flocculated system and show slow sedimentation. This is demonstrated by measuring the transmission over time for suspensions with 150 mg/mL API in Wfl and by determining the sedimentation degree for the highly concentrated samples (300 mg/mL API in Wfl). For transmission measurements, the Cilengitide concentration is limited to 150 mg/mL, otherwise the transmitted light signal is too low. Particles suspended in DMPG or PS 80/SO containing formulation may sediment faster due to the reduced particle interaction. But the rate may also be comparable due to the high solid content which possibly affects the rate more than the reduced interaction.

Suspensions with 150 mg/mL Cilengitide and the equivalent ratio of surfactant mix (2.5 mg/mL PS 80/SO 40/60) or DMPG (1 mg/mL) without isotonic agents show slow sedimentation with 3.1 $\mu\text{m}/\text{mL}$ for the DMPG containing suspension and 1.7 $\mu\text{g}/\text{mL}$ for the suspension in Wfl and in presence of the surfactant mix (Figure 80). Particles suspended in DMPG containing medium might sediment faster as they are more separated and thus, interact less with each other.

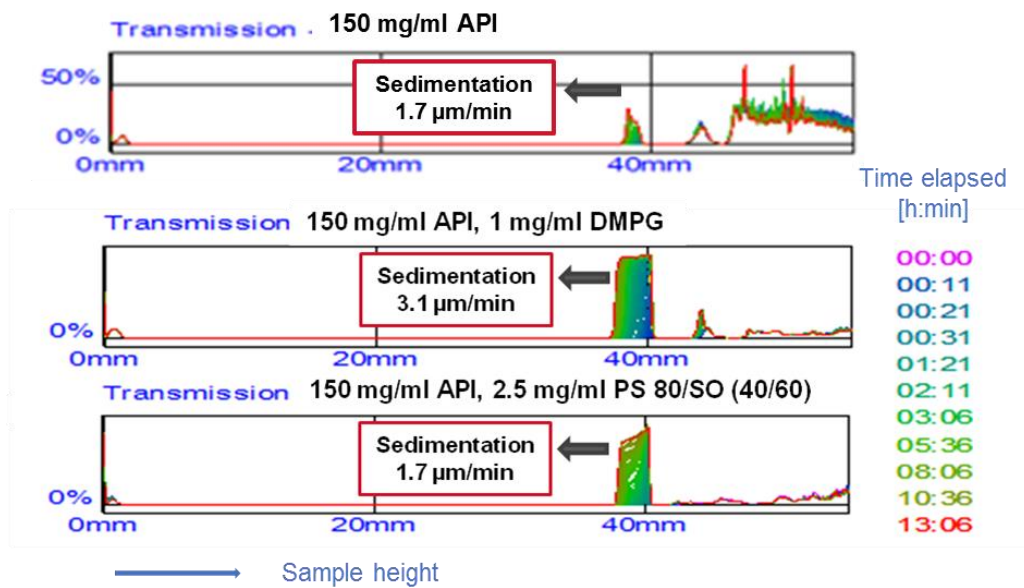


Figure 80: Transmission profile dependent on time and sample height and the calculated sedimentation rate of suspensions containing 150 mg/mL API in WfI (above), with 1 mg/mL DMPG (middle) or 2.5 mg/mL PS 80/SO (40/60) (below).

The sedimentation degree after one year of storage is shown in Figure 81. The PS 80/SO containing samples have a similar sedimentation degree as the suspension in WfI ($F = 0.86$). The samples with NaCl or glucose added are comparable. Without isotonicity agent F is slightly higher. Suspensions with DMPG show a much smaller sediment volume. It appears that the addition of DMPG disrupts the scaffold-like structure which is based on electrostatic repulsion of the particles. The separated particles build a more compact sediment. In contrast, the strongly interacting structure remains in presence of the PS 80/SO mix.

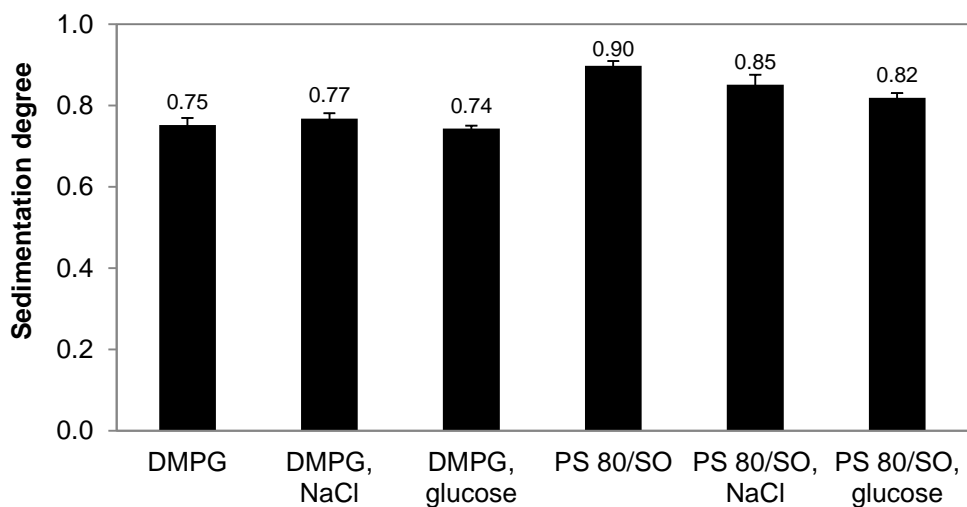


Figure 81: Sedimentation degree calculated for suspensions with 300 mg/mL API stored for one year (2 - 8 °C). Error bars represent standard deviation from triplicate measurements.

In general, the sedimentation rate of all tested formulations is low enough to allow for sufficient time to withdraw the homogenized suspension in reproducible doses from the vial. The overall high sedimentation degree suggests a good stability with respect to caking.

6.2.4 Resuspendability

According to the Ph. Eur. suspensions should be resuspendable with gentle shaking. Consequently, the time required for the resuspension of the formulations is determined as a function of storage time (Figure 82). Advantageous performance of the PS 80/SO samples is expected due to the less compressed sediment. Beads can be used to facilitate the resuspension [98]. Three metal beads made of stainless steel with a 1 mm diameter were added in some samples as indicated.

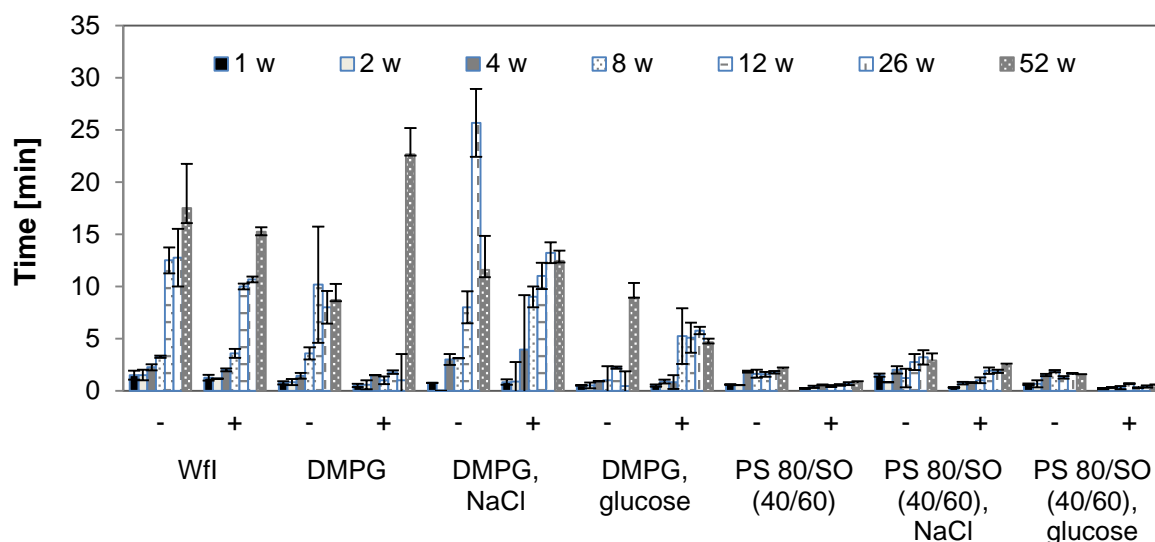


Figure 82: Time required for resuspension of formulations containing 300 mg/mL API, 2 mg/mL DMPG or 5 mg/mL PS 80/SO (40/60) and 150 mM NaCl or 300 mM glucose stored for one year at 2 – 8 °C with (+) or without (-) beads. Error bars represent standard deviation from triplicate measurements.

The suspensions in Wfl and with 2 mg/mL DMPG require comparable time for resuspension. The maximum time is about 25 min for the DMPG suspension with NaCl after 26 weeks of storage (without beads). For DMPG containing samples without isotonic agent beads generally reduce the time (except for the sample stored for 52 weeks) while the beads have no clear beneficial effect on the suspensions in Wfl and the DMPG formulations with NaCl or glucose. The NaCl containing samples tend to be more difficult to resuspend compared to the other DMPG formulations. Thus, the DMPG samples can be resuspended after storage up to 1 year, but the time required for resuspension becomes too long to be acceptable. In contrast, the

PS 80/SO containing samples are easily resuspendable in less than 3.2 ± 0.7 min up to one year and show lower variability as compared to the WfI and DMPG containing samples. The PS 80/SO 40/60 containing suspensions without isotonicity agent or with glucose added require less time to be resuspended as compared to NaCl containing samples, particularly with beads added. The glucose containing sample stored for one week and with beads added requires the minimum time for resuspension with only 0.2 ± 0.05 min. This advantage of the PS 80/SO systems is in line with the expectations due to the less compressed sediment after storage and the lower viscosities at the higher shear rates.

6.2.5 Syringeability

The syringeability during storage is compared by measuring the required time to draw out 1 mL of the formulation using a 25 Gauge needle (Figure 83). Contrary to the WfI suspensions, all analyzed formulations can be drawn out of the vial except for the DMPG containing suspension with NaCl and stored for 26 weeks. In this case, persistent agglomerates are observed which cannot be disintegrated by vigorous shaking (Figure 84). The DMPG containing suspensions require significantly more time to be withdrawn as compared to the PS80/SO samples. In some cases air bubbles have to be removed leading to the higher times for the DMPG samples. The addition of isotonicity agents does not influence the syringeability. Soft agglomerates are observed in case of samples containing DMPG and NaCl stored for 4 weeks, DMPG and glucose stored for 12 weeks and PS 80/SO and NaCl stored for 8 weeks. The soft agglomerates can be destroyed by manual, vigorous shaking contrary to the persistent agglomerates.

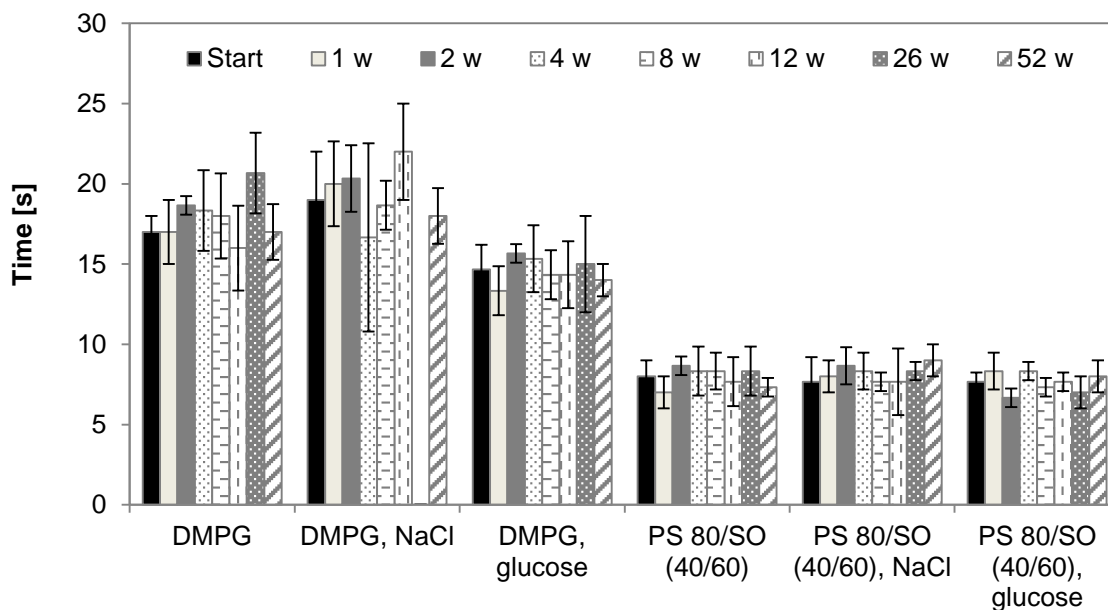


Figure 83: Time required for drawing out 1 mL of the vial for formulations containing 300 mg/mL API and 2 mg/mL DMPG or 5 mg/mL PS 80/SO (40/60) and 150 mM NaCl or 300 mM glucose stored for one year at 2 – 8 °C. Error bars represent standard deviation from triplicate measurements.



Figure 84: Agglomerates observed for the formulation containing 2 mg/mL DMPG and 150 mM NaCl after 4 weeks storage.

6.2.6 Injectability

Furthermore, the required force to eject the redispersed suspension from the syringe with a 25 Gauge needle and with 10 mm/s is measured with the Texture analyzer as a function of formulation and storage time (Figure 85). Even the highly viscous aqueous suspension is injectable as discussed before. All formulations are comparable and can be ejected with less than 5 N during the whole storage period.

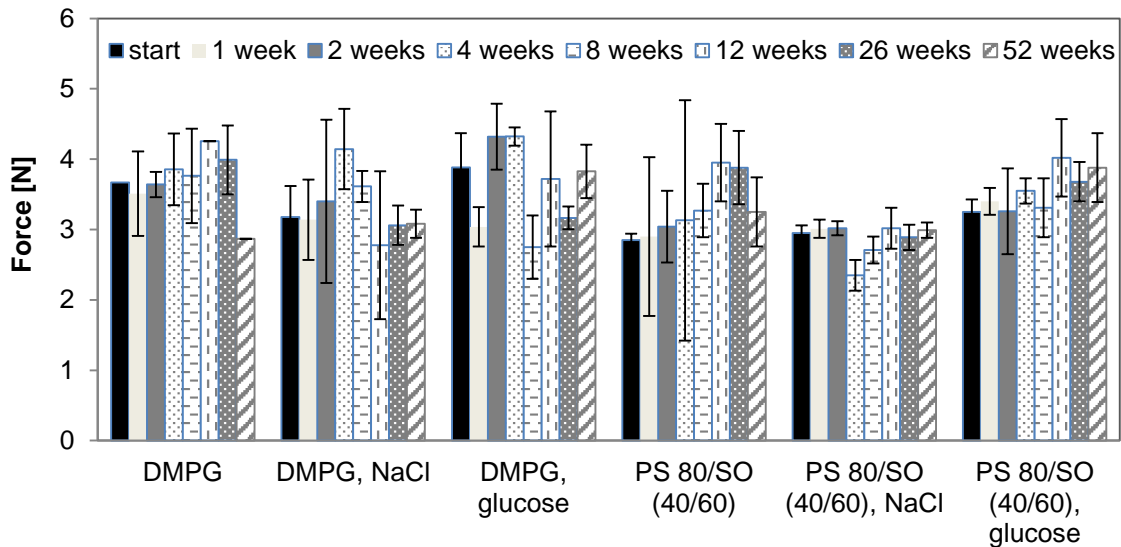


Figure 85: Injection force required for suspensions containing 300 mg/mL API, 2 mg/mL DMPG or 5 mg/mL PS 80/SO (40/60) and 150 mM NaCl or 300 mM glucose over one year using a 25 Gauge needle, a volume of 1 mL and a speed of 10 mm/s. Error bars represent standard deviation from triplicate measurements.

Overall, all the formulations show an acceptable particle size stability during the storage period of one year at 2 – 8 °C. The sedimentation rate is generally low enough to allow for sufficient time to withdraw the homogenized suspension in reproducible doses. The particles of the DMPG containing samples sediment faster as compared to the Wfl and PS 80/SO formulations and interact less with each other building a compact sediment which is hard to resuspend. The PS 80/SO containing suspensions exhibit a loose sediment which is rapidly resuspendable. Furthermore, the surfactant mix containing formulations exhibit a significantly faster and easier syringeability compared to the phospholipid containing systems. Persistent agglomerates are seen for the formulation with DMPG and NaCl stored for 26 weeks prohibiting the withdrawal. Soft agglomerates are seen for suspensions with DMPG and NaCl after 4 weeks storage, DMPG and glucose after 12 weeks storage and also for PS 80/SO containing formulations with NaCl after 8 weeks storage. Finally, the required force of all suspensions is low and constant during storage as seen for the Wfl formulations.

6.3 Conclusion

The viscosity of the highly viscous formulation containing 300 mg/mL Cilengitide is successfully reduced by the addition of surfactants. However, the variation of pH or the addition of ions does not significantly influence the viscosity. An increase of particle size offering a lower viscosity is not suitable for a formulation applied via a 25 Gauge needle.

Suspensions containing DMPG or other phospholipids show a significant lower viscosity around the isoelectric point at pH 5.5. The interaction between the phospholipid and the particle surface is strongest leading to a densely covered particle surface. The particles are separated due to weakened interparticle forces and introduction of repulsive forces resulting in a deflocculated system which is physically unstable. At pH 7, the viscosity is sufficiently low and no caking is observed. These formulations with additionally NaCl or glucose are used for final evaluation of the stability. In contrast, suspensions with PS 80/SO mixtures are stable, flocculated systems over the whole pH range and viscosity is independent on pH. Mixture ratio and concentration do not significantly affect the viscosity in the low shear range. It is found that pure PS 80 does not sufficiently lower the viscosity. At high shear rates, suspensions with 5 mg/mL PS 80/SO (40/60) show lowest viscosity. They are finally used for stability evaluation in combination with NaCl or glucose.

The evaluation of the storage stability shows an acceptable particle size stability for all formulations during storage at 2 - 8 °C over one year. The sedimentation rate of the suspensions with DMPG or PS 80/SO is very low ensuring an adequate dosing. The sedimentation degree of DMPG containing systems is lower than the PS 80/SO systems indicating a more compressed sediment. This is in line with the higher times needed for resuspension of these formulations. With respect to syringeability suspensions with PS 80/SO require less time to be drawn out of the vial compared to DMPG containing formulations. However, agglomerates are observed during storage for all DMPG containing formulations and for formulations with PS 80/SO combined with NaCl which comprise the syringeability. Even though soft agglomerates can be destroyed by vigorous shaking these suspensions are not suitable as final formulation. The injectability of all formulations via a 25 Gauge needle is feasible. Finally, a formulation with PS 80/SO (40/60) with glucose is recommended.

Considering the interaction mechanism for DMPG and Cilengitide it is found that DMPG bicelles built in water are destroyed when dissolved Cilengitide is added. The formation of smaller, spherical micelles is seen in Cryo-TEM pictures and is connected with a turbidity reduction. Thus, the theory for DMPG acting as a ball bearing is not confirmed. Hydrophobic interactions between the myristoyl chain of DMPG and the phenylalanine and valine moieties of Cilengitide are observed at all pH values. Furthermore, it is expected that electrostatic interaction takes place between the negatively charged phosphate group and the positively charged arginine of Cilengitide. The hydrophobic interaction is most pronounced at the isoelectric point of Cilengitide leading to a densely covered particle surface. This is confirmed by a Zeta potential maximum of the suspended particles at pH 5 – 6. The particles are separated due to reduced interparticle forces and introduced repulsive forces. Finally, a deflocculated, instable system is formed which is not suitable as final formulation. However,

DMPG partly interacts with the Cilengitide particle surface at pH 7 reducing the viscosity by lowering the interparticle forces. The surface is only partly covered confirmed by a slight increase of the Zeta potential. A flocculated state exist which does not show caking.

7 Final summary of the thesis

The aim of the thesis was to develop a highly concentrated, physically stable suspension of Cilengitide for subcutaneous application with a target concentration of 300 mg/mL API. The anhydrous polymorph A1 is the most stable polymorph without any tendency for conversion into another polymorphic form and thus, suitable for the development of a subcutaneous suspension. The molecule has an acidic carboxyl group of aspartic acid and a basic guanidinium group of arginine leading to a detected isoelectric point of 5.5. The surface of a Cilengitide A1 molecule is hydrophobic due to the outwardly orientated amino acids phenylalanine and valine. The non-micronized raw material contained needle- and rod-shaped particles with a size of approximately 570 μm and showed good flowability in contrast to micronized material containing particles of approximately 30 μm . However, the non-micronized material would not have been applicable via a 25 Gauge needle due to the large particles. Consequently, the influence of stirring on particle size and structure of non-micronized material suspended in water was evaluated to possibly find a comminuting method ensuring a suitable particle size distribution with a maximum of 100 μm .

Cilengitide particles built a continuous, scaffold-like structure when suspended in water and homogenized. Particle sizes comparable to micronized material resulted after stirring of non-micronized material. Particles broke at predetermined breaking points leading to similar particle sizes. Since long stirring times were required and difficulties in upscaling were expected the use of non-micronized material was not recommended despite the advantage of very good flow properties. Micronized particles are rather stable against comminuting methods with higher energy levels like ultrasound, Ultraturrax[®] and ball mill treatment. The API concentration and the addition of metal beads to possibly facilitate resuspension also did not affect the particle size distribution.

The physical stability of suspensions was evaluated including particle size, sedimentation behavior, resuspendability, viscosity, syringeability and injectability. An acceptable particle size stability was seen upon storage at 2-8 °C, 25 °C / 60 % r.H. and 45 °C / 75 % r.H. The particles settled as flocs building a loose sediment. The sedimentation rate decreased with increasing API concentration due to spatial hindrance. For the samples with 300 mg/mL API a very slow sedimentation rate was found easily enabling an adequate dosing and application. The highly concentrated suspensions could be resuspended within short times due to the loosely packed sediment. Overall, the physical stability of 300 mg/mL Cilengitide suspended in WfI was acceptable. However, suspensions containing the target concentration of 300 mg/mL API were too viscous to be withdrawn out of the vial. The rheological characterization of differently concentrated suspensions was performed with special attention

to shear rates of $\dot{\gamma} = 0.2 \text{ 1/s}$ and $\dot{\gamma} = 12.6 \text{ 1/s}$ characterizing the withdrawal from the vial (syringeability) and $\dot{\gamma} = 1000 \text{ 1/s}$ to reflect the injection of the suspension with a 25 Gauge needle. It was seen that the viscosity significantly increased with increasing concentration mainly in the low shear range compromising the syringeability of the highly concentrated suspensions. All the samples showed a marked shear-thinning behavior resulting in low viscosity at high shear rates. Thus, the injection of even 300 mg/mL suspensions with a 25 Gauge needle was feasible and confirmed by ejection force measurements. Consequently, a viscosity reduction of the highly concentrated suspension was essential to ensure the syringeability.

Several strategies for viscosity reduction were evaluated. The variation of the pH and the addition of ions did not affect the viscosity substantially. A decrease in viscosity by use of larger particles was not suitable. Utilizing "non-micronized" material, despite a $D(0.95)$ value of about $40 \mu\text{m}$, needle shaped particles longer than $120 \mu\text{m}$ were detected. These particles blocked the 25 Gauge needle and such larger particles would need to be completely rounded out. Finally, the addition of surfactants successfully lowered the viscosity of the highly concentrated suspension. Phospholipids, mainly dimyristoylphosphoglycerol (DMPG), decreased the viscosity by introducing electrosteric repulsive forces and by reducing particle interaction. The viscosity reduction was most pronounced at pH 5.5 where hydrophobic interaction was strongest and the surface of Cilengitide particles was densely covered with DMPG molecules resulting in particle separation. Despite of this, these formulations were physically unstable as caking was observed and thus, not suitable as final formulation. The theory for DMPG acting as a ball bearing reducing the interparticle interaction could not be confirmed. Spherical DMPG bicelles were destroyed when adding Cilengitide and spherical micelles formed. Varying the hydrophobic chain length of the phospholipid did not show any effect. Mixtures of the commonly used non-ionic surfactants polysorbate 80 (PS 80) and sorbitan monooleate (SO) lowered the viscosity comparable to the phospholipids. The viscosity reduction generally did not depend on mixing ratio and concentration. In contrast to the phospholipid containing formulations, the pH did not affect the viscosity and thus, the PS 80/SO containing formulations were more robust.

For the final evaluation of the physical stability and performance, suspensions with 2 mg/mL DMPG or 5 mg/mL PS 80/SO (40/60) and 150 mM NaCl or 300 mM glucose at pH 7 were used. All systems showed a comparable initial particle size and acceptable particle size stability. The sedimentation rate was generally low ensuring adequate dosing. Samples with PS 80/SO showed more loosely packed sediments compared to the DMPG containing formulations. Consequently, the PS 80/SO formulations could be resuspended considerably faster. During storage for DMPG containing formulations with NaCl or glucose and PS 80/SO

in combination with NaCl particle agglomerates were formed compromising the syringeability due to needle clogging. The time needed to draw 1 mL out of the vial was less for PS 80/SO systems than for suspensions with DMPG. The injectability was given for all formulations.

Summarizing, a physically stable, highly concentrated suspension for subcutaneous application by adding 5 mg/mL PS80/SO (40/60) in combination with glucose was achieved. The viscosity was efficiently reduced by the addition of either a phospholipid or a mixture containing PS 80 and SO. However, the PS80/SO containing systems combined with glucose showed superior storage stability with respect to resuspendability and syringeability. Consequently, they are recommended as suitable final formulations. In future studies, the effect of surfactant and viscosity on the API pharmacokinetics needs to be studied. Furthermore, a more general evaluation of the concept of surfactant based viscosity reduction of aqueous API suspensions would be interesting.

8 References

1. Nash, R.A., *Suspensions*. Encyclopedia of Pharmaceutical Technology, 2007: p. 3597-3610.
2. Akers, M.J., A.L. Fites, and R.L. Robison, *Formulation Design and Development of Parenteral Suspensions*. Journal of Parenteral Science & Technology, 1987. **41**(3): p. 88 - 96.
3. Liu, J., et al., *Reversible self-association increases the viscosity of a concentrated monoclonal antibody in aqueous solution*. Journal of Pharmaceutical Sciences, 2005. **94**(9): p. 1928-1940.
4. Miller, M.A., et al., *Low Viscosity Highly Concentrated Injectable Nonaqueous Suspensions of Lysozyme Microparticles*. Langmuir, 2009. **26**(2): p. 1067-1074.
5. Jain, K.K., *Drug Delivery Systems*. Methods in Molecular Biology, ed. J.M. Walker. Vol. 437. 2008.
6. Dechantsreiter, M., et al., *Cyclische Adhäsionsinhibitoren*. 1997.
7. Brittain, H.G., D.J.R. Grant, and P.B. Myrdal, *Effects of Polymorphism and Solid-State Solvation on Solubility and Dissolution Rate*, in *Polymorphism in Pharmaceutical Solids*. p. 436-480.
8. Scaringi, C., et al., *Integrin inhibitor cilengitide for the treatment of glioblastoma: A brief overview of current clinical results*. Anticancer Research. **32**(10): p. 4213-4224.
9. Beekman, K.W., et al., *Phase II Evaluations of Cilengitide in Asymptomatic Patients with Androgen-Independent Prostate Cancer: Scientific Rationale and Study Design*. Clinical Genitourinary Cancer, 2006. **4**(4): p. 299-302.
10. Manegold, C., et al., *Randomized phase II study of three doses of the integrin inhibitor cilengitide versus docetaxel as second-line treatment for patients with advanced non-small-cell lung cancer*. Investigational New Drugs. **31**(1): p. 175-182.
11. Vermorken, J.B., et al., *Phase I/II trial of cilengitide with cetuximab, cisplatin and 5-fluorouracil in recurrent and/or metastatic squamous cell cancer of the head and neck: findings of the phase I part*. Br J Cancer. **104**(11): p. 1691-1696.
12. Nash, R.A., *Pharmaceutical Suspensions*, in *Pharmaceutical Dosage Forms: Disperse Systems*, H.A. Liebermann, R.M. M, and G.S. Banker, Editors. 1996: New York. p. 1-46.
13. Martin, A. and P. Bustanante, in *Physical Pharmacy*. 1993: Philadelphia. p. 477-484.
14. Floyd, A.G. and S. Jain, *Injectable Emulsions and Suspensions*, in *Pharmaceutical Dosage Forms: Disperse Systems*, M.R. HA Lieberman, GS Banker, Editor. 1996: New York. p. 261-318.
15. Rueb, C.J. and C.F. Zukoski, *Rheology of suspensions of weakly attractive particles: Approach to gelation*. Journal of Rheology (1978-present), 1998. **42**(6): p. 1451-1476.
16. Nutan, M.T.H. and I.K. Reddy, *General Principles of Suspensions*, in *Pharmaceutical Suspensions: From Formulation Development to Manufacturing*, A.K. Kulshreshtha, O.N. Singh, and G.M. Wall, Editors. 2010: New York. p. 39-66.
17. Kayes, J.B., *Pharmaceutical suspensions: relation between zeta potential, sedimentation volume and suspension stability*. Journal of Pharmacy and Pharmacology, 1977. **29**: p. 199-204.
18. Rupprecht, H., *Gesichtspunkte zur Optimierung arzneilicher Suspensionen*. Pharmazeutische Zeitung, 1975. **35**: p. 1265-1273.
19. Tadros, T.F., *Rheology of Dispersions - Principles and Applications*. 2010, Weinheim.
20. Martin, A., *Physikalische Pharmazie*, H. Leuenberger, Editor. 2002: Stuttgart.
21. Wu, W. and G. Nancollas, *A New Understanding of the Relationship Between Solubility and Particle Size*. Journal of Solution Chemistry, 1998. **27**(6): p. 521-531.
22. Simpson, J.P. and M.J. Akers, *Quality Assurance and Regulation*, in *Injectable Dispersed Systems - Formulation, Processing, and Performance*, D.J. Burgess, Editor. 2005. p. 583-619.

References

23. Jezek, J., et al., *Viscosity of concentrated therapeutic protein compositions*. Advanced Drug Delivery Reviews. **63**(13): p. 1107-1117.
24. Aktaş, Z. and E.T. Woodburn, *Effect of addition of surface active agent on the viscosity of a high concentration slurry of a low-rank British coal in water*. Fuel Processing Technology, 2000. **62**(1): p. 1-15.
25. Benna, M., et al., *Effect of pH on Rheological Properties of Purified Sodium Bentonite Suspensions*. Journal of Colloid and Interface Science, 1999. **218**(2): p. 442-455.
26. Fukuda, Y., et al., *Influence of additive content of anionic polymer dispersant on dense alumina suspension viscosity*. Chemical Engineering Science, 2001. **56**(9): p. 3005-3010.
27. Güngör, N., et al., *The effect of SDS surfactant on the flow and zeta potential of bentonite suspensions*. Materials Letters, 2001. **51**(3): p. 250-254.
28. Zhou, Z., P.J. Scales, and D.V. Boger, *Chemical and physical control of the rheology of concentrated metal oxide suspensions*. Chemical Engineering Science, 2001. **56**(9): p. 2901-2920.
29. Tadros, T., *Interparticle interactions in concentrated suspensions and their bulk (Rheological) properties*. Advances in Colloid and Interface Science. **168**(1-2): p. 263-277.
30. Curtis, R.A., J.M. Prausnitz, and H.W. Blanch, *Protein-protein and protein-salt interactions in aqueous protein solutions containing concentrated electrolytes*. Biotechnology and Bioengineering, 1998. **57**(1): p. 11-21.
31. Saluja, A. and D.S. Kalonia, *Nature and consequences of protein-protein interactions in high protein concentration solutions*. International Journal of Pharmaceutics, 2008. **358**(1-2): p. 1-15.
32. Briceno, M.I., *Pharmaceutical Emulsions and Suspensions*, in *Drugs and the pharmaceutical Science*, F. Nielloud and G. Marti-Mestres, Editors. 2000: New York. p. 557-607.
33. Shi, F.N. and T.J. Napier-Munn, *A model for slurry rheology*. International Journal of Mineral Processing, 1996. **47**(1-2): p. 103-123.
34. Krieger, I.M. and T.J. Dougherty, *A mechanism for non-Newtonian flow in suspension of rigid spheres*. Transaction of the Society of Rheology, 1959. **3**: p. 137-152.
35. Boersma, W.H., J. Laven, and H.N. Stein, *Shear Thickening (Dilatancy) in Concentrated Dispersions*. A.I.Ch.E. Journal, 1990. **36**(3): p. 321.
36. Genovese, D.B., *Shear rheology of hard-sphere, dispersed, and aggregated suspensions, and filler-matrix composites*. Advances in Colloid and Interface Science, 2012. **171-172**(0): p. 1-16.
37. Logos, C. and Q.D. Nguyen, *Effect of particle size on the flow properties of a South Australian coal-water slurry*. Powder Technology, 1996. **88**(1): p. 55-58.
38. Yang, H.G., et al., *Rheological behavior of titanium dioxide suspensions*. Journal of Colloid and Interface Science, 2001. **236**(1): p. 96-103.
39. Chang, C. and R.L. Powell, *Effect of particle size distributions on the rheology of concentrated bimodal suspensions*. Journal of Rheology, 1994. **38**(1): p. 85-98.
40. Dabak, T. and O. Yucel, *Modeling of the concentration particle size distribution effects on the rheology of highly concentrated suspensions*. Powder Technology, 1987. **52**(3): p. 193-206.
41. Storms, R.F., B.V. Ramarao, and R.H. Weiland, *Low shear rate viscosity of bimodally dispersed suspensions*. Powder Technology, 1990. **63**(3): p. 247-259.
42. Clarke, B., *Rheology of coarse settling suspensions*. Transactions of the Institution of Chemical Engineers, 1967. **45**: p. 251-256.
43. Yuan, J. and H.H. Murray, *The importance of crystal morphology on the viscosity of concentrated suspensions of kaolins*. Applied Clay Science, 1997. **12**(3): p. 209-219.
44. Graham, A.L., et al., *Rheological behavior of a suspension of randomly oriented rods*. Applied Physics Letters, 1987. **50**(3): p. 127-129.

45. Zhang, X., et al., *The importance of surface hydration and particle shape on the rheological property of silica-based suspensions*. *Ceramics International*, (0).
46. Kulshreshtha, A.K., O.N. Singh, and G.M. Wall, *Pharmaceutical Suspensions: From Formulation Development to Manufacturing*. 2010.
47. Duman, O. and S. Tunç, *Electrokinetic and rheological properties of Na-bentonite in some electrolyte solutions*. *Microporous and Mesoporous Materials*, 2009. **117**(1-2): p. 331-338.
48. Desai, H., N.R. Biswal, and S. Paria, *Rheological Behavior of Pyrophyllite-Water Slurry in the Presence of Anionic, Cationic, and Nonionic Surfactants*. *Industrial & Engineering Chemistry Research*. **49**(11): p. 5400-5406.
49. Günster, E., et al., *Effect of cationic surfactant adsorption on the rheological and surface properties of bentonite dispersions*. *Journal of Colloid and Interface Science*, 2006. **303**(1): p. 137-141.
50. Patapoff, T.W. and O. Esue, *Polysorbate 20 prevents the precipitation of a monoclonal antibody during shear*. *Pharmaceutical Development and Technology*, 2009. **14**(6): p. 659-664.
51. Işçı, S., et al., *The modification of rheologic properties of clays with PVA effect*. *Materials Letters*, 2004. **58**(12-13): p. 1975-1978.
52. Chari, R., et al., *Long- and short-range electrostatic interactions affect the rheology of highly concentrated antibody solutions*. *Pharmaceutical Research*, 2009. **26**(12): p. 2607-2618.
53. Zhou, Z., *Rheology of metal oxide suspensions*. 2000, The University of Melbourne.
54. Heller, H. and R. Keren, *Rheology of Na-rich Montmorillonite suspension as affected by electrolyte concentration and shear rate*. *Clays and Clay Minerals*, 2001. **49**(4): p. 286-291.
55. Zaman, A.A. and B.M. Moudgil, *Role of electrostatic repulsion on the viscosity of bidisperse silica suspensions*. *Journal of Colloid and Interface Science*, 1999. **212**(1): p. 167-175.
56. Abu-Jdayil, B., *Rheology of sodium and calcium bentonite - water dispersions: Effect of electrolytes and aging time*. *International Journal of Mineral Processing*. **98**(3-4): p. 208-213.
57. Rosen, M.J. and J.T. Kunjappu, *Surfactants and interfacial Phenomena*. 4th edition ed. 2012.
58. Lafuma, F., K. Wong, and B. Cabane, *Bridging of colloidal particles through adsorbed polymers*. *Journal of Colloid and Interface Science*, 1991. **143**(1): p. 9-21.
59. Heath, D. and T.F. Tadros, *Influence of pH, electrolyte, and poly(vinyl alcohol) addition on the rheological characteristics of aqueous dispersions of sodium montmorillonite*. *Journal of Colloid and Interface Science*, 1983. **93**(2): p. 307-319.
60. Kamibayashi, M., H. Ogura, and Y. Otsubo, *Viscosity behavior of silica suspensions flocculated by associating polymers*. *Journal of Colloid and Interface Science*, 2005. **290**(2): p. 592-597.
61. Luckham, P.F. and S. Rossi, *The colloidal and rheological properties of bentonite suspensions*. *Advances in Colloid and Interface Science*, 1999. **82**(1-3): p. 43-92.
62. He, M., Y. Wang, and E. Forssberg, *Slurry rheology in wet ultrafine grinding of industrial minerals: A review*. *Powder Technology*, 2004. **147**(1-3): p. 94-112.
63. Hiemenz, P.C. and R. Rajagopalan, *Principles of Colloid and Surface Chemistry*. 3th edition ed. 1997.
64. Schott, H., *Deflocculation of swelling clays by nonionic and anionic detergents*. *Journal of Colloid and Interface Science*, 1968. **26**(2): p. 133-139.
65. Tunç, S., O. Duman, and B. Kancı, *Rheological measurements of Na-bentonite and sepiolite particles in the presence of tetradecyltrimethylammonium bromide, sodium tetradecyl sulfonate and Brij 30 surfactants*. *Colloids and Surfaces A: Physicochemical and Engineering Aspects*. **398**(0): p. 37-47.

66. Raw, A.S., et al., *Regulatory considerations of pharmaceutical solid polymorphism in Abbreviated New Drug Applications (ANDAs)*. *Advanced Drug Delivery Reviews*, 2004. **56**(3): p. 397-414.
67. Lee, A.Y., D. Erdemir, and A.S. Myerson, *Crystal Polymorphism in Chemical Process Development*, in *Annual Review of Chemical and Biomolecular Engineering, Vol 2*, J.M. Prausnitz, Editor. 2011. p. 259-280.
68. Bauer, J., et al., *Ritonavir: An Extraordinary Example of Conformational Polymorphism*. *Pharmaceutical Research*, 2001. **18**(6): p. 859-866.
69. Dechantsreiter, M.A., et al., *N-Methylated Cyclic RGD Peptides as Highly Active and Selective $\alpha\beta 3$ Integrin Antagonists*. *Journal of Medicinal Chemistry*, 1999. **42**(16): p. 3033-3040.
70. Jonczyk, A., et al., *Novel solid materials of $\{[2s, 5r, 8s, 11s]-5\text{-benzyl-11-(3-guanidino-propyl)-8-isopropyl-7-methyl-3,6,9,12,15-pentaoxo-1,4,7,10,13-pentaaza-cyclopentadec-2-yl}\}$ -acetic acid and methods for obtaining them*. 2010, Google Patents.
71. Garad, S., et al., *Preclinical Development for Suspensions*, in *Pharmaceutical Suspensions - From Formulation Development to Manufacturing*, A.K. Kulshreshtha, O.N. Singh, and G.M. Wall, Editors. 2010. p. 127-176.
72. Machkovech, S. and T. Foster, *Aqueous Suspensions*, in *Long Acting Injections and Implants*, J.C. Wright and D.J. Burgess, Editors. 2012, Springer US. p. 137-151.
73. Wieckhusen, D., A. Glausch, and M. Ahlheim, *Injectable depot formulation comprising crystals of iloperidone*, in *US20050250813 A1*. November 10, 2005.
74. Dermapharm AG Grünwald, G., *Volon® A 40 Kristallsuspension Triamcinolonacetamid, Gebrauchsinformation: Information für Anwender*. 2014.
75. Wu, L., J. Zhang, and W. Watanabe, *Physical and chemical stability of drug nanoparticles*. *Advanced Drug Delivery Reviews*, 2011. **63**(6): p. 456-469.
76. Enomoto, Y., M. Tokuyama, and K. Kawasaki, *Finite volume fraction effects on Ostwald ripening*. *Acta Metallurgica*, 1986. **34**(11): p. 2119-2128.
77. Mueller, S., E.W. Llewellyn, and H.M. Mader, *The rheology of suspensions of solid particles*. *Proceedings of the Royal Society A*, 2010. **466**: p. 1201-1228.
78. Bauer, K., K.-H. Frömring, and C. Führer, *Lehrbuch der pharmazeutischen Technologie*. 7. ed. 2002: Wissenschaftliche Verlagsgesellschaft Stuttgart.
79. Bogdanowich-Knipp, S.J., et al., *Solution stability of linear vs. cyclic RGD peptides*. *The Journal of Peptide Research*, 1999. **53**(5): p. 530-541.
80. Loftsson, T., *Chapter 5 - Stability of Peptides and Proteins*, in *Drug Stability for Pharmaceutical Scientists*, T. Loftsson, Editor. 2014, Academic Press: San Diego. p. 109-114.
81. Li, C. and M. Akinc, *Role of Bound Water on the Viscosity of Nanometric Alumina Suspensions*. *Journal of the American Ceramic Society*, 2005. **88**(6): p. 1448-1454.
82. Falkowski, P., M. Szafran, and T. Mizerski, *Nanometric alumina slurry deflocculated by addition of selected monosaccharides*. *Polish Ceramic Bulletin*, 2006. **99**: p. 553-560.
83. Falkowski, P., et al., *Application of monosaccharides derivatives in colloidal processing of aluminum oxide*. *Journal of the European Ceramic Society*. **30**(14): p. 2805-2811.
84. Garidel, P. and A. Blume, *1,2-Dimyristoyl-sn-glycero-3-phosphoglycerol (DMPG) monolayers: influence of temperature, pH, ionic strength and binding of alkaline earth cations*. *Chemistry and Physics of Lipids*, 2005. **138**(1-2): p. 50-59.
85. Tamashiro, M.N., V.B. Henriques, and M.T. Lamy, *Aqueous Suspensions of Charged Spherical Colloids: Dependence of the Surface Charge on Ionic Strength, Acidity, and Colloid Concentration*. *Langmuir*, 2005. **21**(24): p. 11005-11016.
86. Meyer, H.W., et al., *Bilayer fragments and bilayered micelles (bicelles) of dimyristoylphosphatidylglycerol (DMPG) are induced by storage in distilled water at 4°C*. *Colloids and Surfaces A: Physicochemical and Engineering Aspects*, 2001. **183-185**: p. 495-504.

87. Fernandez, R.M., et al., *Influence of salt on the structure of DMPG studied by SAXS and optical microscopy*. *Biochimica et Biophysica Acta - Biomembranes*, 2008. **1778**(4): p. 907-916.
88. Riske, K.A., H.-G. Döbereiner, and M.T. Lamy-Freund, *Gel-Fluid Transition in Dilute versus Concentrated DMPG Aqueous Dispersions*. *The Journal of Physical Chemistry B*, 2001. **106**(2): p. 239-246.
89. Epand, R.M., et al., *Formation of a new stable phase of phosphatidylglycerols*. *Biophysical Journal*, 1992. **63**: p. 327-332.
90. Epand, R.M. and S.-W. Hui, *Effect of electrostatic repulsion on the morphology and thermotropic transitions of anionic phospholipids*. *FEBS Letters*, 1986. **209**(2): p. 257-260.
91. Spinozzi, F., et al., *Melting Regime of the Anionic Phospholipid DMPG: New Lamellar Phase and Porous Bilayer Model*. *Langmuir*. **26**(9): p. 6484-6493.
92. Riske, K.A., et al., *Mesoscopic Structure in the Chain-Melting Regime of Anionic Phospholipid Vesicles: DMPG*. *Biophysical Journal*, 2004. **86**(6): p. 3722-3733.
93. Barroso, R.P., et al., *Aqueous dispersions of DMPG in low salt contain leaky vesicles*. *Chemistry and Physics of Lipids*. **165**(2): p. 169-177.
94. Garidel, P., et al., *Structural and morphological investigations of the formation of quasi-crystalline phases of 1,2-dimyristoyl-sn-glycero-3-phosphoglycerol (DMPG)*. *Physical Chemistry Chemical Physics*, 2001. **3**: p. 1504-1513.
95. Kleinschmidt, J.H., et al., *Interaction of Bee Venom Melittin with Zwitterionic and Negatively Charged Phospholipid Bilayers: A Spin-Label Electron Spin Resonance Study*. *Biophysical Journal*, 1997. **72**(2, Part 1): p. 767-778.
96. Dempsey, C.E. and B. Sternberg, *Reversible disc-micellization of dimyristoylphosphatidylcholine bilayers induced by melittin and [Ala-14]melittin*. *Biochimica et Biophysica Acta (BBA) - Biomembranes*, 1991. **1061**(2): p. 175-184.
97. Kleinschmidt, J.H. and L.K. Tamm, *Structural Transitions in Short-Chain Lipid Assemblies Studied by ³¹P-NMR Spectroscopy*. *Biophysical Journal*, 2002. **83**(2): p. 994-1003.
98. Grau, U.D. and W.D. Pohler, *Device for dispensing medicinal suspensions*, in *EP19870102367*. 1987, Hoechst Aktiengesellschaft Germany.